UNIVERSITÀ
DEGLI STUDI
DI PADOVA

UNIVERSITÀ DEGLI STUDI DI PADOVA

Dipartimento di Biomedicina Comparata e Alimentazione

SCUOLA DI DOTTORATO DI RICERCA IN

SCIENZE VETERINARIE

XXVIII CICLO

COMPARATIVE MOLECULAR TARGETS FOR ANTICANCER CHEMOTHERAPY: NEW INSIGHTS AND PERSPECTIVES

Direttore della Scuola: Ch.mo Prof. Gianfranco Gabai

Supervisore: Ch.mo Prof. Mauro Dacasto

Dottorando: Eleonora Zorzan

ABSTRACT

The past thirty years have reported the introduction of multiple anticancer therapies targeting various aspects of the cancer hallmarks, which are essential for successful tumor propagation and dissemination. In this sense, the evolution of molecular-scale technology has been central to the identification of new cancer targets.

The receptor tyrosine kinase (RTK) Hardy-Zuckerman 4 feline sarcoma virus homolog (*c-KIT*) is a critical regulator of growth, differentiation, migration and proliferation in the hematopoietic system, in germ cells and melanocytes. Since it activates a number of intracellular signaling pathways implicated in the tumor progression, it is one of the most studied proto-oncogenes as well as the target of drugs belonging to the family of tyrosine kinase inhibitors (TKIs). Actually, TKIs are employed for the treatment of human and canine *c-KIT*-dependent tumors as an alternative to standard chemotherapy. Nevertheless, multiple resistance phenomena frequently occur.

Recently, the discovery of G-quadruplex (G4) structures highlighted a new role for DNA in cancer biology. DNA G4 are four-stranded globular nucleic acid secondary structures, formed in specific G-rich sequences with biological significance; among these ones, the human telomeres and the promotorial region of oncogenes such as *c-KIT*.

In the first part of this dissertation, three compounds were proved to bind *in silico c-KIT* G4 and were tested in human and canine cell lines to check for their potential usefulness as therapeutic agents. Interesting results, e.g. *c-KIT* mRNA and protein inhibition, were obtained with an anthraquinone derivative (AQ1) that caused a block of cell proliferation.

In another study, the occurrence of *c-KIT* mutations was investigated in matched primary and metastatic canine cutaneous mast cell tumor (MCT), to make a recommendation for the best therapeutic choice. In dogs, 10-30% of MCTs possess *c-KIT* mutations, and the relevance of the mutational status for the therapy with TKIs is nowadays accepted also in this species; however, little is known on *c-KIT* mutational status in metastatic MCTs. In all analyzed dogs, there was a perfect concordance between *c-KIT* mutational status in primary MCT and the relative lymph node metastasis. This has a relevant implication for clinical practices.

Finally, during the Ph.D. program, a collaboration was established with the Centre de Recherche en Cancérologie de Marseille, and particularly with Dr. Patrice Dubreuil. In his most recent articles, he discovered a set of genes that are frequently mutated in human systemic mastocytosis (SM) and cooperate with *c-KIT* in the disease malignant evolution. In the last study illustrated in this Ph.D. thesis, the mutational profile of these hotspot genes in canine MCTs samples has been screened, in order to find molecular similarities between the two diseases, thereby justifying the use of domestic dog as an animal model in comparative oncology.

RIASSUNTO

Negli ultimi trent'anni, l'evoluzione delle tecnologie in campo medico-scientifico ha permesso la più profonda conoscenza dei meccanismi molecolari alla base dello sviluppo, della crescita e della diffusione del tumore. Tutto ciò ha permesso di sviluppare le cosiddette terapie mirate**,** identificando nuovi bersagli terapeutici.

Il recettore tirosin-chinasico *c-KIT* è un fattore critico per la regolazione della crescita, differenziazione, migrazione e proliferazione delle cellule germinali, di quelle del sistema ematopoietico e dei melanociti. *c-KIT* è anche coinvolto nell'attivazione di numerosi meccanismi intracellulari implicati nella progressione tumorale e, allo stesso tempo, è uno dei proto-oncogeni più studiati ed il bersaglio di farmaci appartenenti alla famiglia degli inibitori tirosin-chinasici (TKIs). Attualmente, i TKIs sono approvati come trattamento alternativo alla chemioterapia tradizionale in tumori *c-KIT* dipendenti in uomo e cane tuttavia, fenomeni di resistenza a questi farmaci si verificano frequentemente.

Negli ultimi anni, la scoperta di strutture secondarie del DNA chiamate G-quadruplex (G4) ha evidenziato un nuovo ruolo degli acidi nucleici nella biologia tumorale. Tali conformazioni si formano in specifiche sequenze del DNA ricche in residui di guanina, localizzate principalmente nei telomeri e nelle regioni promotoriali di alcuni oncogeni come *c-KIT*.

Nella prima parte di questa tesi di dottorato, tre composti scelti sulla base della loro capacità di legare e stabilizzare le conformazioni G4 sono stati testati in linee cellulari stabilizzate di uomo e cane al fine di determinare la loro efficacia come potenziali agenti terapeutici. In questo senso, alcuni risultati interessanti in termini di blocco della proliferazione nonché della trascrizione e traduzione di *c-KIT* si sono ottenuti con un derivato della famiglia degli antrachinoni chiamato AQ1.

In un altro studio proposto, il profilo mutazionale di *c-KIT* è stato analizzato in una coorte di campioni di mastocitoma del cane composti da tumore primitivo e relativa metastasi linfonodale. Nel cane infatti, la percentuale tra il 10 ed il 30% dei mastocitomi presenta almeno una mutazione di *c-KIT* nel tumore primitivo, tuttavia, poche conoscenze si hanno relativamente al profilo mutazionale nelle metastasi. Dai risultati ottenuti, tutti i cani analizzati hanno dimostrato avere una perfetta concordanza tra tumore primitivo e metastasi in termini di status mutazionale di *c-*

KIT con rilevanti implicazioni cliniche per la scelta della miglior terapia da attuare da parte degli oncologi veterinari.

Infine, nel corso del secondo anno di dottorato, è nata una collaborazione con il Dr. Patrice Dubreuil del Centre de Recherche en Cancérologie de Marseille, a Marsiglia. Nei suoi recenti articoli sulla mastocitosi dell'uomo, egli ha scoperto un set di geni che presentano mutazioni in talune percentuali di casi e cooperano con *c-KIT* nello sviluppo delle forme più gravi ed aggressive della malattia. Nell'ultima pubblicazione illustrata in questa dissertazione, è stato eseguito lo *screening* del profilo mutazionale di questi nuovi geni in campioni di mastocitoma di cane al fine di trovare analogie molecolari che possano giustificare l'uso del cane come animale modello nell'oncologia comparata.

CONTENTS

LIST OF ABBREVIATIONS 1

1. GENERAL INTRODUCTION 3
- 1.1 CANCER TARGETED THERAPY 3
- 1.2 RECEPTOR TYROSINE KINASE 7
- 1.3 TYROSINE KINASE INHIBITORS 7
  - 1.3.1 LIMITS AND SECOND GENERATION TKIs 9
- 1.4 c-KIT 11
- 1.5 HUMAN *c-KIT* MUTATIONS AND RELATED DISEASES 13
  - 1.5.1 MASTOCYTOSIS 14
- 1.6 CANINE *c-KIT* MUTATIONS AND RELATED DISEASES 16
  - 1.6.1 CANINE MCT 16
- 1.7 G-QUADRUPLEX (G4) 19
  - 1.7.1 G-QUADRUPLEX IN PROMOTER REGIONS 20
  - 1.7.2 G-QUADRUPLEX IN CANINE *c-KIT* PROMOTER 22

2. AIMS OF THE THESIS 25

3. SCREENING OF CANDIDATE G-QUADRUPLEX LIGANDS FOR THE HUMAN *C-KIT* PROMOTORIAL REGION AND THEIR EFFECTS IN MULTIPLE *IN-VITRO* MODELS 27
- 3.1 ABSTRACT 28
- 3.2 INTRODUCTION 29
- 3.3 MATERIALS AND METHODS 31
  - 3.3.1 LIGANDS 31
  - 3.3.2 FLUORESCENT MELTING ASSAY 31
  - 3.3.3 FLUORESCENT INTERCALATOR DISPLACEMENT (FID) ASSAY 31
  - 3.3.4 SURFACE PLASMON RESONANCE (SPR) 32
  - 3.3.5 POLYMERASE STOP ASSAY 32
  - 3.3.6 CELL CULTURES 33
  - 3.3.7 G4-LIGANDS CYTOTOXICITY 33
  - 3.3.8 TARGET GENES CONSTITUTIVE EXPRESSION 34
  - 3.3.9 DETERMINATION OF G4-LIGANDS EFFICACY BY qPCR 37
  - 3.3.10 DETERMINATION OF G4-LIGANDS EFFICACY BY FLOW CYTOMETRY 38
  - 3.3.11 CONFIRMATORY EXPERIMENTS WITH OTHER CELLULAR MODELS 38
  - 3.3.12 STATISTICAL ANALYSIS 40
- 3.4 RESULTS 40
  - 3.4.1 LIGANDS SELECTION 40
  - 3.4.2 BINDING AFFINITY AND FUNCTIONAL INTERACTION OF SELECTED LIGANDS 44
  - 3.4.3 G4-LIGANDS CYTOTOXICITY 46
  - 3.4.4 TARGET GENES CONSTITUTIVE EXPRESSION 48

3.4.5 EVALUATION OF G4-LIGANDS EFFICACY 51
3.4.6 CONFIRMATORY RESULTS WITH OTHER CELLULAR MODELS 60
3.5 DISCUSSION 66

4. TARGETING CANINE c-KIT PROMOTER BY CANDIDATE DNA G-QUADRUPLEX LIGANDS 71
4.1 ABSTRACT 72
4.2 INTRODUCTION 73
4.3 MATERIALS AND METHODS 74
4.3.1 LIGANDS 74
4.3.2 CELL CULTURES 74
4.3.3 CHARACTERIZATION OF THE G4 SEQUENCE 75
4.3.4 G4-LIGANDS CYTOTOXICITY 75
4.3.5 TIME DEPENDENT CONSTITUTIVE EXPRESSION OF TARGET GENES 75
4.3.6 TRANSCRIPTIONAL EFFECTS OF G4-LIGANDS ON TARGET GENES 78
4.3.7 CONFIRMATORY POST-TRANSLATIONAL EFFECTS OF G4-LIGANDS 78
4.3.8 STATISTICAL ANALYSIS 79
4.4 RESULTS 79
4.4.1 SEQUENCING OF THE C2 c-KIT PROXIMAL PROMOTER 79
4.4.2 CYTOTOXICITY TEST AND qPCR RESULTS 79
4.5 DISCUSSION 86

5. CONCORDANCE OF c-KIT MUTATIONAL STATUS IN MATCHED PRIMARY AND METASTATIC CUTANEOUS CANINE MAST CELL TUMORS AT BASELINE 89
5.1 ABSTRACT 90
5.2 INTRODUCTION 91
5.3 MATERIALS AND METHODS 92
5.3.1 CASE SELECTION – INCLUSION CRITERIA 92
5.3.2 TUMOR SPECIMENS 93
5.3.3 NUCLEIC ACID EXTRACTION 93
5.3.4 c-KIT GENOTYPING 94
5.3.5 TREATMENT AND RESPONSE CRITERIA 95
5.3.6 STATISTICAL ANALYSIS 95
5.4 RESULTS 96
5.4.1 DOGS AND MCT DEMOGRAPHICS 96
5.4.2 c-KIT MUTATION STATUS 97
5.4.3 TREATMENT AND CLINICAL FOLLOW-UP 99
5.4.4 RELATIONSHIP BETWEEN c-KIT MUTATIONAL STATUS AND CLINICOPATHOLOGICAL FEATURES 100
5.5 DISCUSSION 102

6. MUTATIONAL HOTSPOTS OF TET2, IDH1, IDH2, SRSF2, SF3B1, KRAS AND NRAS FROM HUMAN SYSTEMIC MASTOCYTOSIS ARE NOT 105

CONSERVED IN CANINE MAST CELL TUMORS
6.1 ABSTRACT 106
6.2 INTRODUCTION 107
6.3 MATERIALS AND METHODS 109
6.3.1 SAMPLES AND ETHICAL STATEMENT 109
6.3.2 DNA EXTRACTION, PCR AND SEQUENCE ANALYSIS 109
6.3.3 STATISTICAL ANALYSIS 112
6.4 RESULTS 112
6.4.1 GENE SEQUENCES HOMOLOGY AMONG CANINE AND HUMAN SPECIES 112
6.4.2 TARGET GENES MUTATIONAL STATUS IN MCTs SAMPLES 113
6.4.3 TET2 MUTATIONAL STATUS IN DOG MCT 114
6.5 DISCUSSION 117

7. CONCLUSIONS AND FUTURE PERSPECTIVES 121

8. BIBLIOGRAPHY 125
8.1 WEB REFERENCES 140

LIST OF ABBREVIATIONS

2-Cda	2 chlorodeoxyadenosine
ABC	ATP-binding cassette
ABL	Abelson murine leukemia viral oncogene homolog 1
AgNOR	argyrophilic nucleolar organizer region
ALL	acute lymphoblastic leukemia
AML	acute myeloid leukemia
AN	anthracene
ANOVA	analysis of variance
AQ	anthraquinone
ASXL1	additional sex combs like 1 alias
ATP	adenosine triphosphate
ATP5β	ATP synthase, H^+ transporting, mitochondrial F1 complex, beta polypeptide
BCL2	B-Cell CLL/Lymphoma 2
BCR	breakpoint cluster region
BCRP/ABCG2	breast cancer resistance protein
BRAF	B-Raf proto-oncogene
c-KIT	Hardy-Zuckerman 4 feline sarcoma virus homolog
CCZ1	CCZ1 vacuolar protein trafficking and biogenesis associated homolog
CD	cluster of differentiation
CGI-119	the transmembrane BAX inhibitor motif containing 4
CLL	chronic lymphocytic leukemia
CM	cutaneous mastocytosis
CML	chronic myelogenous leukemia
CMML	chronic myelomonocytic leukemia
DMSO	dimethyl sulfoxide
EGFR	epidermal growth factor receptor
EMA	European Medicines Agency
EML4-ALK	echinoderm microtubule associated protein like 4 – anaplastic lymphoma kinase
ERBB2	Erb-B2 receptor tyrosine kinase 2
FBS	fetal bovine serum
Fc	crystallisable fragments
FDA	US Food and Drugs Administration
FFPE	formalin-fixed and paraffin-embedded
FID	fluorescent intercalator displacement
FLT3	Fms-related tyrosine kinase 3
FNA	fine needle aspirate
G4	G-quadruplex
GAPDH	glyceraldehyde-3-phosphate dehydrogenase
GIST	gastrointestinal stromal tumor
GOLGA1	the Golgin A1
HAD	heterocyclic diamidines
HLA	human leukocyte antigen
HNSCC	head and neck squamous cell carcinomas
HPRT1	hypoxanthine phosphoribosyltransferase 1
IC_{50}	half maximal inhibitory concentration
ICGs	internal control genes
IDH1	isocitrate dehydrogenases 1
IDH2	isocitrate dehydrogenases 2
IFNα	interferon alpha

ITD	internal tandem duplication
JAK/STAT	Janus kinase/signal transducers and activators of transcription
JAK2	Janus kinase 2 alias
JM	juxtamembrane domain
KD	kinase domain
KIT1	c-KIT G-quadruplex sequence 1
KIT2	c-KIT G-quadruplex sequence 2
KRAS	Kirsten rat sarcoma viral oncogene homolog
MAPK	mitogen activated protein kinase
MC	mast cells
MCT	mast cell tumor
MDR1/P-gp	P-glycoprotein
MDS	myelodysplastic syndromes
MET	MET proto-oncogene, Receptor Tyrosine Kinase
MPNs	myeloproliferative neoplasms
MTD	maximum tolerated dose
MYC	v-myc avian myelocytomatosis viral oncogene homolog
NCOA3	nuclear receptor coactivator 3
NDI	naphthalene diimide
NHL	non-Hodgkin lymphoma
NRAS	neuroblastoma RAS viral oncogene homolog
NSCLC	non-small cell lung carcinomas
P1GF	placenta growth factor
PDGFA	platelet-derived growth factor alpha polypeptide
PDGFRα	platelet-derived growth factor receptor alpha
PDGFRβ	platelet-derived growth factor receptor beta
Ph	Philadelphia chromosome
Phen	phenantroline
qPCR	quantitative polymerase chain reaction
RAF	Raf proto-oncogene, serine/threonine kinase
RET	Ret proto-oncogene
RQ	relative quantification
RTK	receptor tyrosine kinase
SCF	stem cell factor
SD	standard deviation
SF3B1	the splicing factor 3b subunit 1
SFK	Src family kinase
SM	systemic mastocytosis
SNPs	single nucleotide polymorphisms
SPR	surface plasmon resonance
SRSF2	the serine/arginine-rich splicing factor 2
ß2M	beta-2-microglobulin
TERT	telomerase reverse transcriptase
TET2	methylcytosine dioxygenase 2
TIE2	TEK tyrosine kinase, endothelial
TKIs	tyrosine kinase inhibitors
TO	thiazole orange
TRKB	neurotrophic tyrosine kinase receptor
UPL	universal probe library
VEGF-A	vascular endothelial growth factor A
VEGFR-1	VEGF receptors 1
VEGFR-2	VEGF receptors 2
WHO	World Health Organization
WT	wild-type

1. GENERAL INTRODUCTION

1.1 CANCER TARGETED THERAPY

In developed countries, cancer is a leading cause of death mainly associated with population ageing and lifestyle, with 14.1 million of new cases and 8.2 million of deaths worldwide in 2012. Despite this, early diagnosis, universal access to health cares and the development of even more innovative therapies resulted in a significant improvement of cancer survival (Urruticoechea et al., 2010).

Among the therapeutic strategies, surgery is the oldest and remains an effective treatment for localized primary tumors and associated regional lymphatics (Urruticoechea et al., 2010).

The advent of radiation therapy (1920s) and chemotherapy (1940s) permitted the cure and the control of the metastatic processes but, in contrast to surgery, they are efficient only against a fraction of tumor cells by each treatment. For these reasons, the three processes are complementary: as an example, radiotherapy protocols are today used pre- and post-surgery in a number of tumor locations such as rectal and esophageal carcinomas or breast and central nervous system tumors. Also intraoperative radiation therapy, consisting in the delivery of a single large fraction during surgery with either electrons or low energy photons, is occasionally used. Chemo- and radiotherapy combined approaches (the administration of chemotherapy prior to, during or following radiotherapy) have been shown to improve local control and eradicate micro-metastatic disease (Urruticoechea et al., 2010).

For more than 50 years, the systemic therapy of cancer has been dominated by the use of cytotoxic chemotherapeutics. Most of these drugs are designed to kill or rapidly inhibit all dividing cells through the creation of DNA-damages. They are administered either in single doses or in short courses of therapy at the "Maximum Tolerated Dose" (MTD), which means the highest administrable doses without no life-threatening toxicity levels (Schrama et al., 2006). Owing to the high doses of these anticancer drugs, a wide treatment-free period is needed to permit normal host cells recovery. Moreover, it is nowadays clear that the genetic instability and high mutation rate of cancer cells resulting from chemotherapy carries a high risk of selection for drug-resistant cell clones (Urruticoechea et al., 2010).

The concept of tumor heterogeneity refers to the existence of cell subpopulations harboring distinct phenotypic profiles resulting from the integration, within and between tumors (intra- and inter-tumor heterogeneity), of both genetic and non-genetic influences (Huang et al., 2014). In this sense, the past decade has borne witness to a transformation in cancer treatment options. The elucidation of the molecular basis of cellular transformation, the concept that cancer is a genetic disease of somatic cells and that these genetic and epigenetic alterations underlie an aberrant transcription program has created a novel framework actually changing the clinical practice (Abou-Jawde et al., 2003). Furthermore, the realization that cancer cells need a microenvironment (i.e. fibroblasts, vessels, macrophages, lymphocytes, etc.) to survive and fully display their phenotype opened the door to new therapeutic strategies termed as 'targeted therapy'. The new targets included signaling molecules, cell-cycle proteins, apoptosis modulators, growth factors, and molecules promoting angiogenesis. Although each cancer seems to have its own pattern of signature mutations, some common aberrations in signaling appear in several tumors. These looked as interesting targets for drug development and have changed the concept of therapy (Urruticoechea et al., 2010).

Three main classes of targeted therapies are now routinely employed in a clinical setting: monoclonal antibodies, small molecule inhibitors and fusion proteins (Tobin et al., 2015). The first example of antibody used to cure cancer was trastuzumab (Herceptin®, Genentech) approved in 1998 as a second line treatment for metastatic breast cancer (Nahta et al., 2006; Huang et al., 2014). It is directed against the extracellular domain of the transmembrane Erb-B2 Receptor Tyrosine Kinase 2 (*ERBB2*), which is overexpressed in 20-30% of breast cancer. This high expression is relatively homogeneous among *ERBB2*+ tumor cells, both in the primary tumor and metastatic sites, suggesting for its effectiveness in all disease locations and against most of cancer cells (Nahta et al., 2006). Trastuzumab is generally well tolerated but some infusion-related reactions are likely to occur, including fever, rigors, chills, nausea, dyspnea and hypotension. A cardiac toxicity was the most problematic adverse event ever noted in combination chemotherapy trials (trastuzumab plus standard chemotherapy; Stern and Herrmann, 2005).

The use of the monoclonal chimeric IgG1 antibody IDEC-C2B8, also called Rituximab (Rituxan or MabThera or Zytux, distributed by different brands),

permitted the successful treatment of single patients with non-Hodgkin lymphoma (NHL). The antibody recognizes and binds the CD20 antigen, a transmembrane phosphoprotein essential for B-lymphocytes differentiation and proliferation. Rituximab does not severely compromise the immunity of the patience since immature precursor cells and the other components of the immune system do not possess CD20 (Adams and Weiner, 2005; Stern and Herrmann, 2005). Therefore, despite B-lymphopenia, rituximab has only infusion related toxicity.

The bevacizumab (Avastin®, Genentech, Roche) is a monoclonal antibody that binds and neutralizes all the human vascular endothelial growth factor A (VEGF-A) isoforms. Firstly approved in 2004, it is used in combination with standard chemotherapy for metastatic colon cancer. It is used for treatment of other types of metastatic cancers as certain lung cancers, renal cancers, ovarian cancers, and glioblastoma multiforme of the brain. It acts inhibiting the growth and proliferation of blood vessels, which are part of the body's normal healing and maintenance. In this sense, the main side effects are hypertension and increased risk of bleeding.

One example of fusion protein used against cancer is constituted by Aflibercept (VEGF-Trap; ziv-aflibercept; Zaltrap, Sanofi-Aventis SpA), an intravenously administered recombinant protein, designed to block angiogenesis promoters. Aflibercept is a fully human, recombinant fusion protein acting as a soluble decoy for VEGF receptor. It is formed by the second and the third extracellular binding domains of human VEGF receptors 1 and 2 (VEGFR-1 and VEGFR-2) fused to the crystallisable fragments (Fc) portion of a human immunoglobulin G1. Aflibercept binds to VEGF-A, VEGF-B and to the placenta growth factor (P1GF) to form a stable inert complex; this latter prevents them from binding to their appropriate receptors (Weidle et al., 2012; Syed and McKeage, 2015).

Another molecular target for new therapeutic strategies is constituted by the apoptosis pathway. Apoptosis is one of the major mechanisms of cell death in response to cancer therapies. Modifications in susceptibility to apoptosis by tumor cells not only contribute to neoplastic development, but also can enhance resistance to conventional anticancer therapies (Kang and Reynolds, 2009). The first agent targeting the B-Cell CLL/Lymphoma 2 (*BCL2*) that entered in clinical trials was a *BCL2* antisense oligonucleotide (oblimersen sodium), which has shown chemo-sensitizing effects when combined with conventional chemotherapy in chronic lymphocytic leukemia (CLL) patients, thereby improving survival (Kang and

Reynolds, 2009). More recent advances include the discovery of small molecule inhibitors of the B-cell lymphoma 2 (Bcl-2) family proteins, and three of them have entered clinical trials (gossypol, ABT-737, GX 15-070; Kang and Reynolds, 2009; Fulda, 2015). They are designed to bind the hydrophobic groove of anti-apoptotic Bcl-2 proteins in place of BH3-only proteins (i.e., BH3-mimetics). They can bind Bax or Bak, which can subsequently depolarize mitochondrial membrane potential, favor the cytochrome c release, begin caspase cascade and, consequently, activate apoptosis.

The Figure 1 reassume the most common examples of targeted therapies.

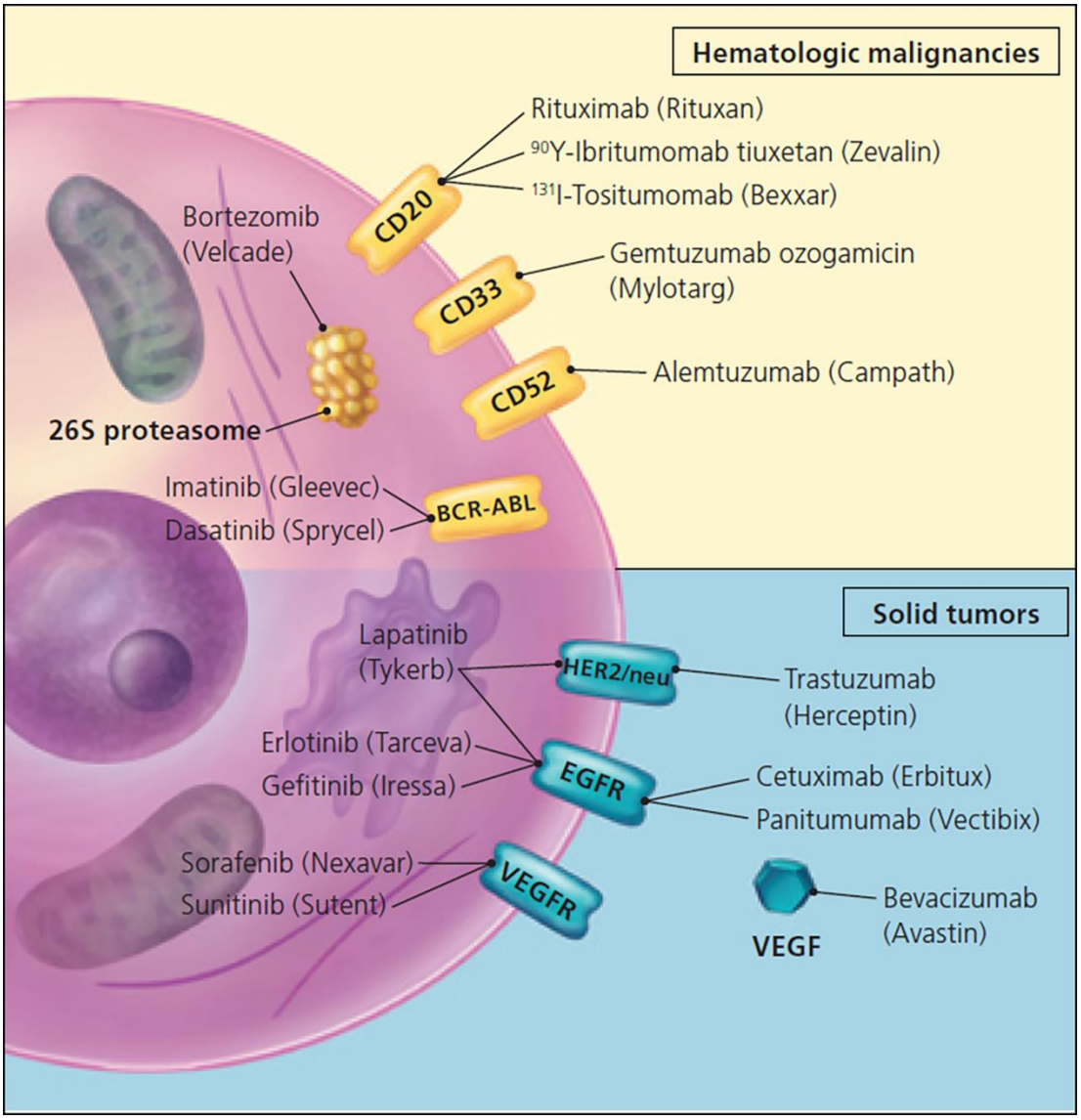

Figure 1. *Mechanisms of targeted therapy. Some drugs (e.g., sorafenib [Nexavar], sunitinib [Sutent], imatinib [Gleevec], dasatinib [Sprycel]) have multiple targets, most of which are not indicated (CD=cluster of differentiation; BCR-ABL= breakpoint cluster region-Abelson; EGFR = epithelial growth factor receptor; VEGFR = vascular endothelial growth*

factor receptor; VEGF = vascular endothelial growth factor). Modified from: Gerber, 2008.

1.2 RECEPTOR TYROSINE KINASE

Tyrosine kinases catalyze the transfer of the γ phosphate group from adenosine triphosphate (ATP) to target proteins. They can be classified either as receptor tyrosine kinases (RTKs) or non-receptor protein kinases (Arora and Scholar, 2005).

RTKs are transmembrane receptors for extracellular signaling molecules, including growth factors and hormones. The typical RTK structure consists of an extracellular ligand-binding domain, a regulatory transmembrane region, and a cytoplasmic kinase domain (KD) that becomes phosphorylated on tyrosine residues upon dimerization or oligomerization (Lemmon and Schlessinger 2010). Once phosphorylated, RTKs recruit adaptor proteins to cause a cascade of protein interactions among intracellular effectors that eventually result in altered gene expression and protein functions. Some examples of these downstream effectors include small GTP kinases (RAS proteins), members of the mitogen activated protein kinase (MAPK) family, phosphoinositide 3-kinases (PI3K) and Janus kinase/signal transducers and activators of transcription (JAK/STAT) proteins. Overall, these proteins regulate critical cellular processes such as cell metabolism, survival, proliferation, differentiation as well as cell–cell communication. Since these processes are essential for cell maintenance and division, it is not surprising that dysregulation of RTKs, or their down-stream effectors, is considered a "driver event" in a wide range of cancers (Sun and Bernards, 2014).

There are approximately 60 receptor tyrosine kinases identified so far, and these ones are divided into around 20 subfamilies defined by the receptor and/or their ligand (Arora and Scholar, 2005). Some examples of RTKs are represented by *c-KIT* or the platelet-derived growth factor receptor alpha (*PDGFRα*) and beta (*PDGFRβ*).

1.3 TYROSINE KINASE INHIBITORS

Small molecule tyrosine kinase inhibitors (TKIs) actually represent a major class of cancer targeted therapeutics.

Their small size (usually <500 Da) allows them to translocate through the plasma membrane and interact with the cytoplasmic domain of cell-surface receptors,

competing with adenosine triphosphate (ATP) for the binding site and, thereby, inhibiting the kinase activity.

In 2000, imatinib mesylate (IM, STI-571 or Gleevec) was introduced for the treatment of chronic myelogenous leukemia (CML; Arora and Scholar, 2005). In over 90% of human patients with CML, and approximately 15-30% of adult patients with acute lymphoblastic leukemia (ALL), the t(9;22) translocation or Philadelphia chromosome (Ph) is a characteristic cytogenetic abnormality. This defect results in the formation of the *BCR-ABL* oncogene by fusing the breakpoint cluster region *(BCR)* on chromosome 22 with the tyrosine kinase Abelson murine leukemia viral oncogene homolog 1 *(ABL)* located on chromosome 9 (An et al., 2010). The fusion protein interacts with multiple downstream signaling pathways mediating the development and maintenance of CML, resulting in altered cellular adhesion, activation of mitogenic signaling, inhibition of apoptosis, and defective DNA repair. Imatinib is the first BCR-ABL tyrosine kinase inhibitor (An et al., 2010) and its mechanism of action is showed in Figure 2 (Deininger and Druker, 2003).

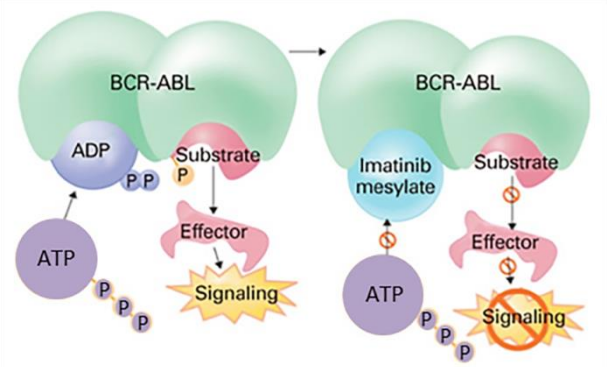

***Figure 2**. Imatinib binding on BCR-ABL. ADP= adenosine diphosphate; ATP= adenosine triphosphate; P= phosphate. Modified from http://kohnpharmaceuticals.weebly.com/biochemical-pathways.html.*

Besides BCR-ABL, imatinib also inhibits c-kit and pdgfr tyrosine kinases in gastrointestinal stromal tumor (GIST; Hirota et al., 1998). Most GIST carry *c-KIT* mutations associated with constitutive activation and receptor phosphorylation. Several clinical trials have shown a significant response to imatinib in more than half

the patients with advanced GISTs; those with mutations in the exon 11 of c-*KIT* had the best response, whereas the few patients without either c-*KIT* or *PDGFRα* mutations were not responsive. Imatinib is now approved for the treatment of patients with *c-KIT*-positive unresectable and/or malignant GISTs (Krause and Van Etten, 2005; Antonescu, 2011).

Other FDA (US Food and Drugs Administration) approved TKIs and their cellular targets are reported in Table 1.

Inhibitor	**Trade Name**	**Target**	**Cancer Type**
Imatinib masylate	Gleevec	ABL, c-KIT, PDGFR	Ph+ CML, GISTs, ALL
Dasatinib	Sprycel	SFK, ABL	CML, ALL
Nilotinib	Tasigna	ABL	CML
Bosutinib	Bosulif	SFK, ABL	CML
Gefitinib	Iressa	EGFR	NSCLC
Erlotinib	Tarceva	EGFR	Lung
Lapatinib	Tykerb	EGFR, ERBB2	Breast, others
Vandetanib	Caprelsa	EGFR, VEGFR, RET	Medullary tryroid
Crizotinib	Xalkori	EML4-ALK	NSCLC
Sunitinib	Sutent	VEGFR, PDGFR, c-KIT, FLT3	GIST, renal
Sorafenib	Nexavar	B-Raf, VEGFR, PDGFR	Renal, hepatocellular, prostate
Pazopanib	Votrient	VEGFR, c-KIT, PDGFR	Renal: soft tissue sarcoma
Regorafenib	Stivarga	VEGFR, TIE2, PDGFR, RET, c-KIT, RAF	Colorectal
Cabozantinib	Cometriq	VEGFR, RET, MET, TRKB, TIE2	Medullary thyroid

Table 1: FDA approved tyrosine kinase inhibitors used for treatment of cancer. SFK= Src family kinase; EGFR= human epidermal growth factor receptor; ERBB2*= Erb-B2 Receptor Tyrosine Kinase 2; RET= Ret proto-oncogene; EML4-ALK= echinoderm microtubule associated protein like 4 – anaplastic lymphoma kinase; FLT3= Fms-related tyrosine kinase 3; BRAF= B-Raf Proto-Oncogene, Serine/Threonine Kinase; TIE2= TEK tyrosine kinase, endothelial; RAF= Raf Proto-Oncogene, Serine/Threonine Kinase; MET = MET Proto-Oncogene, Receptor Tyrosine Kinase; TRKB = Neurotrophic Tyrosine Kinase, Receptor, Type 2. From Miller et al., 2013.*

Gefinitib and erlotinib are other TKIs acting as anti-epithelial growth factor receptor (*EGFR*) drugs in non-small cell lung carcinomas (NSCLC) and head and neck squamous cell carcinomas (HNSCC).

1.3.1 LIMITS AND SECOND GENERATION TKIs

Targeted cancer therapies are less toxic than conventional chemotherapy because they are specific for tumor cells. However, some toxic effects of TK-targeted therapies may be related to inhibition of tyrosine kinase in normal tissues. Defects in cell-mediated immunity have been reported in patients with imatinib-treated CML

and may be a consequence of blockade of c-ABL signaling in T-lymphocytes (Krause et al., 2005).

Other clinical and *in vitro* evidences showed that cells treated with TKIs tend to acquire genetic modifications resulting in resistance to these agents. Up to now, more than 100 mutations have been described affecting more than 70 amino acids and causing resistance by heterogeneous molecular mechanisms. The most common and prevalent mechanism leading to resistance to TKIs therapy is the occurrence of point mutations within the KD, which decrease the affinity of the TKI to the receptor binding domain. Other mutations may affect the binding site, resulting in extensive conformational changes, which impede TKIs bond through steric hindrance.

Around 30% of patients with CML interrupt Imatinib therapy due to intolerance and resistance. Only the T315I mutation (resulting in the substitution of Ile with Thr at the position 315) is responsible for 14% of reported cases. In CML, there are several second-generation ABL kinase inhibitors (i.e. nilotinib and dasatinib) showing increased potency and effectiveness against most of imatinib-resistant BCR-ABL mutants (Weisberg et al., 2007).

Secondary mutations in exon 14 of c-*KIT* and in its exon 17 (activation loop: D816V/H, D820Y, N822Y/K, Y823D), as well as in exon 14 of *PDGFRα* (D842V, ATP binding site: T670I) confer imatinib and sunitinib-resistance in GIST (Chen and Fu, 2011). Sunitinib is a new TKI that exerts its effects on various TKs such as *VEGFR*, *c-KIT*, and *PDGFR* and shows a broad-spectrum antitumor activity by inhibiting both tumor proliferation and angiogenesis.

Although the precise mechanisms behind the incoming of these new alterations are not very clear, one evidence for these phenomena is that specific TKI treatments help tumor to select a preexisting cell population, which has a selective advantage in a sort of striking analogy to a bacterial culture treated with an antibiotic. In addition, TKIs increase patients' genetic instability that promotes the acquisition of new mutations (Chen and Fu, 2011).

Other well-defined mechanisms of resistance in patients are represented by the overexpression of genes, increments in protein level and activation of alternative survival pathways (Deininger and Druker, 2003). About this latter mechanism, *MET* amplification in *EGFR*-mutants NSCLC represents the strongest evidence that cells treated with TKIs tend to undertake new strategies to overcome the inhibition. The activation of *MET*, a transmembrane RTK acting as an hepatocytes growth factor

(HGF) receptor, leads to sustained activation of the PI3K/AKT signaling pathway, bypassing the inhibition of *EGFR* conferred by TKIs (Stewart et al., 2015).

For the antiangiogenic agents (e.g., semaxinib, etc.), there may be additional explanations for the poor responses obtained against cancers up to date. VEGF is thought to be the most potent direct-acting stimulatory regulator of angiogenesis, and its expression is excessive in human cancers; however, there are a myriad of stimulatory and inhibitory factors involved in angiogenesis; some of these are produced by tumor cells, whilst others are produced by host cells. In addition, for each angiogenic factor, multiple regulatory factors and signaling pathways exist. With all this redundancy, inhibiting one factor or one pathway is often not sufficient to inhibit tumor growth. Furthermore, some factors such as VEGF, exist in multiple isoforms, contributing to the difficulty of inhibiting the angiogenic process (Arora and Scholar, 2005).

Finally, in tumor cell lines, multidrug resistance (MDR) is often associated with an ATP-dependent decrease in cellular drug accumulation, which is usually attributed to the overexpression of certain ATP-binding cassette (ABC) transporter proteins. Among ABC-transporters, the overexpression of P-glycoprotein (MDR1/P-gp/ABCB1) and the breast cancer resistance protein (BCRP/ABCG2) confer resistance to imatinib in CML or gefitinib in NSCLN. Further investigations indicated that imatinib, gefitinib, tandutinib, dasatinib, sunitinib and sorafenib are high-affinity substrates of MDR1 and ABCG2 (Ozvegy-Laczka et al., 2005). Collectively, the chemo-immune system seems to recognize targeted TKIs as xenobiotics at the membrane barriers and, in case of active extrusion, protects intracellular targets from the action of the TKIs (Chen and Fu, 2011). These findings suggest that overexpression of ABC-transporters protects tumor cells from TKIs inhibition activity contributing to their pharmacokinetics and pharmacodynamics.

1.4 c-KIT

The *v-kit* oncogene was identified in 1986 in the Hardy-Zuckerman 4 feline sarcoma virus (Besmer et al., 1986), and its human homolog *c-KIT* in 1987 (Yarden et al., 1987). It is located on chromosome segment 4q11 of the human's genome and in the chromosome 13 of dog's genome (Reimann-Berg et al., 2012). In both species, it consists of 21 exons spanning more than 34 kb of DNA. The first exon encodes the

translational initiation codon and the signal peptide. The RTK encoded by the *KIT* gene is a transmembrane protein where exons 2-9 code for the extracellular domain, the transmembrane region is encoded by exon 10, while the remaining exons encode for the intracellular part of the receptor.

The promoter region of murine and human *c-KIT* has been thoroughly investigated (Yamamoto et al., 1993; Maeda et al., 2010). It includes binding sites for AP-2, basic helix-loop-helix proteins, Sp1, Ets, and Myb. Park et al. in 1998, demonstrated the importance of Sp1 for maximal activity of the *c-KIT* promoter, while loss of AP-2 expression caused loss of c-kit expression in malignant melanocytes (Huang et al., 1998). Finally, the basic helix-loop-helix microphthalmia associated transcription factor (MITF) binds to a CACCTG motif and regulates *c-KIT* expression in mast cells (MC) and melanocytes (Huang et al., 1998).

The c-kit ligand is constituted by the stem cell factor (SCF, also called Steel factor or Kit ligand), a growth factor expressed by fibroblasts and endothelial cells; this ligand promotes proliferation, migration, survival, and differentiation of hematopoietic progenitors, melanocytes, and germ cells. It maps to chromosome 12 and 15 in humans and dog genomes, respectively. Both membrane-bound and soluble SCF binds to c-kit and activate its intrinsic tyrosine kinase activity.

The c-kit protein is a member of the class III of RTKs and it consists of 976 amino acids, representing the core protein (110 kDa). Heterogeneous *N*-linked glycosylation results in a mature protein of between 145 and 160 kDa. It is formed by an extracellular part composed of five immunoglobulin-like domains, followed by a single spanning transmembrane region. The intracellular part of c-kit starts with the juxtamembrane domain (JM), a region of great importance for the regulation of c-kit kinase activity and the KD (Lennartsson and Rönnstrand, 2012).

The c-kit activation process mediated by SCF is summarized in Figure 3. In cell membrane, c-kit is diffused as monomer. Each SCF molecule can bind to one c-kit molecule through contacts with the first three Ig-like domains (D1-D2-D3) of the receptor's extracellular region, which have a complementary shape and charge to allow tight binding of SCF (Lemmon and Schlessinger, 2010; Lennartsson and Rönnstrand, 2012). When association with the SCF takes place in two c-kit monomers, their D1-D2-D3 regions are kept structurally unaltered but the two receptors are drawn closer to each other to form a dimer, leading to a reorientation on D4 and D5 (Lemmon and Schlessinger, 2010). Through homotypic interactions

between D4 and D5 across the dimer interface, the transmembrane regions and the intracellular tyrosine KDs get closer to each other, enabling their activation and transphosphorylation along the receptor. These mechanisms leads to initiation of downstream signal transduction.

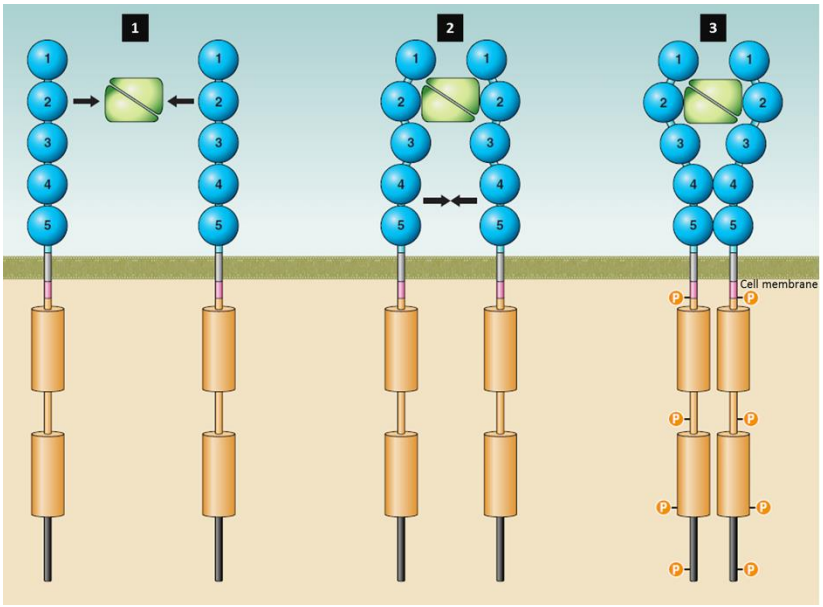

***Figure 3**. Representation of SCF-mediated c-KIT activation. (1) The stem cell factor (SCF) interact, at cell membrane level, with c-KIT Ig-like domains 1-3 of two monomers. (2) The SCF binding drive the two monomers close to each other and favored their interactions between Ig-domains 4 and 5. (3) c-kit homodimer allows for efficient trans-phosphorylation in the juxtamembrane region (Tyr568 and 570), kinase insert region (Tyr703, 721, 730, and 747), kinase domain (Tyr823 and 900) (by Src kinases), and COOH-terminal tail (Tyr936). Modified from Lennartsson and Rönnstrand, 2012.*

The expression pattern of *c-KIT* and *SCF* during mouse embryogenesis suggested that they are involved in migration of cells of the hematopoietic, germ cell, and melanoblast lineages as well as in the differentiation and proliferation of these cells. c-*KIT* expression is down-regulated upon differentiation of hematopoietic progenitors into mature cells of all lineages, except MC, which retain high levels of cell surface c-kit expression (Maeda et al., 2010).

1.5 HUMAN *c-KIT* MUTATIONS AND RELATED DISEASES

The oncogenic *c-KIT* mutations found in neoplasms are gain-of-function mutations resulting in ligand-independent tyrosine kinase activity and consequent ligand-independent proliferation, differentiation and survival of the affected cells.

Dysregulation of *c-KIT* activity plays a central role in the pathogenesis of those malignancies originated from cells dependent on SCF for differentiation/survival, such as MC and Cajal interstitial cells. These include MC proliferative disorders, GIST, melanoma, and acute myeloid leukemia (AML). Increased expression of normal *c-KIT* may also contribute to tumorigenesis in solid lung cancers from small lung cells that constitutively do not express c-*KIT* but are exposed to environments rich in SCF (Cruse et al., 2014).

Gastrointestinal stromal tumors derive from Cajal interstitial cells and multiple activating mutations, involving *c-KIT* exons 8, 11, 13 or 17, have been reported in up to 80% of cases (Corless et al., 2011).

Likewise, approximately 90% of adults with diseases characterized by an abnormal MC proliferation (mastocytosis) have, at least, a point mutation consisting of a substitution of Aspartic acid to Valine in the catalytic domain of c-KIT (D816V) rendering it constitutively active (Arock et al., 2015). The reasons behind the prevalence of exon 17 mutations in hematological malignancies compared to those in exon 11 in GISTs are still unknown. Activating mutations in JM alter the suppressive control effect of this region on the activity of the receptor, while those in the KD are catalytic in nature. Mutations occurring on other exons, such as 8, 9 and 10, coding either for the extracellular domain (8 and 9) than for the RTK transmembrane domain (10), have been described in AML (Malaise et al., 2009), GISTs (Corless et al., 2011) and in childhood patients with mastocytosis, albeit their incidence result much lower (Cruse et al, 2014).

1.5.1 MASTOCYTOSIS

Mastocytosis results from a clonal, neoplastic proliferation of morphologically and immunophenotypically abnormal MC that accumulate in one or more organ systems. It was considered one of eight subcategories of myeloproliferative neoplasms (MPN) in World Health Organization (WHO) classification of tumors of hematopoietic and lymphoid tissues (WHO, 2008).

The clinical presentation of mastocytosis is quite heterogeneous; a skin-limited disease, peculiar in pediatric patients, in which it occurs within the first 2 years of

life, and that commonly results in a spontaneous regression of skin lesions (cutaneous mastocytosis, CM); alternatively, a more aggressive variant with extra-cutaneous involvement, generally seen in adult patients, that may be associated with multi-organ dysfunction/failure and shortened survival (systemic mastocytosis, SM; Arock et al., 2015).

The gold standard for diagnosis, according to WHO criteria, is the presence of multifocal clusters of morphologically abnormal MC in the bone marrow. Minor diagnostic criteria include elevated serum tryptase level, abnormal MC expression of CD25 and/or CD2, and presence of KIT D816V mutation. In 2008, the WHO recognized seven mastocytosis categories, listed in Table 2.

Variant	**Subvariant**
Cutaneous mastocytosis (CM)	Urticaria pigmentosa (UP), maculopapular CM (MPCM), diffuse CM (DCM), mastocytoma of skin
Indolent systemic mastocytosis (ISM)	Smoldering SM, isolated bone marrow mastocytosis
Systemic mastocytosis with an associated clonal hematologic non-mast cell lineage (SM-AHNMD)	SM–acute myeloid leukemia (SM-AML), SM-myelodysplastic syndrome (SM-MDS), SM- myeloproliferative disorders (SM-MPD), SM- Chronic Myelomonocytic Leukemia (SM-CMML), SM- Non-Hodgkin's Lymphoma (SM-NHL).
Aggressive systemic mastocytosis (ASM)	
Mast cell leukemia (MCL)	Aleukemic MCL
Mast cell sarcoma	
Extracutaneous mastocytoma	

Table 2. *WHO systemic mastocytosis variants. From Metcalfe et al., 2008.*

Current therapy in WHO-defined SM is largely palliative and directed against MC degranulation symptoms (e.g. urticarial, angioedema, nausea, vomiting, diarrhea, abdominal pain), symptomatic skin disease (e.g. urticaria pigmentosa) and/or organ dysfunction resulting from MC tissue infiltration (e.g. hypersplenism; Pardanani, 2015).

Among other types of treatments for SM there are cytoreductive agents as interferon-α (IFNα) and 2 chlorodeoxyadenosine (2-Cda). The IFNα acts against all SM subcategories, and improve dermatological, hematological, gastrointestinal, and systemic symptoms associated with histamine release. Imatinib mesylate demonstrates *in vitro* efficacy against wild-type c-*KIT* and certain transmembrane (F522C) and juxta-membrane (V560G) mutations, but not on D816V mutants. New TKIs are currently under investigation for SM treatment and are represented by dasatinib and midostaurin (PKC412). However, treatment of advanced SM remains one of the most challenging areas in clinical hematology; in fact, whereas mediator-related symptoms can be controlled in most cases, MC expansion is usually resistant to most conventional antineoplastic drugs (Valent et al., 2010; Pardanani, 2015).

1.6 CANINE *c-KIT* MUTATIONS AND RELATED DISEASES

In dog MCTs, several c-*KIT* mutations, leading to uncontrolled signaling, have been identified (Bavcar & Argyle, 2012). These mutations are similar to those found in human GIST (Marech et al., 2014).

Approximately 10-30% of canine MCTs present *KIT* mutations, more frequently localized in the JM (exon 11), and mostly consisting of internal tandem duplications (ITDs: Marech et al., 2014; Bonkobara, 2015). Mutations in the extracellular domain, namely in D5 (exons 8 and 9) are less frequent than those found in exon 11 (Letard et al., 2008; Takeuchi et al., 2013). Finally, mutations in other exons 2, 6, 7, 15 and 17 are quite infrequent (<3%: Bonkobara, 2015).

Increased *c-KIT* mRNA levels and gene mutations occurring in exons 11 and 17 were also observed in canine AMLs (Usher et al., 2009). In addition, also canine GIST evidenced *c-KIT* mutations occurring in the JM (Frost et al., 2003).

1.6.1 CANINE MCT

MCT is one of the most common tumor occurring in dogs. It is characterized by an abnormal MC accumulation in tissues, and mostly it appears as a solitary non-painful cutaneous mass with preferred localization in the head/neck and in the arts. Systemic symptoms, such as anorexia, erythema, abdominal discomfort, edema, gastrointestinal ulceration, vomiting, and melena, are less common; these ones are frequently associated with visceral forms of MCT with a poorer prognosis and/or

with paraneoplastic disease due to the release of bioactive constituents from MC granules (Welle et al., 2008; Blackwood et al., 2012).

The MCT clinical presentation varies according to the tumor grade: well-differentiated cutaneous MCTs consist of slow growing, hairless and solitary lesions, while poorly differentiated cutaneous MCTs are characterized by rapid growing, ulcerated and pruritic lesions, sometimes surrounded by small "satellite lesions" (Blackwood et al., 2012).

Upon the suspicion of a MCT, the definitive diagnosis can be achieved through cytology examination, for the most part using fine needle aspirate (FNA). Histological examination is also an important tool for MCTs grading and prognosis (Sabattini et al., 2015). Various histological grading systems have been proposed, but the mostly used one is the classification proposed by Patnaik et al. (1984), which divides MCTs into three grades: grade I MCTs (well-differentiated), which are mostly benign and slowly developed; grade III MCTs (poorly differentiated) that exhibit aggressive growth with local invasion. They are also more prone to metastasize and show a high recurrence potential. Finally, grade II (intermediately differentiated) MCTs; these latter are more difficult to predict, thereby accounting for more subjective and inconsistent classifications (Blackwood et al., 2012; Sabattini et al., 2015). The Patnaik grading scheme has inherent weaknesses characterized by subjective criteria and inter-observer variability. In particular, this traditional and widely accepted grading system has failed to reliably differentiate between aggressive and nonaggressive grade II MCTs (Giantin et al., 2014). There is another grading system, proposed by Kiupel and co-authors (2011), which divided tumors into high or low grade MCTs. Such a classification has improved prediction of metastasis and/or new tumor development, tumor mortality and survival (Takeuchi et al., 2013; Sabattini et al., 2015).

Since histological grading alone is not suitable to predict the MCT biological behavior and treatment response, some supplementary prognostic markers have been investigated. Amon these ones, *c-KIT* mutational status has been identified as a useful prognostic and therapeutic marker. Furthermore, the expression of c-kit protein can be immunohistochemically characterized, and has been correlated with histopathological grading and prognosis in some studies, albeit not consistently (Takeuchi et al., 2013; Sailasuta et al., 2014; Patruno et al., 2014; Costa Casagrande et al., 2015). Other prognostic markers have been investigated, such as cellular

proliferation markers (e.g. mitotic index, the argyrophilic nucleolar organizer region AgNOR, the immunohistochemical markers Ki-67 and proliferating cell nuclear antigen, PCNA), angiogenesis markers and DNA ploidy analysis (Blackwood et al., 2012; Fonseca-Alves, 2015; Gil da Costa, 2015; Sabattini et al., 2015).

Complementary to histological grading, clinical staging is recommended to define the nature and extent of MCT, especially after diagnosis of a poorly differentiated tumor or when an expensive treatment is planned; this should include, at least, FNAs of draining lymph nodes and abdominal ultrasound. In cases of nodal metastasis presence, full staging is required with abdominal ultrasound (along with spleen and liver biopsies aspiration) and, if the case, bone marrow aspiration and lung radiographs (Blackwood et al., 2012). A clinical staging system was proposed by WHO: stage 0 is usually assigned to single tumors incompletely excised from the dermis without regional lymph node involvement; stages I and II comprise single tumors confined to the dermis without or with regional lymph node involvement, respectively; in stage III are included multiple dermal tumors, or large infiltrating tumors with or without regional lymph node involvement; stage IV includes any tumor with distant metastasis or recurrence with metastasis (Rogers, 2010). However, stage and prognosis do not directly correlate in all clinical situations (Blackwood et al., 2012).

The prognostic indicators outlined above serve to aid in the therapeutic approach of MCT. Surgery is the treatment of choice in localized, non-metastatic canine MCTs. Most of dogs with low to intermediate grade MCTs experience longer survival times with complete surgical excision alone if compared with high grade MCTs. During surgery, safety margins should be included all around the mass. In cases in which a surgical excision with adequate margins is not feasible and/or poor prognostic factors such as histologic intermediate to high grade MCTs are encountered, radiation therapy and/or systemic chemotherapy is indicated. Due to the risk of radiation-induced MC granulation and consequent systemic effects, radiotherapy is generally avoided as a sole therapy. It is preferentially used as a postoperative adjunctive therapy after incomplete excision. Best results are achieved where radiation is planned prior to surgery, rather than afterthought following by an inadequate surgery (Blackwood et al., 2012).

The most commonly used cytotoxic agents for the treatment of canine MCT include vinblastine (VBL) and lomustine (CCNU); in addition, systemic

corticosteroids have been shown to have some clinical efficacy. Indeed, the response rate to prednisone has been shown to be 20%, with remission times comprised between 10 and 20 weeks (London and Seguin, 2003). The use of an adjuvant systemic protocol (corticosteroids, CCNU and VBL), following surgical excision of intermediate grade MCT with evidence of local-regional lymph node metastasis, showed a median survival time of 1359 days (Lejeune et al., 2013).

Recently, two TKIs have been approved by the European Medicines Agency (EMA) for the therapy of canine MCTs:

(1) Toceranib phosphate (Palladia®, Pfizer Animal Health), approved for the use in recurrent, non-resectable grade II/III MCTs. Dogs with mutated *c-KIT* showed the highest response rate (69% against 37%: London et al., 2009).

(2) Masitinib (Masivet ®, AB Science), approved for non-resectable grade II/III MCTs, particularly those with a *c-KIT* mutation.

1.7 G-QUADRUPLEX (G4)

G4, discovered by Gellert and collaborators in 1962, are stable DNA secondary structures alternative to the double helix of Watson and Crick. The basic elements that formed a G4 are showed in Figure 4.

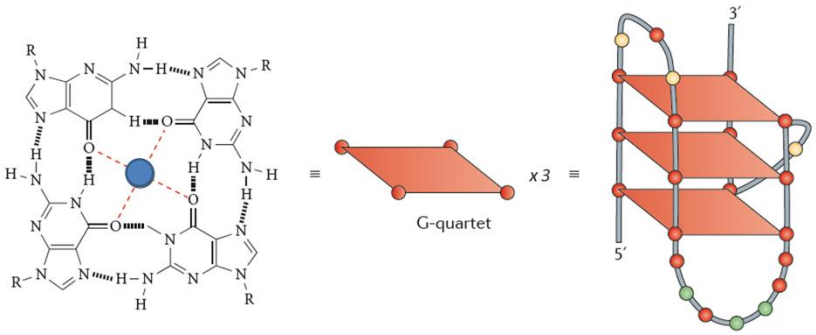

Figure 4. *The dominant G4 conformation in the B-cell lymphoma 2 (BCL-2) promoter as an example of G4 structure. Modified from Balasubramanian et al., 2011.*

G4 originate in guanine-rich nucleic acids sequences when four guanine form a square planar platform called G-tetrad through cyclic Hoogsteen hydrogen bonding, in which each of the four bases is the donor and the acceptor of two hydrogen bonds (Bryan and Baumann, 2011). Stacked G-quartets form a G4 structure, and the interpose sequences are extruded as single-strand loops (although tetra-molecular G4

structures may also lack loops). The sequence and size of the loop regions varies but are usually small (1–7 nucleotides nucleotides), and smaller loops result in more stable G4 structures, as do longer G-tracts. Spaces between the loops, termed grooves, are bounded by charged phosphodiester backbones.

This structure is stabilized by monovalent cations (mostly K^+ and Na^+) that occupy the central cavities and neutralize the electrostatic repulsion of inwardly pointing guanine oxygens (Bochman et al., 2012).

Oligonucleotides containing G-stretches can form monomeric, dimeric or tetrameric G4 by folding/assembling one, two or four separate strands (Phan, 2009). DNA strands may be oriented in anti-parallel, parallel, or hybrid configuration. G4 conformation is influenced by both the DNA sequence and the conditions used in the folding reaction, such as the nature of the stabilizing cation. Thus it is difficult to predict the propensity of a sequence to fold into a particular structure, and each sequence needs to be characterized under different folding conditions.

Also the stability of G4 varies; it depends on the identity of the stabilizing cation, the DNA length and sequence, the length of intervening loops and, finally, the strand stoichiometry and alignment. In this respect, there have been some recent progresses in developing computational methods for predicting G4 stability.

Many proteins have been shown to interact with G4 structures; these proteins may bind and stabilize G4 or unwind and destabilize them.

One of the most important G4 structures are telomeres and telomerases. Human telomeres comprise tandem repeats of the DNA motif (TTAGGG) for ~5–10 kb, together with associated telomeric proteins. The shortening of telomeres to a critical length is a signal for cellular senescence. This phenomena is counteracted by telomerase, the telomere-specific reverse transcriptase that contains the RNA template to direct the addition of telomeric DNA by the catalytic telomerase reverse transcriptase (*TERT*) component. Telomerase is upregulated in ≥85% of tumors, providing a telomere maintenance mechanism that contributes to cellular immortalization and tumor progression. Telomeric DNA can fold into compact G4 structures inhibiting the activity of telomerase. There are a large number of small-molecule ligands showing a high binding affinity for G4, and most of them cause telomere dysfunction *in vivo* and inhibit telomerase activity *in vitro* (Moye et al., 2015).

1.7.1 G-QUADRUPLEX IN PROMOTER REGIONS

The potential for G4 formation in promoter regions is largely concentrated in genes associated with cell growth and proliferation. These oncogene promoters are typically TATA-less with G-rich regions in their proximal promoters; among these ones, there are the v-myc avian myelocytomatosis viral oncogene homolog (*MYC*), *VEGF*, *BCL-2*, *PDGFRβ*, the Kirsten rat sarcoma viral oncogene homolog (*KRAS*), as well as *c-KIT* (Onel et al., 2014). Furthermore, these structures seem to be underrepresented in tumor suppressor genes (Bochman et al., 2012). These evidences suggest that G4s may play a functional role in gene regulation (Bryan and Baumann, 2011).

MYC is an oncogene most commonly found to be altered in cancer, and its promoter is the one most extensively studied in terms of G4 formation (Chen and Yang, 2012). It encodes for a transcription factor that regulates the expression of several genes (Bidzinska et al., 2013). The G4-forming region within the *MYC* promoter is a sequence of 27-nucleotides , e.g. a Nuclease Hypersensitive Element (NHE) III1, which regulates most of the gene's transcriptional activity (Chen and Yang, 2012; Onel et al., 2014). This sequence contains five consecutive runs of guanine ("G-runs"), and may fold into several G4s and loop isomers with different stabilities; the major G4 formed in K+ solution involves four consecutive 3G-runs that adopt a parallel folding (Myc2345), with the major loop isomer being 1:2:1 (Chen and Yang, 2012; Onel et al., 2014).

In *MYC*, the G4 structure is a negative regulator of the expression because a single base mutation, which destabilizes the chair form, increases *MYC* expression up to three-fold. Furthermore, compounds that stabilize this G4 structure (i.e., the cationic porphyrin TMPyP4) decrease *c-MYC* expression (Siddiqui-Jain et al., 2002; Tian et al., 2010).

Two G-rich sequences capable of forming G4s have been identified in the promotorial region of human proto-oncogene *c-KIT*: KIT1 and KIT2, respectively located -12 /-34, and -64 / -84 base pairs upstream the transcription start site (TSS: McLuckie et al., 2011). They are located within a nuclease hypersensitive region, and are separated by 31 bp which contain an active SP1 site. Both sequences form G4s under physiological conditions, as proved by NMR and X-ray crystallography (Bryan and Baumann, 2011). A large number of G4 ligands have been reported in the literature, and TMPyP4 is the ligand most extensively studied to date. It inhibits both

telomerase (half maximal inhibitory concentration, $IC_{50} \cong 0.7–10$ μM) and *Taq* DNA polymerase ($IC_{50} \cong 2$ μM). It exhibits some promising anticancer activities *in vivo*, but it has very poor DNA specificity, causes anaphase bridges in sea urchin embryos, and is highly toxic *in vivo*. When administered at 0.1 mM (a dose near its MTD in cell cultures), TMPyP4 elicits a dramatic effect on gene expression, and it down-regulates the transcription of both *c-MYC* and the catalytic subunit of telomerase. Moreover, it binds to duplex, triplex, G4, single stranded and bulk genomic DNA with similar affinities (*K*d ≅ 200 nM); therefore, it cannot be considered a structure-selective ligand.

Telomestatin (SOT-095), a natural product isolated from *Streptomyces anulatus* 3533-SV4, is one of the strongest and most specific inhibitors of telomerase reported to date ($IC_{50} \cong 1$ μM).Telomestatin has molecular dimensions similar to those of G-tetrad DNA, and can bind to various G4 with modest affinity (*K*d ≅ 30 nM). Telomestatin exhibits good selectivity for intramolecular versus intermolecular G4 structures, and it has a 70-fold lower affinity for duplex DNA. Telomestatin induces telomere shortening in treated cells more rapidly than through a single mechanism involving telomerase inhibition. Recent studies have shown that telomere uncapping and the loss of telomeric DNA is related to the competition between telomestatin and POT1, a shelterin protein that binds to the 3' single-stranded overhang (Gomez et al., 2006; Luedtke, 2009). While it is unknown if this type of activity might be cancer-selective, telomestatin induces senescence and apoptosis in a number of different tumor cell types and exhibits less toxicity towards normal progenitor cells (Luedtke, 2009).

1.7.2 G-QUADRUPLEX IN CANINE *c-KIT* PROMOTER

In 2014, part of this PhD study aimed to characterize the canine *KIT* proximal promoter. Similarly to the human *KIT* proto-oncogene, two putative quadruplex sequences were identified and reported in Figure 5: canine KIT1 ("d_kit1", -117 to 138 bp upstream the ATG), and KIT2 ("d_kit2", -154 to -174 bp upstream the ATG). Both positions were not referred to TSS, because the 5'UTR of canine *KIT* gene has not yet been fully characterized. Da Ros and co-authors published these results in the same year (Da Ros et al., 2014). Canine KIT1 showed a high degree of sequence

homology with its human counterpart and shared a common overall parallel G4 folding in a K+ containing solution (Da Ros et al., 2014).

On the other hand, human and canine KIT2 sequences largely differ to each other. Two isoforms of canine KIT2 were identified; although a defined structure has not yet been attributed, it is conceivable that the multiplicity of folded structures that human KIT2 can form in solution may also occur in the canine species (Da Ros et al., 2014).

Overall, the potential functional role of the aforementioned G4 motifs may be of important relevance, not only for the canine, but also as a comparative model for human disease (Da Ros et al., 2014).

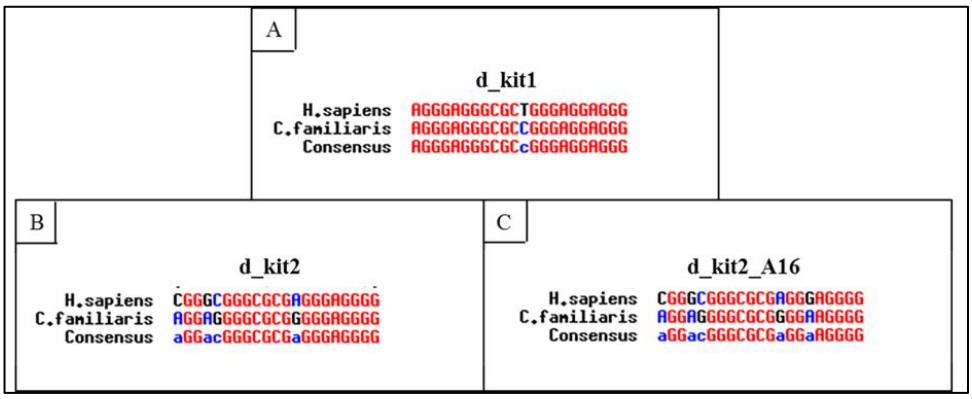

Figure 5. *Sequences involved in the formation of the two G4s present in the promoter regions of human and canine KIT (Rankin et al., 2005; Da Ros et al., 2014).*

2. AIMS OF THE THESIS

In human and canine cancer, *c-KIT* represents one of the best examples of therapeutic target, and its inhibition allows oncologists to treat tumors whose malignancy is partly or completely dependent on its activity.

The present thesis groups together four scientific contributions related to *c-KIT* expression in human and canine tumors; overall, it attempted the exploration of new strategies for anticancer chemotherapy targeting *c-KIT* in multiple *in vitro* models. In particular, the specific aim of the first part of the thesis (chapters 3 and 4) consisted in the identification of candidate *c-KIT* G4 ligands that could stabilize G4 DNA secondary structures in the *c-KIT* promoter region and, hence, block its transcription in human and canine established cell lines. These studies were conducted in collaboration with the research group of Claudia Sissi, a Full Professor affiliated to the Department of Pharmacological Sciences of the University of Padua; she performed the compounds library screening.

The other two publications (chapters 5 and 6) aimed to cover some scientific gaps in canine and comparative oncology. Precisely, in chapter 5 the characterization of *c-KIT* mutational profile in primary canine MCT and its own metastases was undertaken, to make a more careful recommendation about the use of *c-KIT* mutational analysis (and, consequently, decision therapy) in the clinical setting; in chapter 6, the occurrence of mutations in genes already known to be involved in pathogenesis of human SM (TET2, SF3B1, SRSF2, KRAS, NRAS, IDH1, IDH2) was investigated in canine MCT, to find out analogies between the two neoplastic diseases. Part of chapter 3 and the whole work discussed in chapter 6 were carried out, during my eight-months foreign internship, at the Centre de Recherche en Cancérologie de Marseille and under the supervision and support of Dr. Patrice Dubreuil and his research group.

3. Screening of candidate G-quadruplex ligands for the human *c-KIT* promotorial region and their effects in multiple *in-vitro* models

Adapted from: **Zorzan E., Da Ros S., Musetti C., Zorro Shahidian L., Ramos Coelho N.F., Bonsembiante F., Létard S., Gelain M. E., Palumbo M., Dubreuil P., Giantin M., Sissi C., and Dacasto M., 2015. Screening of candidate G-quadruplex ligands for the human *c-KIT* promotorial region and their effects in multiple *in-vitro* models. Oncotarget, under revision.**

3.1 ABSTRACT

The V-Kit Hardy-Zuckerman 4 Feline Sarcoma Viral Oncogene Homolog (c-*KIT*) encodes for a tyrosine kinase receptor (RTK) and it is implicated in the pathogenesis of gastrointestinal stromal tumors, melanoma and acute leukemia. Two guanine-rich strands within *c-KIT* promoter can fold into G-quadruplex structures (G4). In this study, an "in house" library of compounds was screened for the recognition of the two G4 regions, hypothesizing a possible down-regulation of gene expression and the consequent discovery of potentially selective anticancer drugs.

The cytotoxicity of the three most promising G4 ligands was measured in MCF7 and HGC27 cell lines, and transcriptional effects on *c-KIT* as well as on other oncogenes known to possess G4 structures in their promoters were investigated at different concentrations and times of culture. An anthraquinone derivative (AQ1) was the most effective inhibitor of *c-KIT* mRNA and protein amounts in both cell lines.

Confirmatory experiments were executed in other *in vitro* models which strictly depend on *c-KIT* for survival (α155, HMC1.2 and ROSA cell lines), and an encouraging block of cell proliferation was noticed, also in cell lines having *c-KIT* mutations.

In conclusion, AQ1 represent a promising compound for the treatment of *c-KIT*-dependent tumors, worth of further and more in depth molecular investigations.

3.2 INTRODUCTION

The *c-KIT* proto-oncogene (*c-KIT*) codes for a tyrosine kinase receptor (c-kit) that, when activated by stem cell factor (SCF) in mast cells, melanocytes, and Cajal interstitial cells, is involved in a broad range of physiological processes, including cell proliferation, migration, maturation and survival (Metcalfe, 2008; Gregory-Bryson et al., 2010).

c-KIT is dysregulated in many diseases, including cancer (Lennartsson and Rönnstrand, 2012); in neoplastic diseases, its increased expression and auto-phosphorylation allows tumor cells to develop independently from growth and survival signals (Hanahan and Weinberg 2000; Pittoni et al., 2011). Furthermore, several mutations, potentially leading to c-kit activation in the absence of SCF binding, have been reported (Liang et al., 2013). Gain of function mutations can be found in gastrointestinal stromal tumor (GIST, >90%), mast cell tumors (>70%), nasal T-cell lymphomas (>17%), seminoma/dysgerminoma (>9%) and some acute myeloid leukemia (>68%; Ashman and Griffith, 2013).

Less than fifteen years ago, tyrosine kinase inhibitors (TKIs) were approved for the treatment of human cancers overexpressing c-kit. The immediate results obtained by using TKIs were promising; nevertheless, drug-resistance phenomena have been observed for some TKIs such as imatinib (Rosenzweig, 2012). It has been hypothesized that several cellular mechanisms contribute to drug resistance; moreover, the same drug may show differential clinical responses depending on the presence of a wild type or a mutated *c-KIT* genotype (Ustun et al., 2011). To overcome this limit, the promoter region of *c-KIT* has been considered attractive as a molecular target (Rankin et al., 2005; Fernando et al., 2006). G-rich sequences are known to fold into non-canonical structures named G4. They are formed by stacked G-tetrads, each constituted by four guanines connected by a Hoogsteen-hydrogen bonds network to provide a square planar platform (Bryan and Baumann, 2011). Clusters of guanines are typically present at telomere level, however, they are also frequently found in the promoter regions of proto-oncogenes including *c-KIT*, where G4 structures have been assumed to act as regulatory elements for gene expression (Balasubramanian et al., 2011; Bryan and Baumann, 2011). Within the human *c-KIT* promoter, two guanine-rich (G-rich) sequences have been identified: KIT1 and KIT2,

occurring respectively between positions -12 and -34 bp and positions -64 and -84 bp upstream the transcription starting site (McLuckie et al., 2011).

Therefore, the idea of applying G4 targeting ligands that can induce/stabilize these non-canonical tetrahelices, is considered a novel approach in cancer treatment (Balasubramanian et al., 2011) and the goal is the identification of compounds capable of repressing target gene transcription through the stabilization of G4 structures.

Up-to-date, several small molecules that efficiently bind the G4 form of *c-KIT* have been identified. For some of them a drug-mediated inhibition of *c-KIT* expression has been confirmed: these include trisubstituted isoalloxazines, naphthalene diimide derivatives, substituted indenoisoquinolines and benzo[a]phenoxazines (Bejugam et al., 2007; Gunaratnam et al., 2009; Bejugam et al., 2010; McLuckie et al., 2011).

To further optimize the promising outcome of these derivatives, here we set up a library of "in house" available compounds and composed of derivatives which can be clustered into six different families according to their main scaffold: anthraquinone (AQ; Zagotto et al., 2011), anthracene (AN; Folini et al., 2010), phenantroline (Phen; Musetti et al., 2009; Bianco et al., 2010; Bianco et al., 2013), naphthalene diimide (NDI; Milelli et al., 2012) and heterocyclic diamidines (HAD; Nanjunda et al., 2012). Within each family of compounds, structural variations concern mostly the side chains in terms of composition or relative localization on the pharmacophore. This represents a precise choice. Indeed, upon stacking of the planar core, the side chains are available to achieve selective recognition of the G4 loops and grooves which are the structural domains that mainly define the unique conformational signature of G4s. According to this model, compounds able to drive the preferential recognition of nucleic acid structures which are structurally divergent in these portions, might be expected to modulate the affinity/selectivity towards different G4 arrangements.

Giving the purpose of the present study, the whole library has been screened against both the G-rich *c-KIT* sequences to select the most promising candidates (G4-ligands) for the suppression of *c-KIT* expression by efficient stabilization of KIT1 and/or KIT2 G4 structures. From the binding studies, three positive hits were selected and subsequently tested for cytotoxicity. Finally, their effects on *c-KIT* mRNA levels and protein expression were evaluated in different human cancer cell lines including some well-known *in vitro* models of *c-KIT*-dependent tumors.

3.3 MATERIALS AND METHODS

3.3.1 Ligands

AQ and AN derivatives were synthesized by Prof. G. Zagotto (University of Padua, Italy); NDI were synthesized by Prof. V. Tumiatti and A. Milelli (University of Bologna, Italy), HAD by Prof. D. W. Boykin (Georgia State University, USA) and Phen analogues by Prof. A. P. Krapcko (University of Vermount, USA). Stock solutions (1 mM) of each library member were prepared in dimethyl sulfoxide (DMSO, Sigma-Aldrich Co., St. Louis, USA) and stored at -20°C. For positive hits (AQ1, AQ7 and AN6), 10 mM stock solutions were prepared in DMSO and freshly diluted in culture medium the day of the experiment.

3.3.2 Fluorescence melting assay

Fluorescence melting analyses were performed with a Roche Light Cycler® 480 II (Roche Applied Science, Indianapolis, USA), using an excitation source at 488 nm and recording the fluorescence emission at 520 nm. Samples (20 µl final volume) containing 0.25 µM DNA were loaded on a 96-well plate in 10 mM LiOH pH 7.5 with H_3PO_4, containing 50 mM KCl and increasing concentrations of ligands. Samples were first heated to 95°C at a rate of 0.1°C/s, maintained at 95°C for 5 min and then annealed by cooling to 30°C at a rate of 0.1°C/s. Then samples were maintained at 30°C for 5 min before being slowly heated to 95°C (1°C/min) and annealed at a rate of 1°C/min. For the analyses with double strand oligonucleotides, the two complementary strands were annealed before ligand addition and melting acquisition. Each curve was repeated at least three times and errors were ± 0.4°C. Melting temperatures were determined from the first derivatives of the melting profiles using the Roche Light Cycler software (Roche Diagnostics, Mannheim, Germany).

3.3.3 Fluorescent Intercalator Displacement (FID) assay

FID screening assay was performed in a 96-well plate reader Victor3TM 1420 Multilabel Counter Perkin Elmer (Perkin Elmer, Waltham, USA) set at 25°C. An excitation λ of 485 nm and emission λ of 535 nm were used. Before data acquisition the 96-well plate was shaken for 2 s. In each well, 80 µl of reaction mixture containing oligonucleotide (1 µM), *Thiazole Orange (*TO, Sigma-Aldrich Co., St.

Louis, USA) (2 μM) and increasing concentrations of each compound (1-2-8 μM) in 10 mM Tris, 50 mM KCl, pH 7.5 were loaded. Fluorescence titrations were performed in a Perkin Elmer LS55 Luminescence spectrometer (Perkin Elmer, Waltham, USA) equipped with a cell holder termostated at 25°C and using an excitation wavelength of 501 nm. For FID, a solution containing 0.62 μM of target DNA and 1.24 μM of TO was added of increasing concentrations of tested compounds in 10 mM Tris, 50 mM KCl, pH 7.5. The percentage of TO displacement was calculated as TO displacement = 100 - [$(F/F_0) \times 100$], where F_0 is the fluorescence in the absence of ligand and F the fluorescence recorded at each point of titration. TO displacement was plotted as a function of compound concentration. From these plots the EC_{50} (half maximal effective concentration) was calculated. Each titration was repeated at least in triplicate.

3.3.4 Surface Plasmon Resonance (SPR)

Surface Plasmon Resonance measurements were performed on a Biacore X100 (GE Healthcare Life Sciences, Little Chalfont, United Kingdom) set up with a streptavidine-coated sensor chips prepared for use by conditioning with injections of 1 M NaCl, 50 mM NaOH in 50% isopropanol for 1 min and finally extensively washed with a 0.22 μm filtered buffer (10 mM Tris pH7.5, 50 mM KCl, 0.025% P20). Previously annealed, 5'-biotinylated oligonucleotides were then immobilized on one cell of the chip surface by flowing a 50 nM DNA solution at a 1 μl/min flow rate until the level of 400 response unit (RU) was obtained. A second cell was left blank as control. Sensorgrams were acquired using serial dilution of tested ligands in the same buffer. To avoid interference by DMSO, its concentration was kept constant and added to the running buffer too (1.7%). Compounds solutions were injected at a 25 μl/min flow rate until a constant steady-state was reached (60-200 s). After each run, a 30 s regeneration step was performed with 10 mM glycine pH 2.5 followed by a 60 s stabilization period in the running buffer. The experimental RU values were recorded at the steady state. Data were fitted according to a binding site model.

3.3.5 Polymerase stop assay

A 20 nM equimolar mixture of ^{32}P 5'-labeled primer and the human telomeric template sequence HT4-temp d[$TC_2A_2CTATGTATAC(T_2AG_3)_4ACATATCGATGA_3T_2GCTATAGTGAGTCGTA$

T_2A] was annealed in the required polymerase buffer and subsequently added of increasing tested ligand concentrations. After incubation (30 min at room temperature), 2.5 U of Taq polymerase (Thermo Scientific, Waltham, USA) and 100 µM dNTPs mixture were added to each sample and the resulting solutions were kept for 30 min at 55°C. Reaction products were resolved by gel electrophoresis (12% polyacrylamide gel with 7 M urea) in 1X TBE (89 mM Tris base, 89 mM boric acid, 2 mM Na_2EDTA). Gels were dried and resolved bands were visualized on a PhosphorImager (GE Healthcare, Little Chalfont, United Kingdom).

3.3.6 Cell cultures

The breast adenocarcinoma human cell line MCF7 (Leibniz Institute DSMZ-German Collection of Microorganisms and Cell Cultures) and the human gastric carcinoma cell line HGC27 (European Collection of Cell Cultures) were maintained in 25 or 75 cm^2 flasks under a humidified 5% CO_2 atmosphere, at 37°C. Cells were grown in Eagle's Minimal Essential Medium (EMEM, Gibco® Life Technologies, Carlsbad, USA) supplemented with 10% fetal bovine serum (Gibco® Life Technologies, Carlsbad, USA), 2 mM L-glutamine (Euroclone, Milan, Italy), 1% non-essential amino acids (Euroclone, Milan, Italy) and 1% penicillin/streptomycin (Euroclone, Milan, Italy). MCF7 were cultured in presence of 10 µg/ ml of human insulin (Elli Lilly & Co., Indianapolis, USA).

The human mast cell leukemia HMC1.2, containing both juxtamembrane and catalytic *c-KIT* domain mutations (V560G and D816V), was kindly provided by Dr. Joseph Butterfield (Mayo Clinic, Rochester, MN, USA). This cell line, as well as the human mast cell leukemia α155 (possessing only the V560G mutation), the human prostate cancer cell line PC3, the human lymphoma cell line KARPAS 299 and ROSA mast cell lines (WT and transfected with KITD816V; Saleh et al., 2014) were cultured in RPMI medium (Gibco® Life Technologies, Carlsbad, USA) supplemented with 10% FBS, 2 mM L-glutamine and 1% penicillin/streptomycin.

Cell number and viability were checked by using Trypan Blue dye exclusion test (Sigma-Aldrich Co., St. Louis, USA). For all the experiments, cells were used from passage 5 to passage 25 maximum.

Cell cultures were checked for Mycoplasma contamination both before and at the end of experiments through PCR Mycoplasma Test Kit (PromoKine, Heidelberg, Germany).

3.3.7 G4-ligands cytotoxicity

MCF7 and HCG27 cells were seeded at concentrations comprised between $0.3x10^4$ and $0.5x10^4$ cells/well in a 96-well flat bottom plate (Sarstedt Italia, Verona, Italy). After 24 hours, AQ1 or AN6 were added at concentrations from 0.01 µM up to 10 µM for 72 hours. Additional wells exposed to the vehicle (DMSO, 0.1% final concentration) and medium alone were prepared, too. At the end of the experiment, 20 µl of CellTiter-Blue® Cell Viability Assay (Alamar Blue, Promega, Madison, USA) were added to each well and the fluorescence was measured at 560 nm as excitation wavelength and 590 nm as emission wavelength, by using a VICTOR™X4 Multilabel Plate Reader (Perkin Elmer, Waltham, USA). Three separate experiments were executed and each concentration was tested in sestuplicate. For AQ7, the sulforhodamine B *(*Sigma-Aldrich Co., St. Louis, USA) assay was used as proliferation test instead of Alamar Blue. Both cell lines were exposed to a range of concentrations up to 10 µM for 0, 24, 48, 72, and 96 hours. Three separate experiments were executed, and each concentration was tested in sestuplicate.

3.3.8 Target genes constitutive expression

Since no information about the constitutive expression of *c-KIT* were available in literature, a first set of experiments were undertaken to define the best experimental settings for measuring G4-ligands efficacy.

Cells were seeded onto 6-well plates at concentration of $5x10^5$ and $4x10^5$ cells/well (for MCF7 and HGC27, respectively) and collected after 6, 24, 48, 72 and 96 hours. Monolayers were washed with 1 ml of fresh PBS, scraped off and centrifuged at 100*g* for 5 min. Cell pellets were resuspended in 0.5 ml of TRIzol®reagent (Invitrogen™, Life Technologies, Carlsbad, USA), and total RNA was extracted according to manufacturer's instructions. Nucleic acids yield and purity (260/280 and 260/230 nm absorbance ratios) were measured by using the Nanodrop ND-1000 Spectrophotometer (Nanodrop Technologies, Wilmington, UK), whilst their quality was checked by 1% agarose gel electrophoresis. Total RNA (1 µg) was reverse transcribed by using the High Capacity cDNA Reverse Transcription Kit (Life Technologies, Foster City, USA) and following the manufacturer instructions.

The full list of primers used in the present study for qPCR analysis is reported in Table 1.

Gene	UPL probe	Primers (5'- 3')	Source
MYC	#67	F : TGGTGCTCCATGAGGAGACA R : GTGGCACCTCTTGAGGACCA	Gunaratnam et al., 2009
PDGFA	#77	F: ACACGAGCAGTGTCAAGTGC R: CCTGCAGTATTCCACCTTGG	Iqbal et al., 2012
PDGFRB	#14	R: TGCTCATCTGTGAAGGCAAG F: TGGCATTGTAGAACTGCTCG	Chanakira et al., 2012
BCL2	#75	F: ATGTGTGTGGAGAGCGTCAA R: GCCGTACAGTTCCACAAAGG	Brassesco et al., 2010
B2M	#42	F: AGGCTATCCAGCGTACTCCA R: TGTCGGATGGATGAAACCCA	designed *ex novo*
GAPDH	#60	F: CTCTGCTCCTCCTGTTCGAC R: ACGACCAAATCCGTTGACTC	designed *ex novo*
HPRT1	#22	F: TGATAGATCCATTCCTATGACTGTAGA R: CAAGACATTCTTTCCAGTTAAAGTTG	designed *ex novo*
KIT	#29	F: GGCACGGTTGAATGTAAGGC R: CAGGGTGTGGGGATGGATTT	designed *ex novo*
KRAS	#62	F: GGAGCTGGTGGCGTAGGCAAG R: GCCCTCCCCAGTCCTCATGT	designed *ex novo*
hTERT	#68	F: GGAGAACAAGCTGTTTGCGG R: AGCCATACTCAGGGACACCT	designed *ex novo*

***Table 1**. Primers and probes used for the qPCR analysis either obtained from previous publications or specifically designed for this study. UPL=Universal Probe Library; F= forward; R= reverse*

Despite *c-KIT*, which is the main target of this study, we also analyzed other 6 genes known to contain putative G4 structures in their promoter region: such as the V-Myc Avian Myelocytomatosis Viral Oncogene Homolog (*MYC*), the Kirsten rat sarcoma viral oncogene homolog (*KRAS*), the b*eta*-type platelet-derived growth factor receptor (PDGFRβ), the B-cell lymphoma 2 (*BCL2*), the Platelet-Derived

Growth Factor Alpha Polypeptide (*PDGFA*) and the Telomerase Reverse Transcriptase (*hTERT*). Gene-specific primers for *MYC, PDGFA, BCL2* and *PDGFRß* were selected from previously published studies (Gunaratnam et al., 2009; Brassesco et al., 2010; Chanakira et al., 2012; Iqbal et al., 2012), and the most appropriate Universal Probe Library (UPL) probe was later determined by using the UPL Assay Design Centre web service (Roche Diagnostics, Mannheim, Germany). For the remaining genes, primers were designed *ex novo* by using the Primer3 software (*http://primer3.ut.ee/*). Assay specificity was evaluated either *in silico*, by using the BLAST tool, than experimentally by Power SYBR Green I (Life Technologies, Carlsbad, CA) amplification and melting curve analysis.

Quantitative real-time RT-PCR (qPCR) reactions (10 µl final volume) consisted of 1X LightCycler 480 Probe Master (Roche Applied Science, Indianapolis, USA), 300 or 600 nM forward and reverse primers (Eurofins MWG Operon, Ebersberg, Germany) derived from the assay set-up, 200 nM human UPL probe (Roche Applied Science, Indianapolis, USA) and 2.5 µl of 1:7.5 diluted cDNA. The analysis was performed in a LightCycler 480 Instrument (Roche Applied Science, Indianapolis, IN) using standard PCR conditions (95°C for 10 min; 45 cycles at 95°C for 10 s and at 60°C for 30 s; 40°C for 30 s). Calibration curves, using 3-fold and 4-fold serial dilutions of a cDNA pool, were performed, and corresponding values of slope, efficiency (E) and dynamic range, for each cell line, are reported in Table 2.

Gene	MCF7			HGC27		
	Slope	**Efficiency (%)**	**Dynamic range (Ct)**	**Slope**	**Efficiency (%)**	**Dynamic range (Ct)**
B2M	-3,192	105,7	18,78 - 32,06	-3,34	99,1	18,74 - 30,85
BCL2	-3,41	96,5	25,82 - 34,13	-3,27	102,2	24,90 - 33,43
GAPDH	-3,48	93,7	15,81 - 30,59	-3,28	102	16,20 - 30,64
HPRT1	-3,324	99,9	20,23 - 32,63	-3,3	101	20,96 - 33,18
KIT	-3,137	108,3	29,01 - 35,78	-3,531	92	29,58 - 39,58
KRAS	-3,34	99	21,50 - 32,28	3,352	98,8	21,30 - 32,41
MYC	-3.3	100.7	26.85 - 33.06	-3,502	93	22,47 - 30,89
PDGFA	-3,169	106,8	22,97 - 31,68	-3,18	106,3	23,87 - 33,02
PDGFRB	Not expressed			-3,36	98,4	24,84 - 32,28
hTERT	-3,11	109,2	33,24 - 38,82	-3,34	99,2	29,38 - 35,78

Table 2. *qPCR assay standard curve values for MCF7 and HGC27.*

Only qPCR assays with E (%) comprised between 90% and 110% were considered acceptable. qPCR data were analyzed with the LightCycler480 software release 1.5.0 (Roche Applied Science, Indianapolis, USA), by using the second derivative method. mRNA relative quantification was performed by using the ΔΔCt method (Livak et al., 2001). Three internal control genes (ICGs), e.g. Hypoxanthine Phosphoribosyltransferase 1 (*HPRT1*), Glyceraldehyde-3-Phosphate Dehydrogenase (*GAPDH*) and Beta-2-Microglobulin (*ß2M*) were amplified in all samples, but only ICGs genes whose expression was not statistically varied during experimental conditions were considered for the relative quantification (RQ). A cDNA pool was used as calibrator.

Experiments were performed in triplicate and, for each experiment, two biological replicates were included.

3.3.9 Determination of G4-ligands efficacy by qPCR

To measure the transcriptional effects of each candidate G4-ligand, cells (24 hours after seeding) were incubated with vehicle (DMSO, 0.1% final concentration) or two sub-cytotoxic doses of G4-ligands (1/3 and 2/3 of IC_{50} value, respectively). Based on constitutive *c-KIT* expression during time culture, cells were collected as

described above after 6, 12 and 24 hours of incubation. Methods used for RNA extraction, reverse transcription and qPCR were the same described in the previous paragraph. ICGs expression was checked within every experimental condition. The choice of the most suitable ICGs to be used for normalization was cell line- and ligand-dependent.

3.3.10 Determination of G4-ligands efficacy by flow cytometry

Cells ($5x10^5$/well and $4x10^5$/well for MCF-7 and HGC-27 cell lines, respectively) were seeded in 6-well plates; after 24 hours, the vehicle (DMSO, 0.1% final concentration) or AQ1 or AN6 (1 µM, final concentration) were added to the medium. Forty-eight hours post-exposure, monolayers were washed twice with PBS 1X 0.02% EDTA, detached and centrifuged at 100*g* for 4 min. Cells were resuspended in RPMI medium (Gibco® Life Technologies, Carlsbad, USA) supplemented with 3,3% FBS (Gibco® Life Technologies, Carlsbad, USA). Fifty µl of the cell suspension were incubated for 15 min at 4°C with 50 µl of a rat anti-mouse monoclonal antibody raised against cell surface c-KIT ($CD117_{PE}$: clone ACK 45, BD Pharmingen, California, USA), concentrated 1:25; then, a wash step with 500 µl of PBS and a centrifugation step at 100*g* at 4°C for 10 min, were performed. After removing the supernatant, 900 µl of PBS 1X were added to the cells. For BCL2 detection, 100 µl of the cell suspension were fixed and permeabilized with the IntraStain kit (DAKO Italia SRL, Milano, Italy) and then incubated with an anti-BCL2 antibody FITC conjugated (clone 124, DAKO Italia SRL, Milano, Italy). For acquisitions, the CyFlow® Space (Partec® GmbH, Münster, Germany) was used. Cells not incubated with the anti-$CD117_{PE}$ and anti-$BCL2_{FITC}$ were considered as negative controls. For each sample, c-kit expression was evaluated either in terms of events that stained for CD117 and in terms of mean fluorescent intensity (MFI), calculated as the ratio of the MFI in neoplastic cells by the MFI of unstained cells. Samples were analyzed by using FlowMax® software (Quantum Analysis GmbH, Münster, Germany), version 2.82.

3.3.11 Confirmatory experiments with other cellular models

Confirmatory proliferation studies were executed on α155, HMC1.2, PC3, $ROSA^{WT}$ and $ROSA^{KITD816V}$ cell lines, by using methods and conditions mentioned above (IC_{50} determination). Cells were treated with AQ1 or AN6 at concentrations

from 0.2 µM up to 3 µM and for 72 hours. To check for the resistance or sensitivity of the used cellular models, an imatinib control (1 µM final concentration) was included in the experimental setting.

As regards qPCR, three independent confirmatory experiments were executed in α155 and HMC1.2 cell lines to confirm the transcriptional effects of AQ1 on *c-KIT* mRNA. About $9x10^5$/well cells were seeded onto 6-well plates, and DMSO or AQ1 were added at final concentrations of 0.1% and 1 µM, respectively. Cells were incubated for 6 and 12 hours and centrifuged at 100*g* for 5 min; pellets were then washed once with 1 ml PBS and, finally, submitted to the same methodological procedure reported above (determination of G4-ligands efficacy by qPCR). For each cell line, values of slope, efficiency and dynamic range of qPCR assays are reported in Table 3.

Gene	**α155**			**HMC1.2**		
	Slope	**Efficiency (%)**	**Dynamic range (Ct)**	**Slope**	**Efficiency (%)**	**Dynamic range (Ct)**
B2M	-3.33	99.6	17.18-31.68	-3.38	97.7	17.46-31.25
GAPDH	-3.37	98	16.43-30.91	-3.40	96.7	17.34-31.36
HPRT1	-3.39	97.1	21.75-35.65	-3.38	97.5	22.14-37.67
KIT	-3.32	99.7	18.00-32.32	-3.30	101	19.08-32.90

Table 3: *qPCR assay standard curve values for α155 and HMC1.2.*

For confirmatory flow cytometry investigations, HMC1.2, α155 and KARPAS 299 cells were seeded in P6-well plates ($3x10^5$ cells/well); then, DMSO or AQ1 were added at final concentrations of 0.1%, and 1 or 2 µM, respectively. After 48 hours, $3x10^5$ cells were collected. HMC1.2 and α155 cells were labeled, at 4°C for 30 min, with mouse monoclonal anti-CD117 SC 13508 (Santa Cruz Biotech, Texas, USA), diluted 1:100. The secondary antibody used was an anti-mouse PE conjugated (diluted 1:50). The high affinity IgE receptor (FcεRI), present on mast cell membrane, was saturated by incubation with human serum for 10 min at room temperature. The human leukocyte antigens (HLA) were used as reference proteins and α155, HMC1.2 and KARPAS 299 cell lines were labeled with monoclonal anti-human leukocyte antigen (HLA) PeCy5 conjugated (W6-32 eBioscience, California,

USA). Unstained cells with the proper isotype control were used to check for non-specific fluorescence signals.

The cytofluorimetric analysis was made in a BD LSRFortessa™ (Becton Dickinson, New Jersey, USA) and data were analyzed by using DIVA™ (BD Pharmingen, California, USA) software. The c-kit expression was evaluated, for each sample, in terms of median fluorescent intensity (mFI), calculated as the ratio of the mFI in neoplastic cells by the mFI of unstained cells. Final results consisted in the mean of three different experiments.

3.3.12 Statistical analysis

The statistical analysis of data was performed by using GraphPad Prism version 5.00 for Windows (GraphPad Software, San Diego, USA). Dose-response curves and IC_{50} values were determined by nonlinear regression analysis, fitting a sigmoid dose-response curve.

Data on the time-dependent constitutive expression of target genes were expressed as -fold change (%) of the respective T_6 value, and analyzed with one-way analysis of variance (ANOVA) followed by Bonferroni post-test.

The statistically significant differences in mRNA levels in cells treated with G4-ligands were checked by the two-way ANOVA followed by Bonferroni post-test to identify if any difference in terms of transcriptional response was dependent either from the dose and/or time of treatment. Each RQ value of treated cells was normalized to the average RQ of the respective time-control samples.

In cell proliferation experiments, the viability data obtained with the different cell lines were analyzed with the Student t-test.

Data from cytofluorimetric analysis were expressed as n–fold changes against control cells; either the Student *t*-test nor the one-way ANOVA were used to unveil statistically significant differences between cells treated with vehicle only and AQ1.

3.4 RESULTS

3.4.1 Ligands selection

As anticipated, all members of the library were previously tested for their ability to stabilize the G4 structure of the human telomeric sequence as well as a random DNA double helix and a general preference for G4 *vs* dsDNA was previously reported for most compounds of the library (Musetti et al., 2009; Bianco et al., 2010; Folini et al., 2010; Zagotto et al., 2011; Milelli et al., 2012; Nanjunda et al., 2012; Bianco et al., 2013). Consistently, as a first preliminary screening tool, we analyzed all the members of our library by fluorescence melting measurements. The induced thermal stabilization on the G4s assumed by the target sequences in the same experimental conditions are reported in Figure 1A and Table 4.

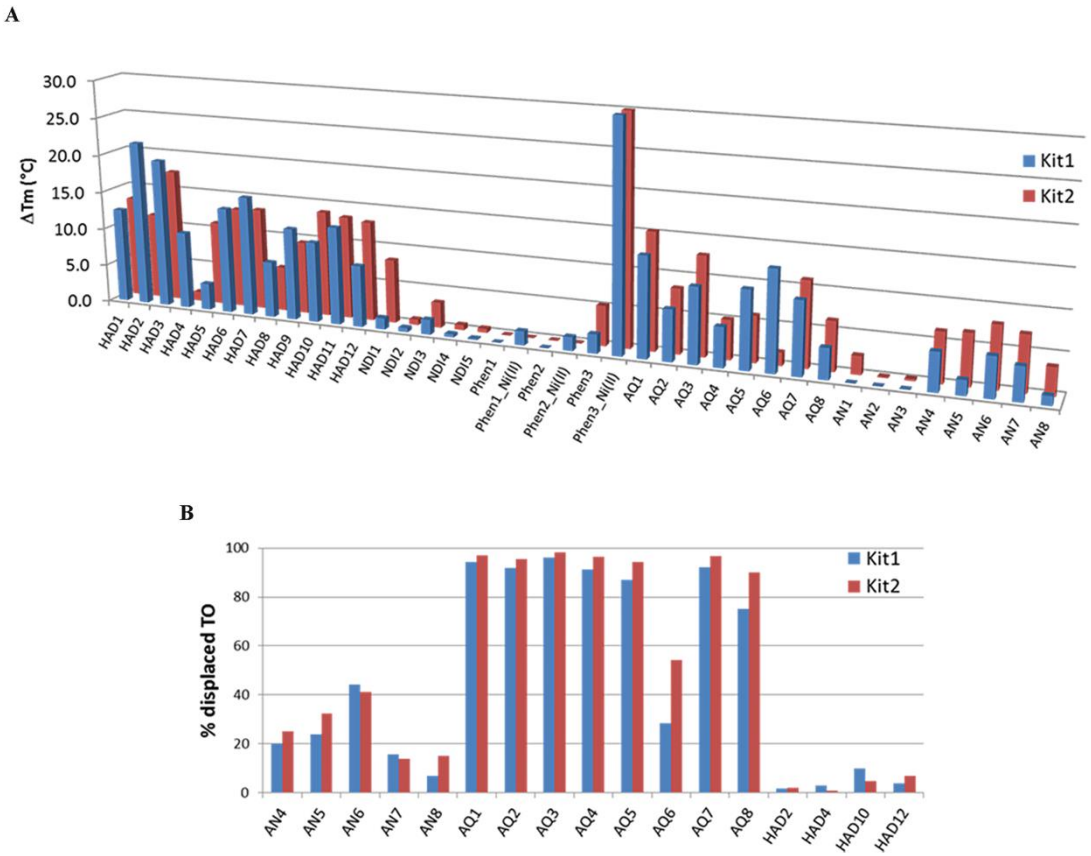

Figure 1. *(A) Increments of the melting temperature of the G4 arrangements of tested c-KIT sequences induced by 1 μM concentrations of tested ligands. Data were acquired in LiP buffer with 50 mM or 1 mM KCl for KIT1 or KIT2, respectively. (B) Percentage of TO displacement from KIT1 or KIT2 induced by a 4-fold excess of AQ, AN and HAD derivatives.*

Compound	Ref	KIT1	KIT2	HTS	dsDNA
HAD1	DB832[a]	12.5	13.3	10.9	2.4
HAD2	DB1450[a]	21.8	11.3	12.8	12.1
HAD3	DB2037[a]	19.6	17.5	16.8	7.8
HAD4	DB1463[a]	10.1	1.2	7.3	2.0
HAD5	DB1438[a]	3.5	11.0	13.3	1.2
HAD6	DB1972[a]	14.0	13.1	9.9	4.2
HAD7	DB1949[a]	15.7	13.4	12.6	2.6
HAD8	DB934[a]	7.4	5.8	5.0	2.9
HAD9	DB1693[a]	12.1	9.5	9.4	2.2
HAD10	DB1694[a]	10.6	13.9	5.6	1.1
HAD11	DB1093[a]	12.9	13.4	11.7	11.5
HAD12	DB1999[a]	8.1	13.1	4.9	2.4
NDI1	2[b]	1.5	8.3	10.3	3.0
NDI2	1[b]	0.6	0.7	9.2	2.8
NDI3	20[b]	2.0	3.3	13.5	4.4
NDI4	22[b]	0.4	0.7	7.0	1.9
NDI5	8[b]	0.2	0.5	10.1	5.0
Phen1	K34[c]	0.0	0.0	0.1	0.0
Phen1_Ni(II)	$(K34)_2Ni(II)$[c]	1.9	0.0	3.1	0.0
Phen2	P120[d]	0.0	0.0	0.1	0.0
Phen2_Ni(II)	$(P120)_2Ni(II)$[d]	1.8	0.0	10.0	0.0
Phen3	P115[e]	2.5	5.2	0.1	0.0
Phen3_Ni(II)	(P115)Ni(II)[e]	30.9	30.6	23.6	0.3
AQ1	D-13[f]	13.1	15.3	18.0	4.6
AQ2	E-13[f]	6.7	8.4	18.9	4.5
AQ3	B-13[f]	9.9	12.9	14.2	2.5
AQ4	C-13[f]	5.2	5.1	9.9	1.4
AQ5	D-15[f]	10.2	6.0	18.2	1.2
AQ6	E-15[f]	13.0	1.7	4.5	0.1
AQ7	B-15[f]	9.5	11.1	7.0	0.3
AQ8	C-15[f]	4.0	6.4	4.3	0.1
AN1	Ant1[g]	0.0	2.4	1.0	1.2
AN2	Ant2[g]	0.0	0.1	0.3	0.6
AN3	Ant9[g]	0.0	0.2	1.0	1.6
AN4	Ant9,10[g]	5.0	6.5	1.7	0.9
AN5	Ant1,5[g]	2.0	6.7	13.6	0.5
AN6	Ant1,8[g]	5.2	8.0	3.0	0.8
AN7	Ant2,6[g]	4.4	7.2	4.7	0.1
AN8	Ant2,7[g]	1.2	3.6	2.0	0.1

Table 4. *Library of tested compounds and variation of the melting temperature they induced at 1 μM concentration of each tested DNA sequence. Errors were ± 0.4 °C. The previously used compound name and the corresponding reference are reported in the ref column.* [a] *Nanjunda et al., 2012,* [b] *Milelli et al., 2012,* [c] *Musetti et al., 2009,* [d] *Bianco et al., 2013,* [e] *Bianco et al., 2010,* [f] *Zagotto et al., 2011,* [g] *Folini et al., 2010.*

Interestingly, some behaviors were conserved among derivatives belonging to the same scaffold. As an example, all tested polyamine derivatives recognized G4 irrespectively of DNA sequence (telomere, KIT1 or KIT2). As regards the NDI derivatives, all of them showed a preferential stabilization of the telomeric G4. Thus, none of these compounds were selected for further investigations. About Phen-derivatives, only their Ni(II) complexes involving two Phen moieties were confirmed to be active, as previously shown on the telomeric sequence; thus, we considered them as not appropriate for *in cells* studies, since in the living environment the distribution among complexes with different stoichiometry can be hardly monitored.

On average, anthraquinone derivatives (AQ) showed higher thermal stabilization in comparison to the tested anthracenes (AN). Moreover, for both families of compounds, some variations in terms of efficiency and selectivity were highlighted according to the nature and relative position of the side chains. This led us to consider them as promising candidates. In order to further reduce the number of hits we added a second screening protocol, a G4 fluorescent intercalator displacement (G4-FID). This assay is based on competitive displacement of TO form DNA by our putative ligands. In agreement with literature data, we confirmed that, in our experimental conditions, TO showed comparable binding constant for KIT1 and KIT2 (Largy et al., 2011). Consequently, this assay provides a direct indication of the affinity ranking order by tested competitors. For comparison, in this assay we included some HAD derivatives which are suggested to bind G4 into the grooves. Accordingly, they were not able to displace the end-stacking agent TO. The results of FID are summarized in Figure 1B.

FID and thermal stabilization data are in good agreement. On average, AQ derivatives were the best TO competitors. This result prompted us to perform full titrations with some derivatives. We focused on the comparison between 1,5 and 2,6 regioisomers within the AQ family (AQ1 and AQ5 vs AQ3 and AQ7, respectively) since they appear to be the best performing compounds (Table 5).

	AQ1	AQ5	AQ3	AQ7	AN6
KIT1	0.32 ± 0.05	0.27 ± 0.02	0.50 ± 0.04	0.24 ± 0.04	4.11 ± 0.7
KIT2	0.35 ± 0.05	0.41 ± 0.03	0.62 ± 0.05	0.25 ± 0.02	3.63 ± 1.00

Table 5. *DC_{50} (50% displacement concentration; μM) derived from TO displaces (FID) by selected ligands (AQ and AN derivatives) with KIT sequences.*

Within the 1,5 series, the aminoacidic composition of the side chain (βAla-Lys in AQ1 vs βAla-Phe-Lys in AQ5) did not cause significant variations in TO displacement. Conversely, the insertion of a phenylalanine moiety seemed to positively affect it within the 2,6 series (βAla-Lys in AQ3 vs βAla-Phe-Lys in AQ7). As far as AN derivatives are concerned, they were confirmed to be remarkably less efficient than AQs. Among them, AN6 was the best performing on both the tested KIT sequences. Noteworthy differences were never observed between KIT1 or KIT2 sequences.

Hence, by merging FID and thermal stabilization results, anthracene derivative AN6 and anthracenedione derivatives AQ1 and AQ7 were selected for further investigations.

3.4.2 Binding affinity and functional interaction of selected ligands

To better characterize the interaction between the selected ligands and the G4 folded form of KIT1 and KIT2, we performed SPR. For this experiment, oligonucleotides labeled at 5'with Biotin-TEG (tetra-ethyleneglycol) were folded in KCl and subsequently immobilized on a gold chip functionalized with streptavidine. Sensorgrams were acquired and the data at the steady state were used to evaluate the binding constants of the selected binders towards the *c-KIT* sequences (Figure 2, Table 6).

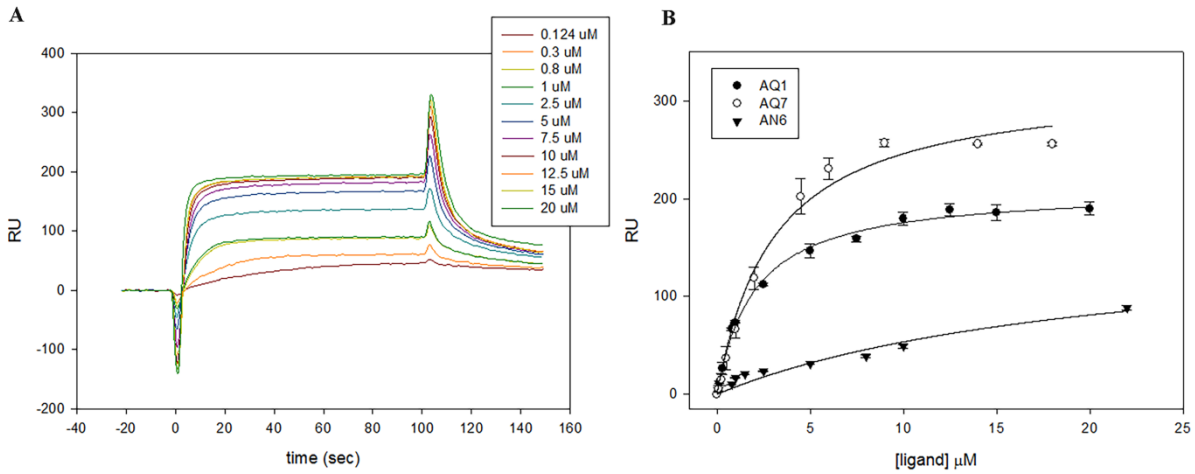

Figure 2. *Representative examples of SPR analysis. (A) Sensorgrams derived from the analysis of AQ1 with KIT2. (B) Plots of the RU at the steady state plotted vs the concentration of injected ligand on chip functionalized with KIT1.*

	KIT1	KIT2
AQ1	1.99 ± 0.15	1.01 ± 0.15
AQ7	3.04 ± 0.43	2.29 ± 0.28
AN6	71.5 ± 20.1	25.5 ± 4.01

Table 6. *Dissociation constants, (Kd, μM) of selected ligands (AQ and AN derivatives) with KIT sequences determined by SPR in 10 mM Tris, 50 mM KCl, pH 7.5, 0.025% surfactant P20.*

All experimental equilibrium data well fitted with a single binding model. Interestingly, all tested ligands showed a preferential, albeit modest, interaction with KIT2. However, in line with the above presented results, the binding constant of AN6 was confirmed to be at least one order of magnitude lower than those provided by AQ derivatives.

Before moving toward the cell system, we assessed if the binding of our ligands to the *c-KIT* sequences can actually impairs the processing of the *c-KIT* promoter. Thus, we performed polymerase stop assay: KIT1 and KIT2 sequences were inserted into a template strand and the elongation of a complementary primer by Taq polymerase was monitored. As shown in Figure 3, increasing concentrations of each ligand in the reaction mixture resulted in a progressive reduction of the full length product. In parallel, a predominant arrest product, which corresponds to the primer elongation up to the G-rich region, appeared. According to the above reported

binding affinity ranking order, this effect occurred at lower ligand concentration when the AQ derivatives were used and with a slight more pronounced efficiency on KIT2 sequence. This reinforces a model in which the G4-ligand complex prevents the oligonucleotide replication by Taq polymerase.

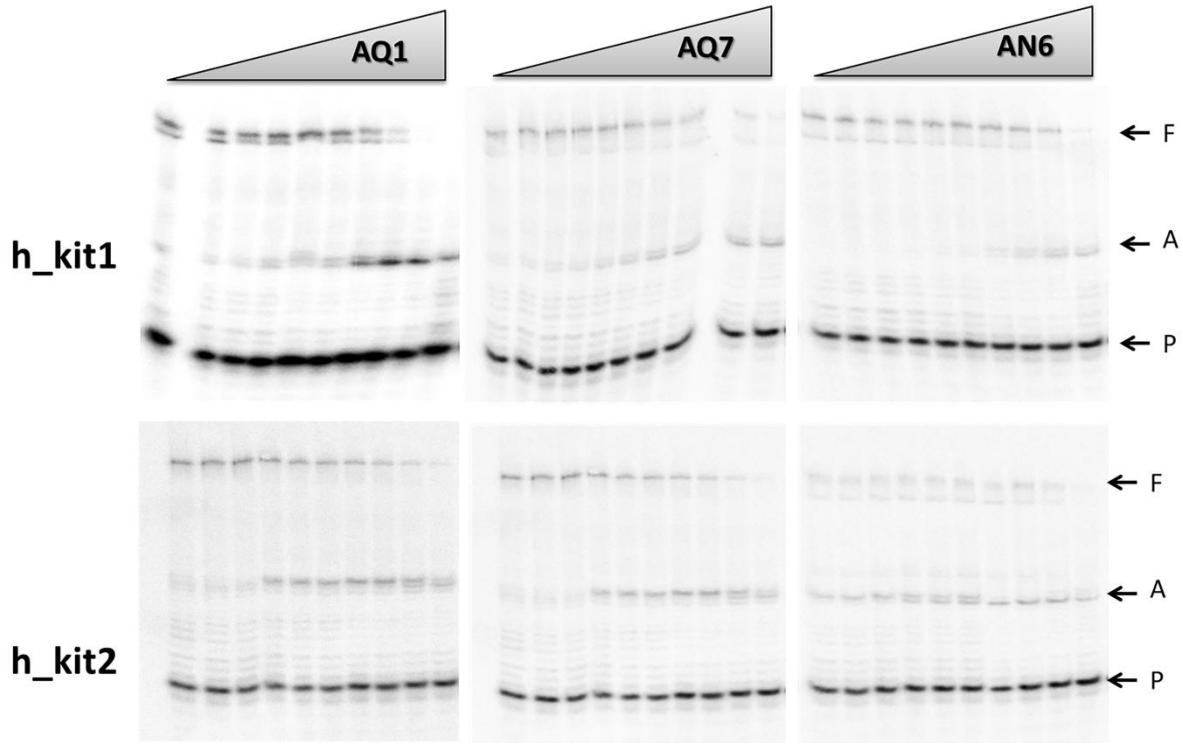

Figure 3. *Polymerase stop assay with 0-15 µM of tested ligands. P, A and F correspond respectively to primer, arrest product and full length product.*

3.4.3 G4-ligands cytotoxicity

In short-term cultures (72 hours) AQ1 and AN6 showed dose-dependent cytotoxic effects in both MCF7 and HGC27 cell lines. Dose-response curves, the relative IC_{50} values and the corresponding linear regression coefficients (R^2) for each G4-ligand are reported in Figure 4. AQ7 was comparatively less cytotoxic, and the IC_{50} value could not be determined even using concentrations up to 10 µM (Figure 4E and 4F).

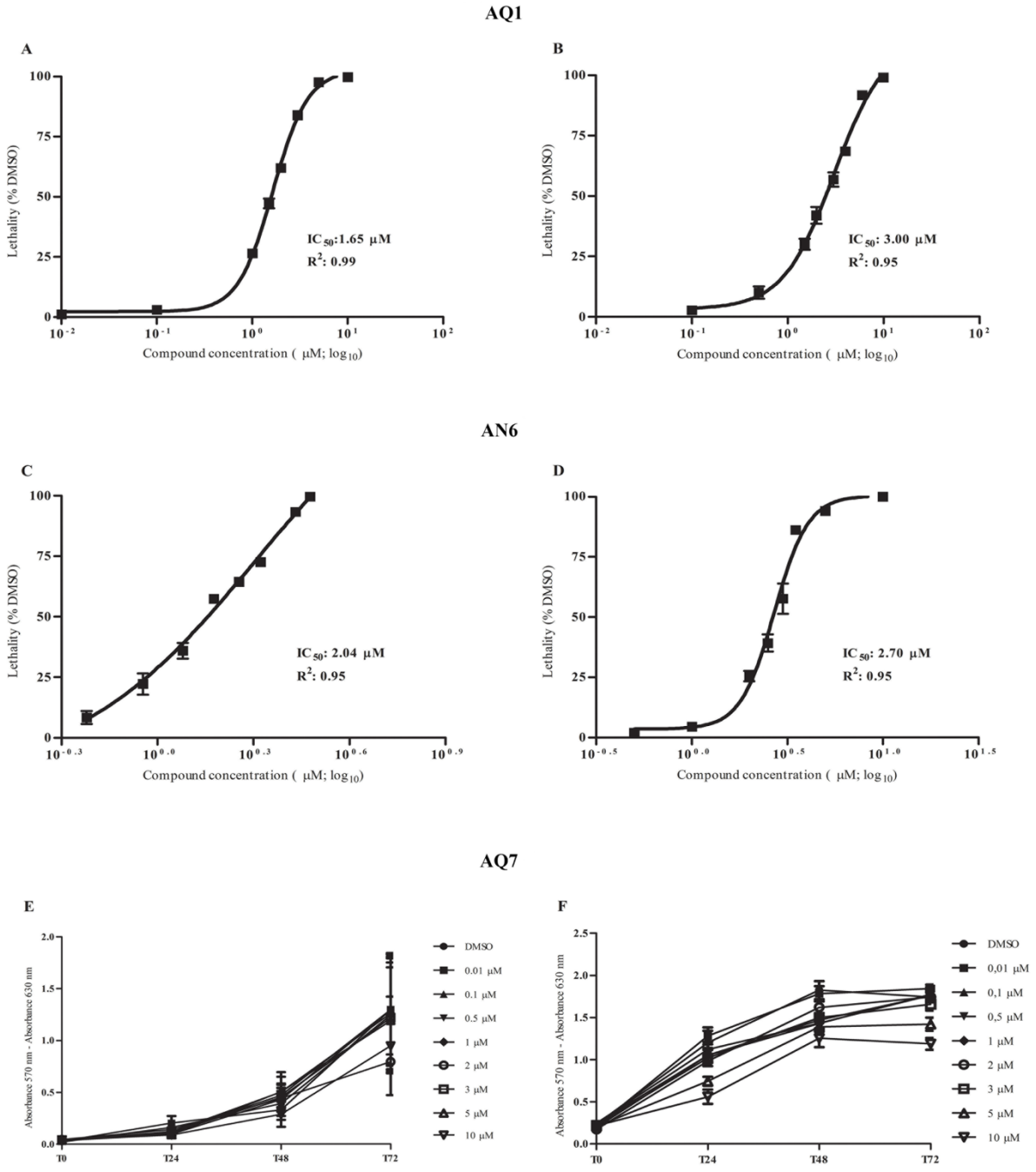

Figure 4. *Dose-response curves and proliferation curves of HGC27 and MCF7 after treatment with the G4-ligands. (A) HGC27 and (B) MCF7 dose-response curves from Alamar Blue experiments to determine IC_{50} values and R^2 following the incubation with AQ1. (C) HGC27 and (D) MCF7 dose-response curves from Alamar Blue experiments to determine IC_{50} values and R^2 after the exposure to AN6. (E) HGC27 and (F) MCF7 proliferation curves from sulforhodamine B experiments following the incubation with AQ7. Data are expressed as mean values ± standard deviation of three independent experiments, each one performed in different passages.*

3.4.4 Target genes constitutive expression

To define the best protocol of exposure to G4-ligands, we measured the time-dependent (from T_6 and up to T_{96}) changes in the constitutive expression of *c-KIT*, as well as of 6 other genes known to contain G4 forming sequences in their promoter region, e.g., *MYC, BCL2, PDGFA, PDGFRβ, KRAS* and *hTERT*. Results are shown in Figure 5.

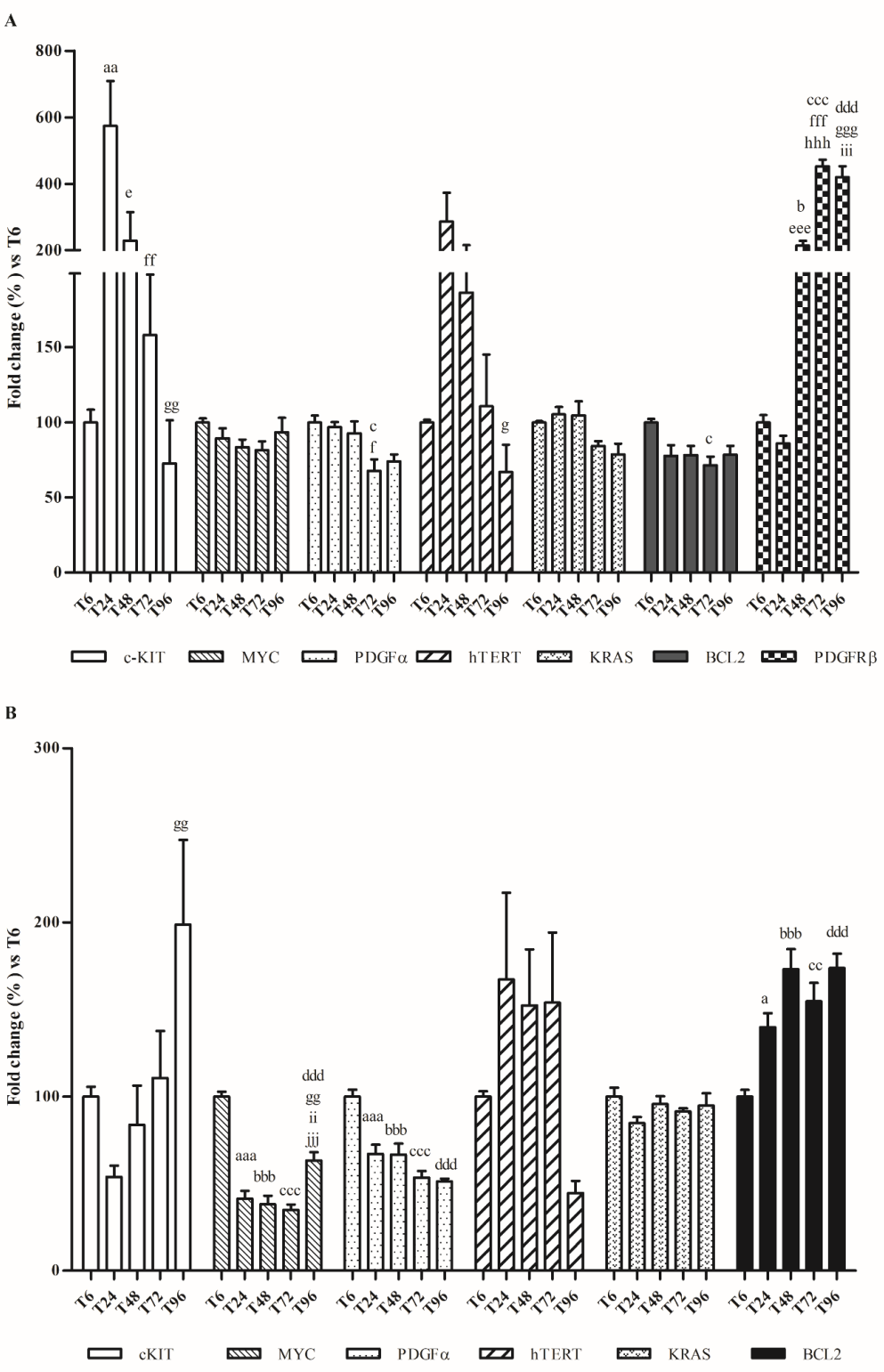

Figure 5. *Effects of culturing time on gene expression. (A) Total RNA was isolated from HGC27 monolayers and mRNA levels of c-KIT, MYC, PDGFA, hTERT, KRAS, BCL2 and PDGFRβ were measured by using a qPCR approach. (B) Total RNA was isolated from MCF7 monolayers and mRNA levels of c-KIT, MYC, PDGFA, hTERT, KRAS and BCL2 were measured by using a qPCR approach. Data (arithmetic means ± S.D.) are expressed as n-fold change (a.u.) normalized to the RQ mean value of cells stopped at T_6, to which an arbitrary value of 100 was assigned.* $^{a,\ aa,\ aaa}$*: P<0.05; P<0.01; P<0.001 T_6 vs T_{24};* $^{b,\ bbb}$*: P<0.05; P<0.001 T_6 vs T_{48};* $^{c,\ cc,\ ccc}$*: P<0.05; P<0.01; P<0.001 T_6 vs T_{72};* ^{ddd}*: P<0.001 T_6 vs*

T_{96}; [e, eee]: P<0.05; P<0.001 T_{24} vs T_{48}; [f, ff, fff]: P<0.05; P<0.01; P<0.001 T_{24} vs T_{72}; [g, gg, ggg]: P<0.05; P<0.01; P<0.001 T_{24} vs T_{96}; [hhh]: P<0.001 T_{48} vs T_{72}; [ii, iii]: P<0.01; P<0.001 T_{48} vs T_{96}; [jjj]: P<0.001 T_{72} vs T_{96}.

Overall, *c-KIT* seemed to be the most variable gene, with a differential pattern of expression between the two cell lines. In the HGC27 cell line, it reached a peak of expression at T_{24}, then it significantly decreased day by day; however, in MCF7 cell line, *c-KIT* expression increased slowly and reached a top at T_{96}. As regards the other genes, no evident time-dependent differences in gene expression were ever noticed, except for *BCL2* in MCF7 and *PDGFRβ* in HGC27 whose mRNA levels significantly increased with time; however, in MCF7 cell line both *MYC* and *PDGFA* mRNAs decreased after T_6. Worth mentioning, *PDGFRβ* gene expression was not detectable in MCF7 cell line. Taking into consideration the present results and since the objective of the treatment was to block the promoter activity, the transcriptional effects of candidate G4-ligands on *c-KIT* gene were investigated in cells incubated for 6, 12 and 24 hours.

Table 7 summarized qPCR and flow cytometry experimental settings chosen for each cell line and ligand.

Cell line	Ligand	IC_{50}	qPCR Concentration Tested	qPCR Time Tested	Flow cytometry Concentration Tested	Flow cytometry Time tested
HGC27	AQ1	1.65	0.5 µM - 1 µM	T6, T12, T24	1 µM - 2 µM[a]	T48
	AQ7	>10 µM	10 µM [b]	T6, T12, T24[b]	/	/
	AN6	2.04	0.5 µM - 1 µM	T6, T12, T24	1 µM	T48
MCF7	AQ1	3.00	1 µM -2 µM	T6, T12, T24	1 µM - 2 µM[a]	T48
	AQ7	>10 µM	10 µM [b]	T6, T12, T24 [b]	/	/
	AN6	2.70	1 µM -2 µM	T6, T12, T24	1 µM	T48
α155	AQ1	/	1 µM	T6, T12	1 µM - 2 µM	T48
HMC1.2	AQ1	/	1 µM	T6, T12	1 µM - 2 µM	T48

Table 7. *qPCR and flow cytometry experimental settings chosen for each cell line and ligand tested in the study.* [a] *2 µM concentration was used only in BCL2 detection experiment,* [b] *data not shown in the manuscript.*

3.4.5 Evaluation of G4-ligands efficacy

The incubation with AQ1 led to an inhibition of *c-KIT* expression (range 2-10-fold) in HGC27 cells (Figure 6A), while in MCF7 cell line the gene was almost completely suppressed after 24 hours (37-fold; Figure 6B). In both cell lines, the down-regulation by treatment was always statistically significant (P<0.0001).

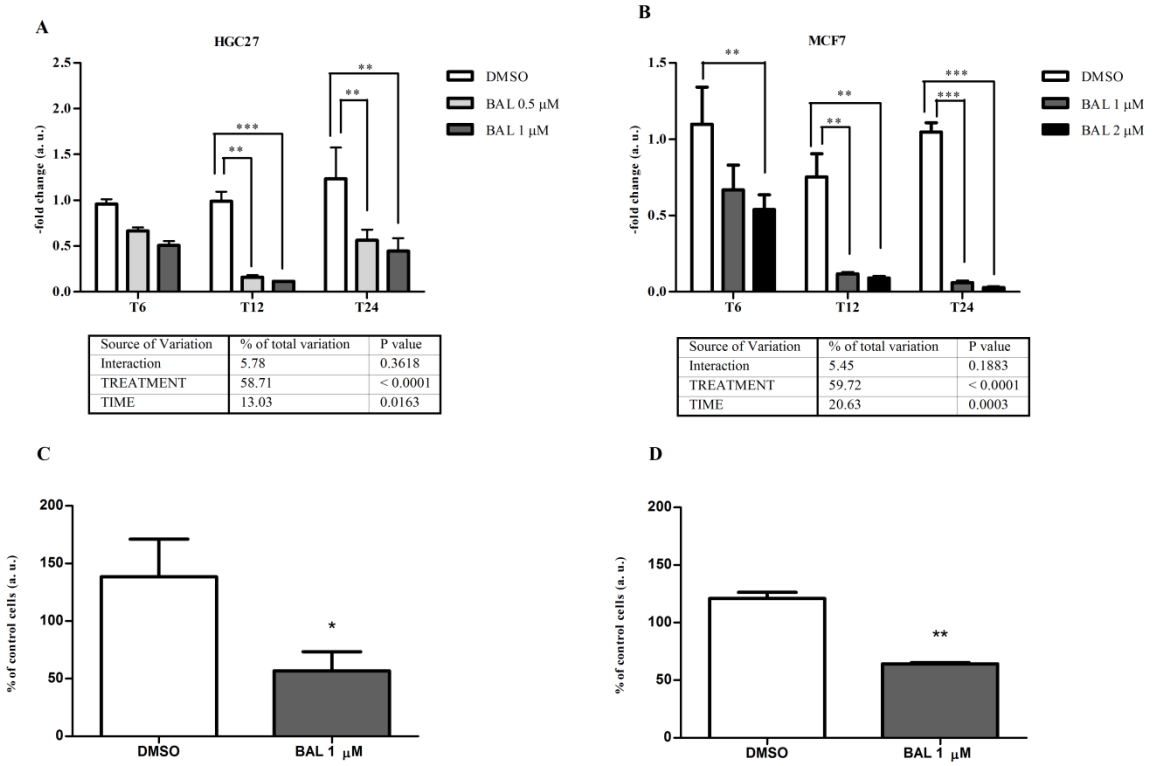

Source of Variation	% of total variation	P value
Interaction	5.78	0.3618
TREATMENT	58.71	< 0.0001
TIME	13.03	0.0163

Source of Variation	% of total variation	P value
Interaction	5.45	0.1883
TREATMENT	59.72	< 0.0001
TIME	20.63	0.0003

Figure 6. *Effect of AQ1 on c-KIT mRNA and protein expression in HGC27 and MCF7 cell lines. The c-KIT mRNA level (A) and (B) was measured by using qPCR approach, and data (arithmetic means ± S.D.) are expressed as n-fold change normalized to the RQ of control cells at each time (T_6, T_{12}, T_{24}) to which an arbitrary value of 1 (a.u.) was assigned. Two-way ANOVA followed by Bonferroni post-test were used to assess statistical differences between doses and time of treatment. The c-kit protein amount (C) and (D) was measured by flow cytometry and data are expressed as n-fold change (a. u.) to the mean fluorescence intensity (MFI) of not treated cells. Student t-test was used to assess statistical differences between cell treated with AQ1 and those treated with the vehicle (DMSO).* *,**,****: P<0.05; P<0.01; P<0.001.*

c-KIT transcriptional results were confirmed, although to a lower magnitude, at the protein level by flow cytometry analysis. A significant decrease of *c-KIT* (2-fold) was observed in HGC27, and a similar trend was also noticed in MCF7 cell line (Figure 6C and 6D, respectively). An example of flow cytometry dot plots, with population gate and histograms showing the fluorescence of CD117, is reported in Figure 7.

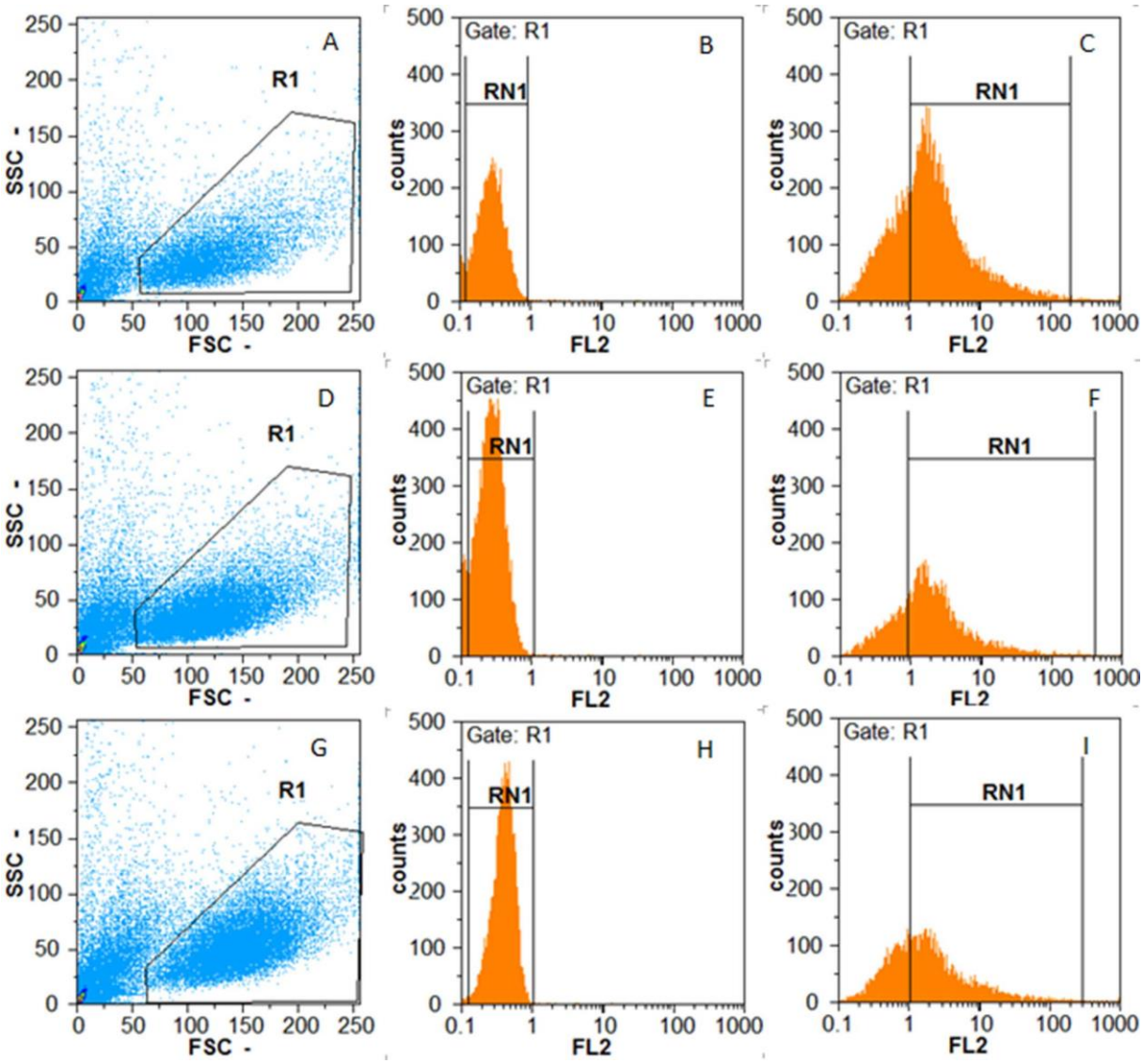

Figure 7. *Evaluation of CD117 expression in HCG27 cells after 24h of incubation:*
Control sample: (A) morphological scatter (forward scatter, FSC; side scatter, SSC); (B) isotype control, histogram; (C) CD117 expression, histogram;
HCG27 cells incubated with DMSO (D) morphological scatter (forward scatter, FSC; side scatter, SSC); (E) isotype control, histogram; (F) CD117 expression, histogram.
HCG27 cells incubated with AQ1 1 µM: (G) morphological scatter (forward scatter, FSC; side scatter, SSC); (H) isotype control, histogram (I) CD117 expression, histogram.

Besides *c-KIT*, AQ1 caused a marked and significant inhibition (P<0.0001) of *BCL2* gene expression in both cell lines (Figure 8).

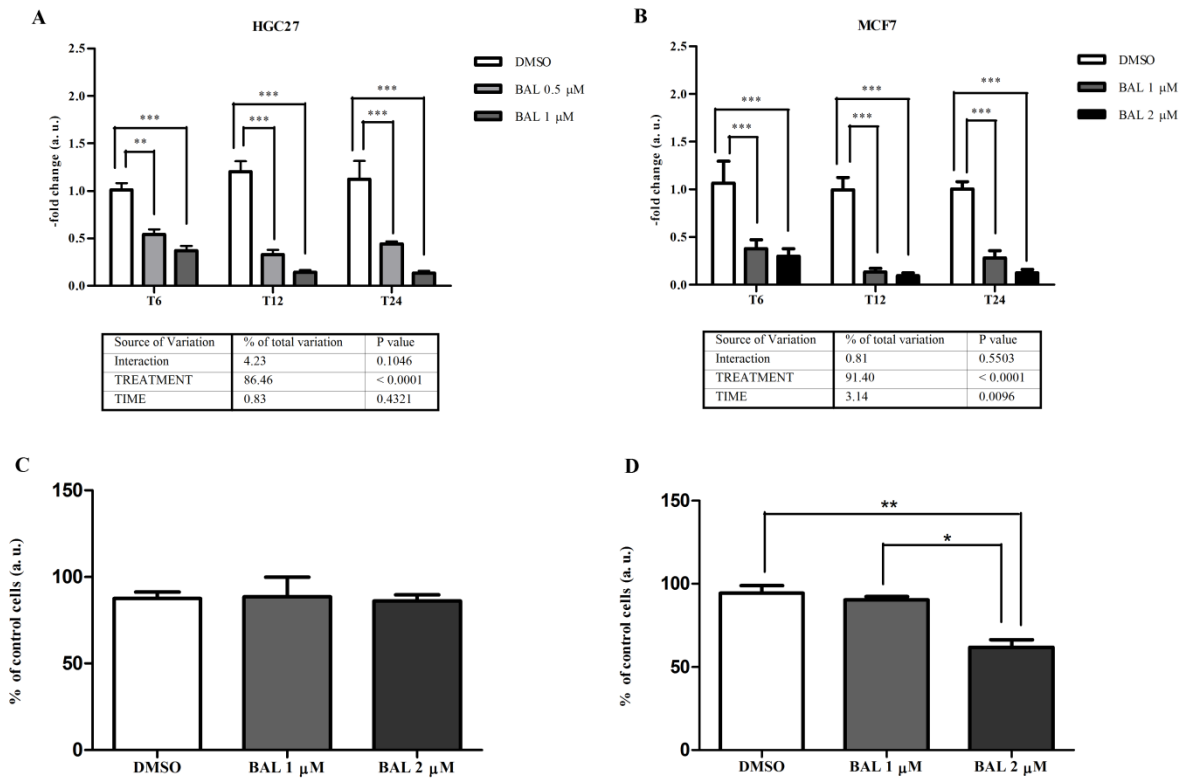

Figure 8. *Effect of treatment with AQ1 on BCL2 mRNA and protein in HGC27 and MCF7 cell lines. The BCL2 mRNA level (A) and (B) was measured by using a qPCR approach, and data (arithmetic means ± S.D.) are expressed as n-fold change normalized to the RQ of control cells at each time (T_6, T_{12}, T_{24}) to which an arbitrary value of 1 (a.u.) was assigned. Two-way ANOVA followed by Bonferroni post-test was used to assess statistical differences between doses and time of treatment.* ****: P<0.001. The bcl2 protein amount (C) and (D) was measured by flow cytometry, and data are expressed as n-fold change (a.u.) of the mean fluorescence intensity (MFI) measured in untreated cells. One-way ANOVA followed by Bonferroni post-test was used to assess statistical differences between cell treated with AQ1 and those treated with the vehicle (DMSO).* *,***: P<0.05; P<0.01.*

The magnitude of such inhibition accounted for 2.5-5 and 4-6 -fold for HGC27 and MCF7, respectively. No post-transcriptional effects were noticed in HGC27 under the present experimental conditions (Figure 8C); however, a significant decrease (P<0.01) of bcl2 protein amount was observed, at 48 hours, only in MCF7 cells with AQ1 treatment at 2 µM (Figure 8D).

Concerning the other oncogenes, known to possess G4 structures in their promoter region, a significant, although of minor importance, down-regulation was observed for *PDGFRβ* in HGC27 (*P*=0.0003; Figure 9), and for *MYC* and *hTERT* in MCF7 with *P*<0.0001 (Figure 10).

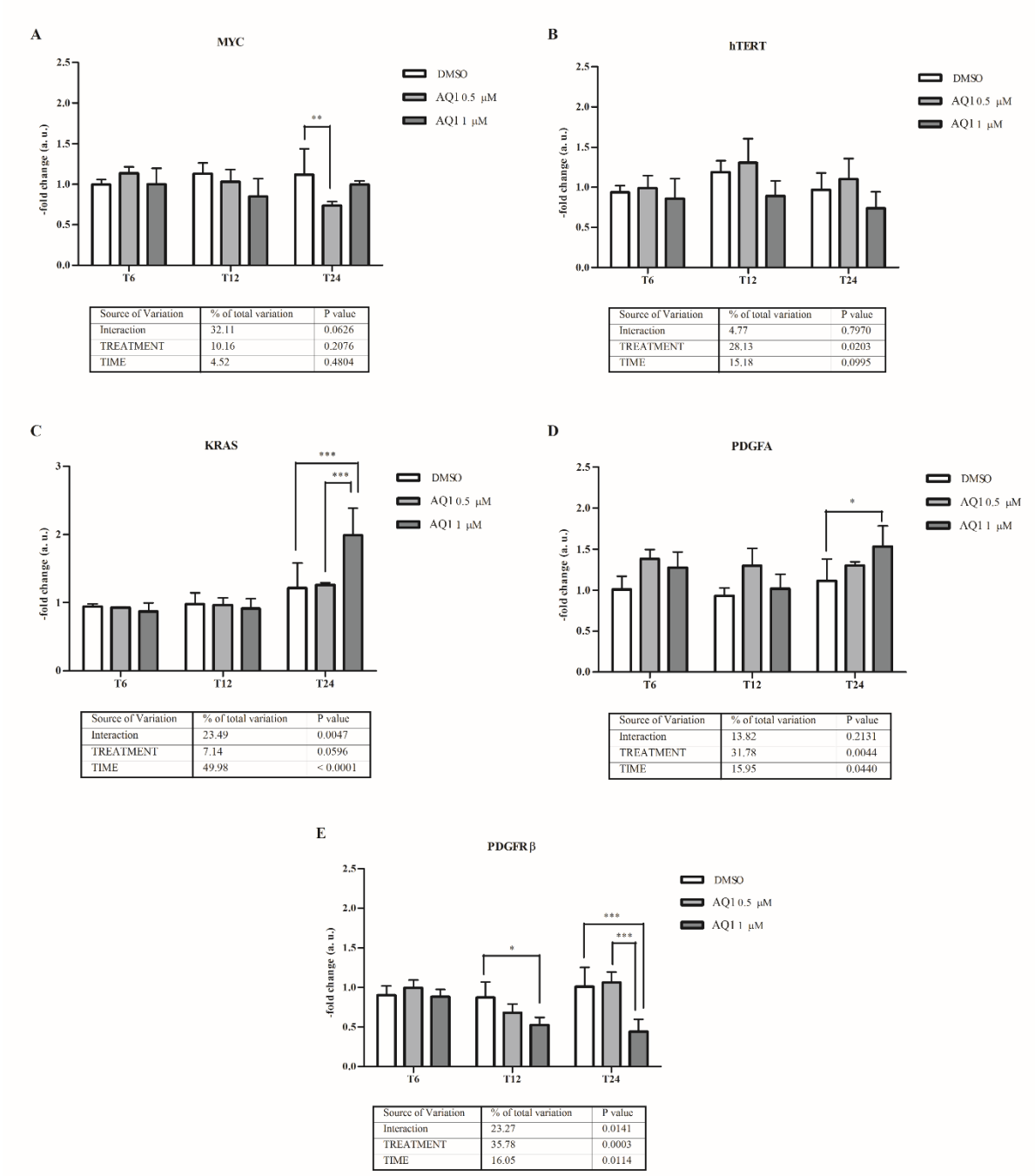

Figure 9. *Effect of AQ1 on mRNA of other oncogenes possessing G4 structures in HGC27. (A) MYC, (B) hTERT, (C) KRAS, (D) PDGFA and (E) PDGFRβ mRNA level were measured using qPCR, and data (arithmetic means ± S.D.) are expressed as n-fold change (a.u.) normalized to the RQ of control cells at each time (T_6, T_{12}, T_{24}) to which an arbitrary value of 1 was assigned. Two-way ANOVA and Bonferroni post-test were used to assess statistical differences between doses and time of treatment.* $^{*, **, ***}$*: P<0.05; P<0.01; P <0.001.*

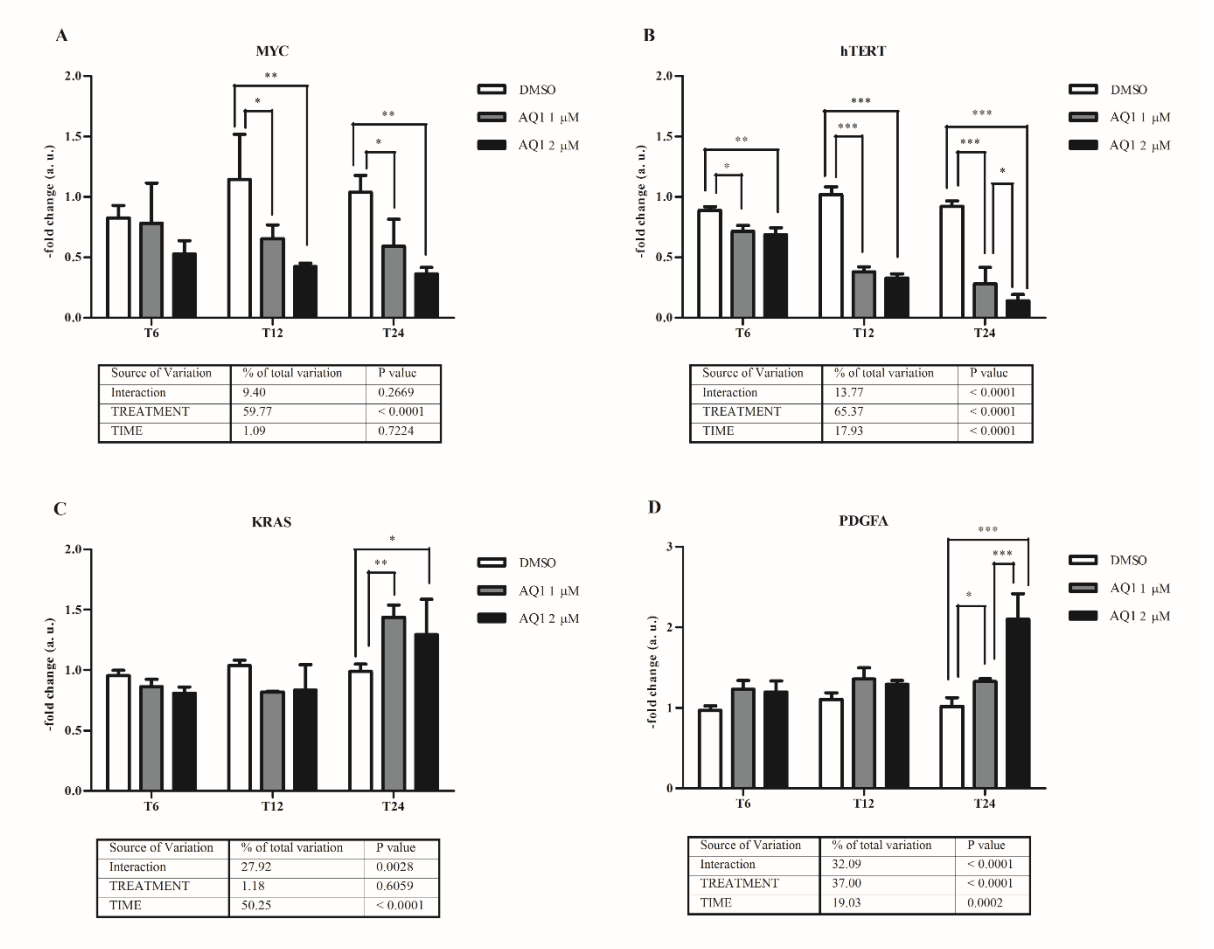

Source of Variation	% of total variation	P value
Interaction	9.40	0.2669
TREATMENT	59.77	< 0.0001
TIME	1.09	0.7224

Source of Variation	% of total variation	P value
Interaction	13.77	< 0.0001
TREATMENT	65.37	< 0.0001
TIME	17.93	< 0.0001

Source of Variation	% of total variation	P value
Interaction	27.92	0.0028
TREATMENT	1.18	0.6059
TIME	50.25	< 0.0001

Source of Variation	% of total variation	P value
Interaction	32.09	< 0.0001
TREATMENT	37.00	< 0.0001
TIME	19.03	0.0002

***Figure 10**: Effect of AQ1 on mRNA of other oncogenes possessing G4 structures in MCF7. (A) MYC, (B) hTERT, (C) KRAS and (D) PDGFA mRNA level were measured using qPCR, and data (arithmetic means ± S.D.) are expressed as n-fold change (a.u.) normalized to the RQ of control cells at each time (T_6, T_{12}, T_{24}) to which an arbitrary value of 1 was assigned. Two-way ANOVA and Bonferroni post-test were used to assess statistical differences between doses and time of treatment. *, **, ***: $p<0.05$; $p<0.01$; $p<0.001$.*

As regards AN6, it did not affect *c-KIT* mRNA in HGC27 cell line, whereas a decrease, only at T_{12} hours and at the highest ligand concentration, was observed in MCF7 cell line ($P<0.05$; Figure 11A and 11B). The amount of c-kit protein was significantly decreased, after 48 hours of incubation in both cell lines ($P<0.01$ and $P<0.05$ in HCG27 and MCF7, respectively; see Figure 11C and 11D). On the contrary, contrasting results were obtained for the other oncogenes under investigation.

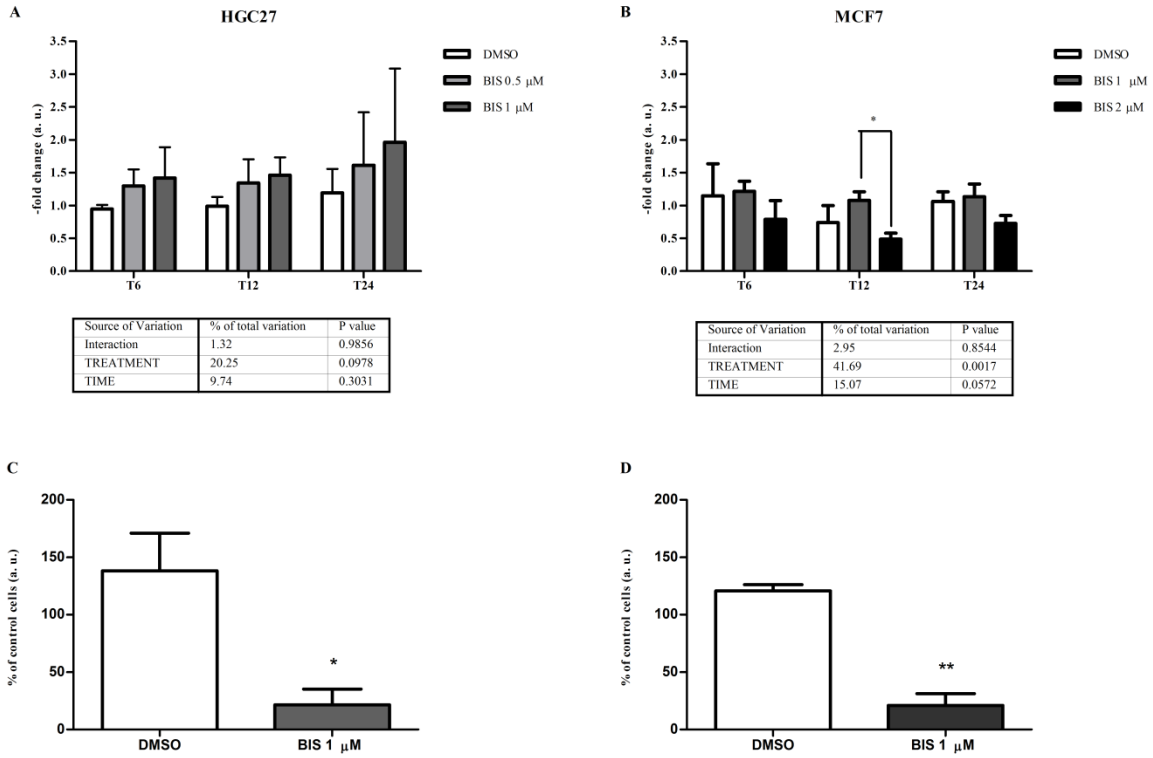

Source of Variation	% of total variation	P value
Interaction	1.32	0.9856
TREATMENT	20.25	0.0978
TIME	9.74	0.3031

Source of Variation	% of total variation	P value
Interaction	2.95	0.8544
TREATMENT	41.69	0.0017
TIME	15.07	0.0572

Figure 11: *Effect of AN6 on c-KIT mRNA and protein expression in HGC27 and MCF7 cell lines. The c-KIT mRNA levels (A and B) were measured by using a qPCR approach; data (arithmetic means ± S.D.) are expressed as n-fold change normalized to the RQ of control cells at each time (T_6, T_{12}, T_{24}), to which an arbitrary value of 1 (arbitrary units, a.u.) was assigned. Two-way ANOVA, followed by Bonferroni post-test, were used to assess statistical differences between doses and time of treatment.* ***: P<0.01. The c-kit protein amounts (C and D) were measured by flow cytometry, and data are expressed as n-fold change (a.u.) with respect to the mean fluorescence intensity (MFI) of untreated cells. Student t-test was used to assess statistical differences between cell treated with AN6 and those treated with the vehicle (DMSO).* *,***: P<0.05; P<0.01.*

The PDGFA mRNA levels increased after AN6 treatment in both cell lines (Figure 12D and 13D), while KRAS and PDGFRβ were up-regulated in HGC27 cell line only (Figure 12C and 12E).

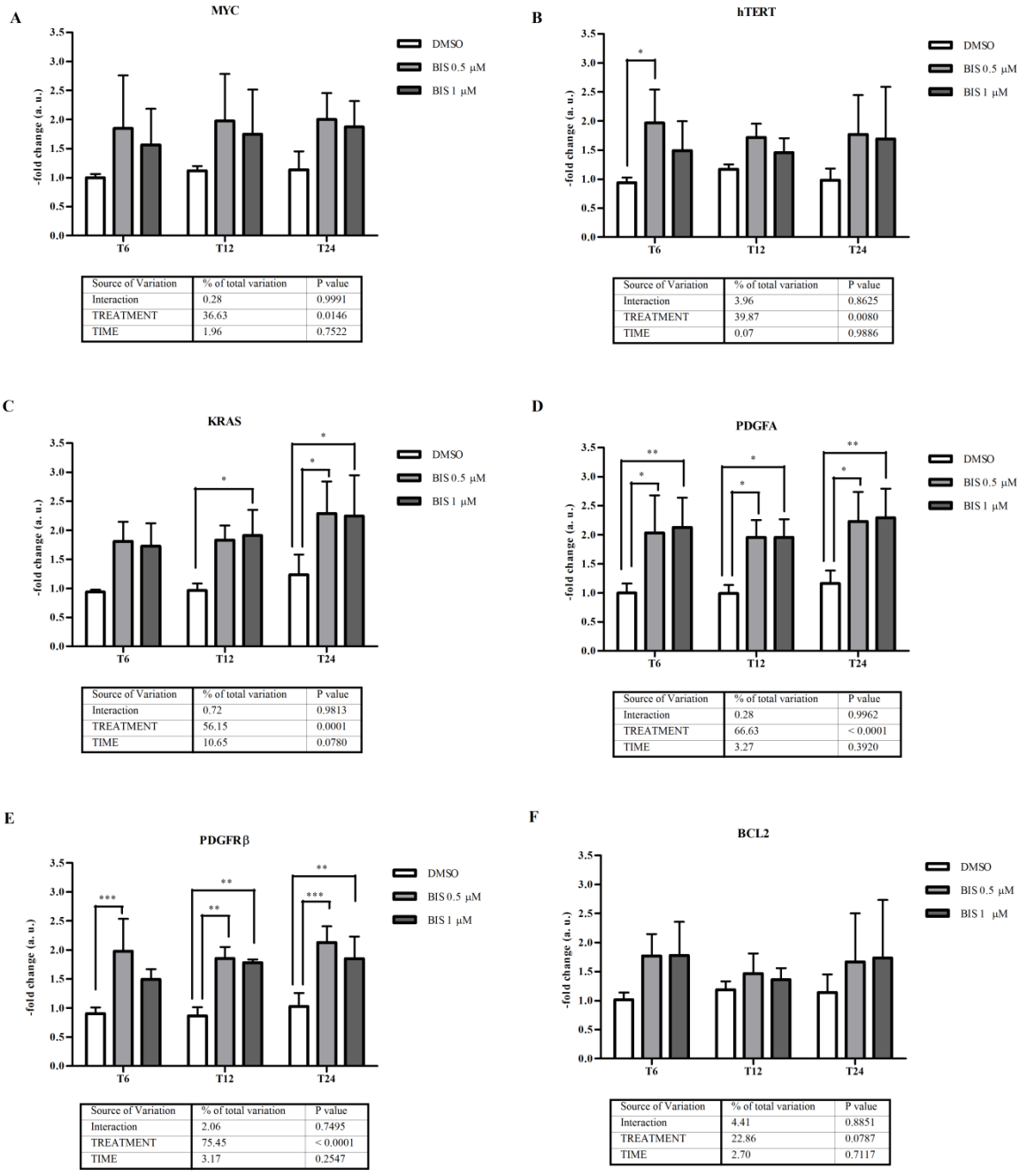

***Figure 12**: Effect of treatment with AN6 on mRNA of oncogenes possessing G4 structures in HGC27. (A) MYC, (B) hTERT, (C) KRAS, (D) PDGFA, (E) PDGFRβ, and (F) BCL2 mRNA levels were measured by using qPCR, and data (arithmetic means ± S.D.) are expressed as n-fold change (a.u.) normalized to the RQ of control cells at each time (T_6, T_{12}, T_{24}) to which an arbitrary value of 1 was assigned. Two-way ANOVA and Bonferroni post-test were used to assess statistical differences between doses and time of treatment. *, **, ***: $p<0.05$; $p<0.01$; $p<0.001$.*

On contrary, in MCF7 cell line a significant blocking effect was noticed for *MYC* and *hTERT* only at the highest tested concentration (P<0.01 and P<0.05; Figure 13A and 13B, respectively).

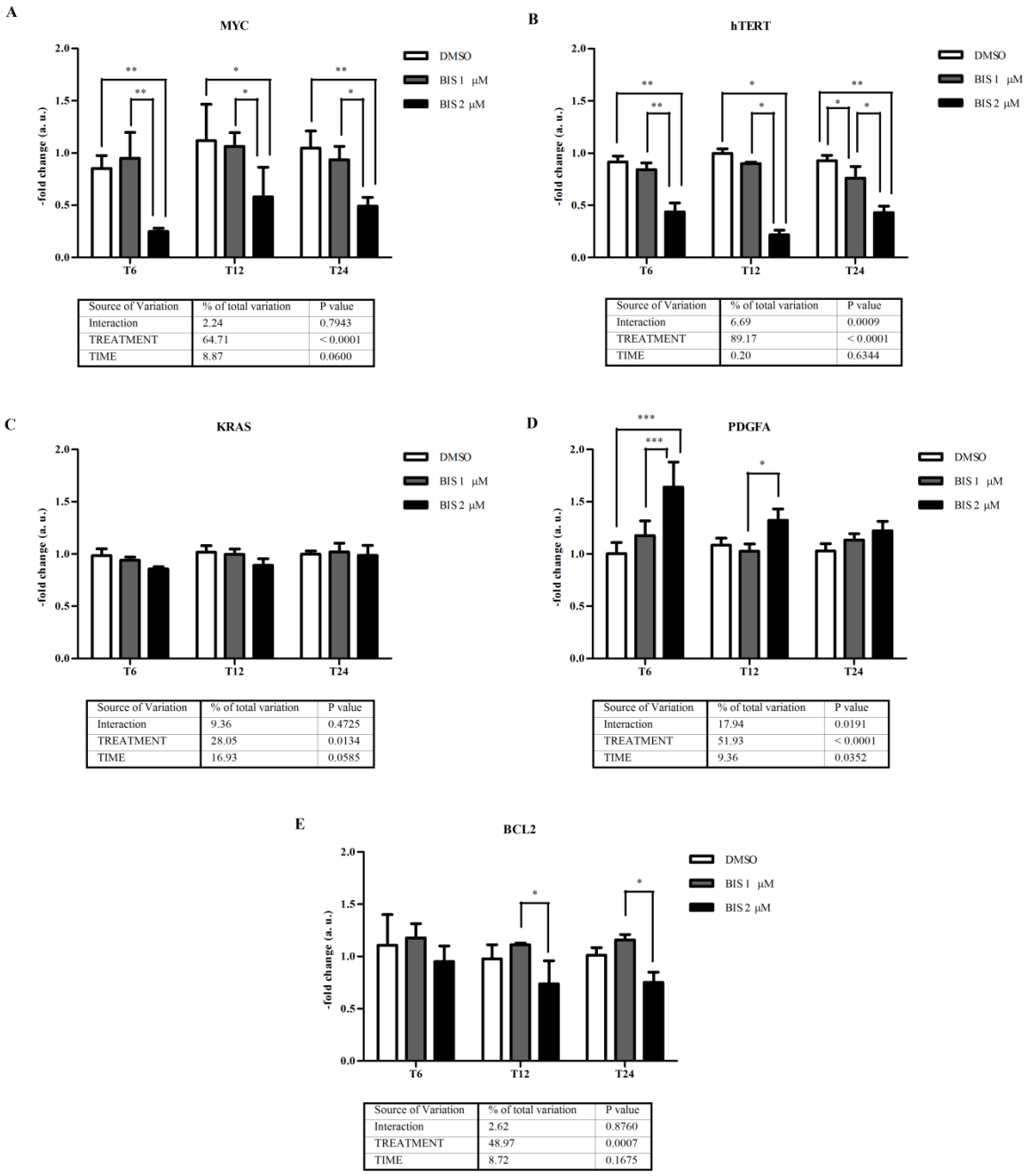

Source of Variation	% of total variation	P value
Interaction	2.24	0.7943
TREATMENT	64.71	< 0.0001
TIME	8.87	0.0600

Source of Variation	% of total variation	P value
Interaction	6.69	0.0009
TREATMENT	89.17	< 0.0001
TIME	0.20	0.6344

Source of Variation	% of total variation	P value
Interaction	9.36	0.4725
TREATMENT	28.05	0.0134
TIME	16.93	0.0585

Source of Variation	% of total variation	P value
Interaction	17.94	0.0191
TREATMENT	51.93	< 0.0001
TIME	9.36	0.0352

Source of Variation	% of total variation	P value
Interaction	2.62	0.8760
TREATMENT	48.97	0.0007
TIME	8.72	0.1675

***Figure 13**: Effect of exposure with AN6 on mRNA of oncogenes possessing G4 structures in MCF7. (A) MYC, (B) hTERT, (C) KRAS, (D) PDGFA and (E) BCL2 mRNA level were measured by using a qPCR approach, and data (arithmetic means ± S.D.) are expressed as n-fold change (a.u.) normalized to the RQ of control cells at each time (T_6, T_{12}, T_{24}) to which an arbitrary value of 1 was assigned. Two-way ANOVA followed by Bonferroni post-test was used to assess statistical differences between doses and time of treatment. *, **, ***: $p<0.05$; $p<0.01$; $p<0.001$.*

Finally, the exposure to AQ7 at 10 µM did not lead to a significant up- or down- regulation of *c-KIT* and the whole set of alternative genes considered in the present study (data not shown).

3.4.6 Confirmatory results with other cellular models

To confirm that the effective molecular target of AQ1 is located in *c-KIT* promoter, a proliferation study was undertaken in a new mast cell line, e.g. the SCF dependent ROSA cell line and, particularly, the WT cell line ($ROSA^{WT}$) as well as its SCF independent sub-clone $ROSA^{KITD816V}$, engineered by lentiviral transfection (Saleh et al., 2014) and consequently regulated by a different promoter. In Figure 14A the viability results obtained treating cells with imatinib at 1 μM as control of stable transfection were reported. As expected, $ROSA^{WT}$ were much more sensitive to the treatment then the sub-clone transfected with the imatinib resistant mutation KITD816V. As reported in Figure 14B, AQ1 significantly inhibited proliferation to a greater extent in $ROSA^{WT}$ than in $ROSA^{KITD816V}$. The absence of G4 in the promoter region of $ROSA^{KITD816V}$ favor the survival of cells under the treatment with AQ1.

The anti-proliferative effects of AQ1 were then tested in other three cell lines: the α155 and the HMC1.2 in which the growth strictly depends on *c-KIT*, and PC3 where *c-KIT* is not constitutively expressed (Simak et al., 2000). As shown in Figure 14C, an overall inhibition of cell proliferation was observed, with a different order of magnitude and significantly less relevant for the non-expressing *c-KIT* PC3 cell line. The same experiment was also repeated on other cell lines where *c-KIT* is not responsible for growth namely TOV112 ovarian cancer cells and KARPAS299 lymphoma cell line. Data obtained corroborated those described with PC3 cell line (data not shown). Interestingly, no differences in term of viability among AQ1 concentrations were noticed between α155 and HMC1.2 cell lines, while a differential response was visible after treatment with imatinib between imatinib-sensitive (α155) and imatinib-resistant (HMC1.2 and PC3) cell lines (Figure 14D). These results suggest that AQ1 and imatinib exert their actions at different molecular levels, because the former compound was not influenced by the mutation as the second.

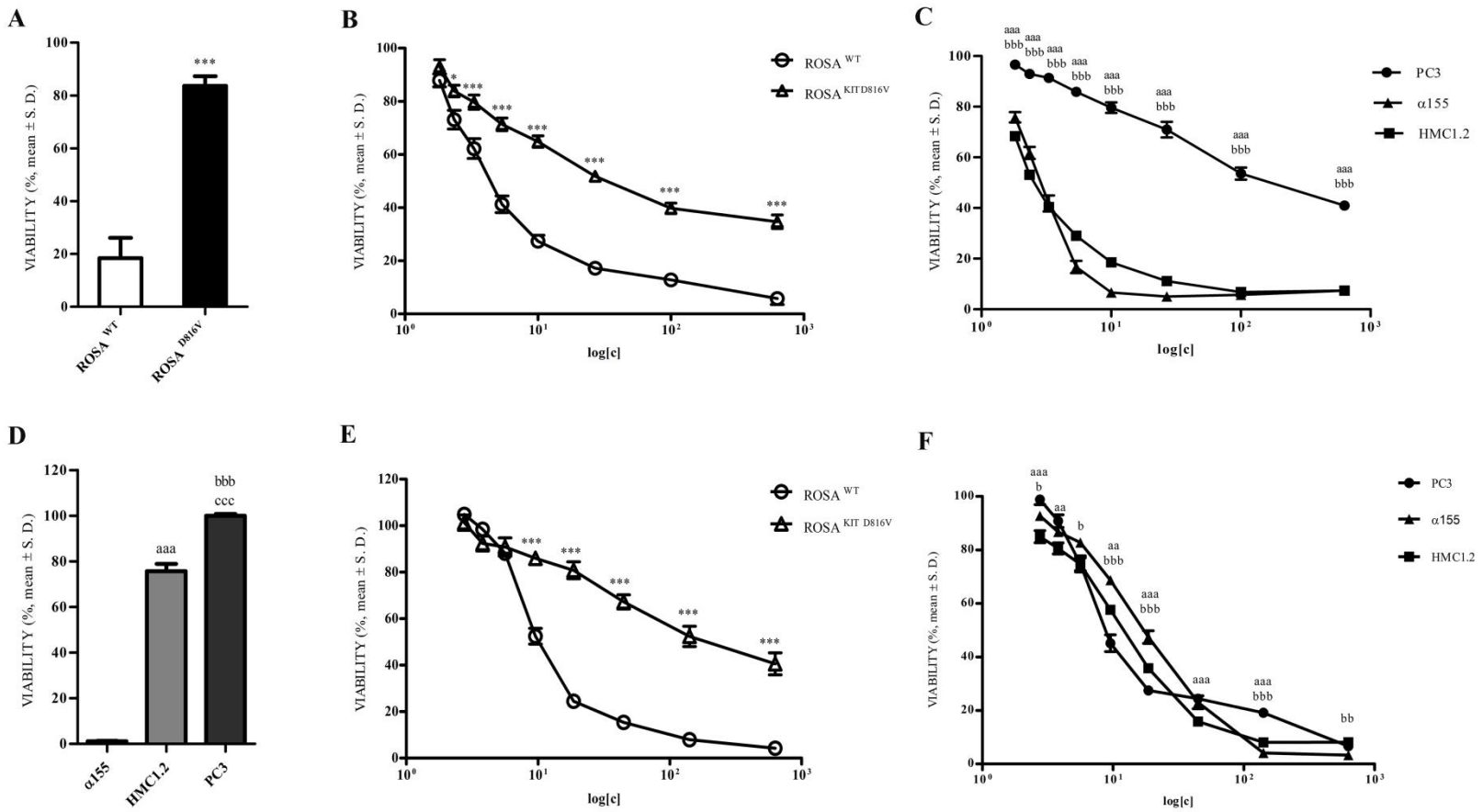

Figure 14. *Effect of exposure (72 hours) to imatinib, AQ1, and AN6 on proliferation of ROSA^{WT}, ROSA^{KITD816V}, α155, HMC1.2 and PC3 cell lines. Data are expressed as percentage of viability ± S.D. against cells treated only with the vehicle (DMSO). (A) Effect of imatinib 1 μM on ROSA cell lines. Student t-test. ***: P<0.001. (B) Effect of AQ1 on ROSA cell lines. Student t-test. *, ***: P<0.05; P<0.001. (C) Effect of AQ1 on α155, HMC1.2 and PC3. Student t-test. ^{aaa}: P<0.001 α155 vs PC3; ^{bbb}: P<0.001 HMC1.2 vs PC3. (D) Effect of imatinib 1 μM on α155, HMC1.2 and PC3 cell lines. One-way ANOVA followed by Bonferroni post-test. ^{aaa}: P<0.001 α155 vs HMC1.2; ^{bbb}: P<0.001 α155 vs PC3; ^{ccc}: P<0.001 HMC1.2 vs PC3. (E) Effect of AN6 on ROSA cell lines. Student t-test. ***: P<0.001. (F) Effect of AN6 on α155, HMC1.2 and PC3. Student t-test. ^{aa}, ^{aaa}: P<0.01; P<0.001 α155 vs PC3; $^{b, bb, bbb}$: P<0.05; P<0.01; P<0.001 HMC1.2 vs PC3.*

As far as AN6 is concerned, it seemed to bind specifically to the *c-KIT* promoter (Figure 14E). Indeed, a different pattern of inhibition between $ROSA^{WT}$ and $ROSA^{KITD816V}$ cells proliferation was noticed. Nevertheless, no antiproliferative effects were ever observed in PC3, α155 and HMC1.2 cell lines (Figure 14F). This would suggest a non-selective action of AN6 towards other G4 sequences, particularly when *c-KIT* is expressed to a lower extent or is undetectable. Consequently, and taking into account also the reduced inhibitory effect on *c-KIT* mRNA, we focused our attention on AQ1.

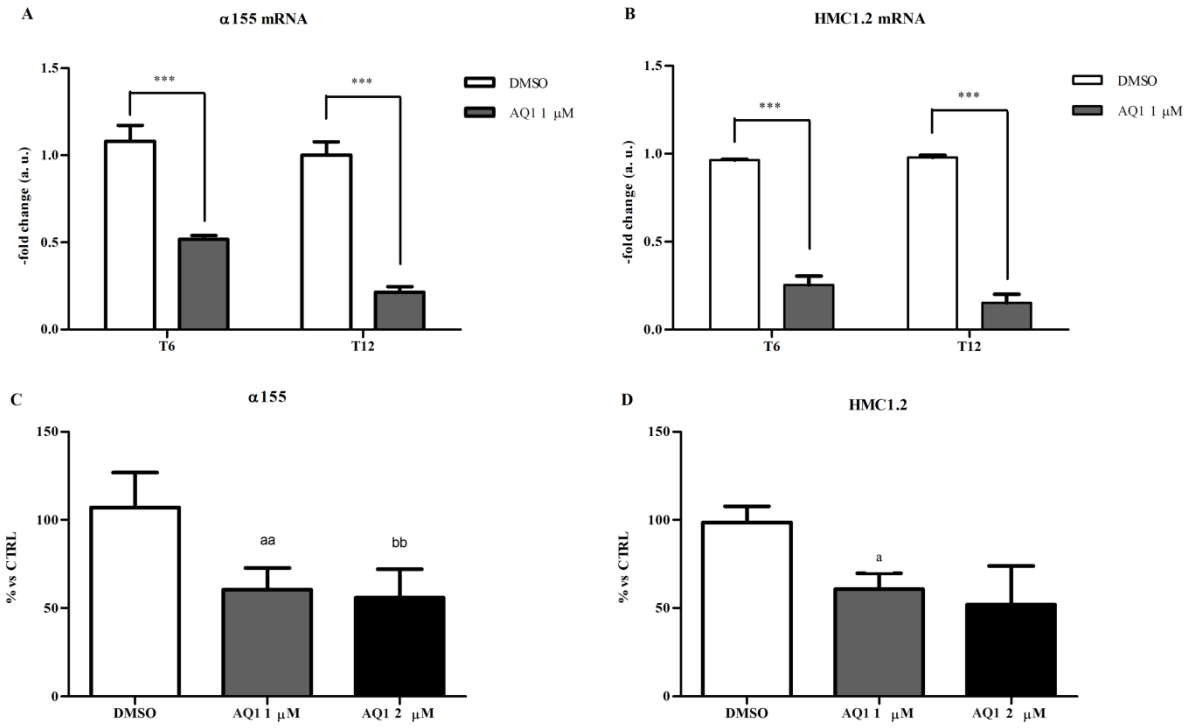

Figure 15. *Effect of AQ1 on c-KIT mRNA and protein in α155 and HMC1.2 cell lines. The c-KIT mRNA levels (A and B) were measured by qPCR, and data (arithmetic means ± S.D.) are expressed as n-fold change normalized to the RQ of control cells at each time (T_6, T_{12}) to which an arbitrary value of 1 (a.u.) was assigned. Two-way ANOVA, followed by Bonferroni post-test, was used to assess statistical differences between doses and time of treatment.* ****: P<0.001. The c-kit protein amounts (C and D) were measured by flow cytometry and data are expressed as n-fold change (a.u.) to the mFI of not treated cells. One-way ANOVA, followed by Bonferroni post-test, was used to assess statistical differences between cell treated with AQ1 and those treated with the vehicle (DMSO).* $^{a, aa}$*: P<0.05; P<0.01 DMSO vs 1 µM AQ1;* ^{bb}*: P<0.01 DMSO vs 2 µM AQ1.*

Following the treatment of α155 and HMC1.2 cell lines with 1 µM AQ1 (final concentration), we measured *c-KIT* mRNA and protein levels by qPCR and FACS, respectively. A significant transcriptional down-regulation was noticed, in both cell lines, after 6 and 12 hours of exposure (Figure 15A and 15B). This result was

confirmed at the post-translational level after 48 hours of exposure (Figure 15C and 15D).

An example of scatter plots and histograms obtained with α155 cell line is reported in Figure 16. Following the treatment with AQ1, the side-scatter of cell population change; this phenomenon might be attributed to a ligand-dependent morphological effect.

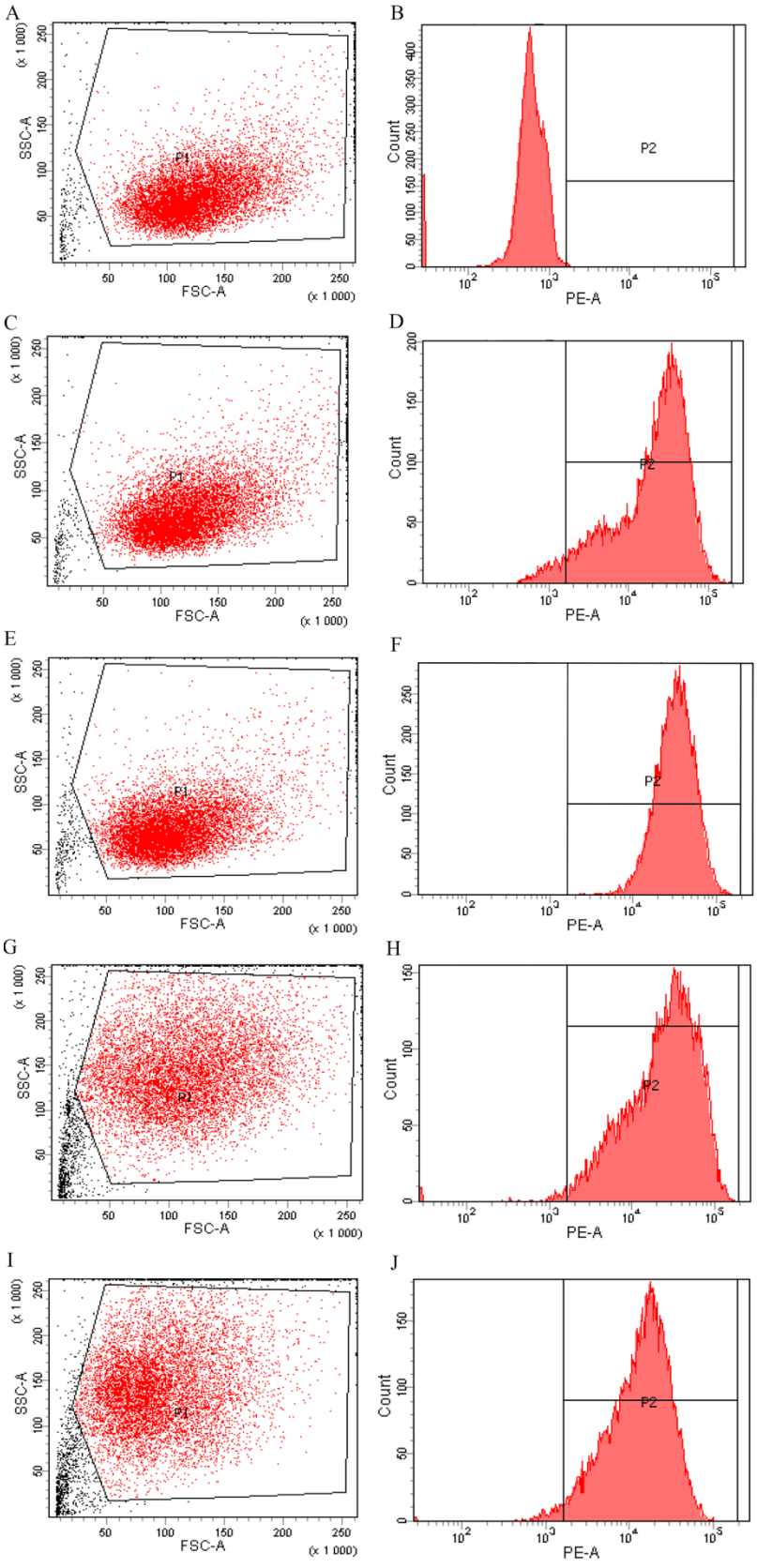

Figure 16: *Flow cytometry analysis of CD117 in α155 cell line. Morphological scatter plot with forward scatter (FSC) vs side scatter (SSC) and c-kit histogram plot of fluorescence intensity (FI) of different samples: (A) and (B) irrelevant antibody IgG; (C) and (D) control cells; (E) and (F) DMSO treated cells FI; (G) and (H) AQ1 1 μM treated cells; (I) and (J) AQ1 2 μM treated cells.*

To demonstrate that the inhibition of *c-KIT* protein was not due to a toxic effect, we performed the same experiment labeling the HLA complex, a protein supposed to be not influenced by the treatment. Data obtained with α155, HMC1.2 and KARPAS299 cell lines (the last one survives independently from *c-KIT*) showed that HLA complex expression was never influenced by AQ1 exposure (see Figure 17).

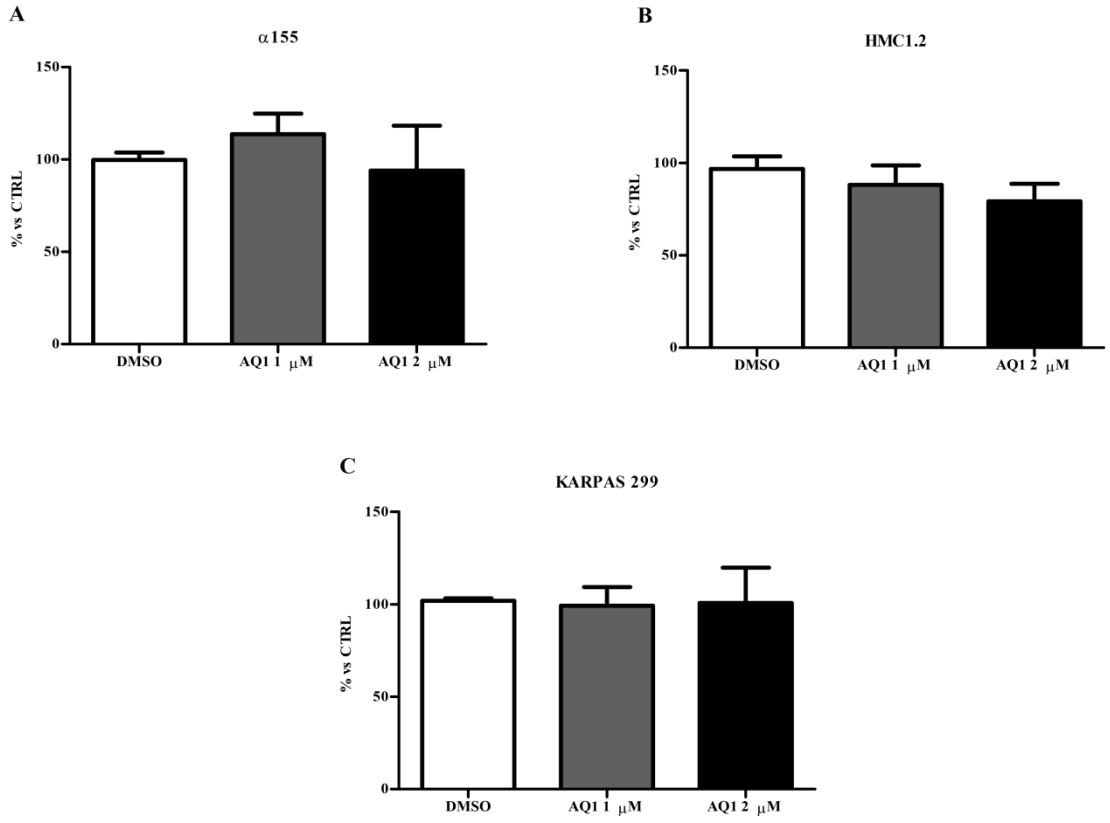

Figure 17: *Effect of treatment with AQ1 on HLA proteins of α155 (A), HMC1.2 (B) and KARPAS299 (C). HLA protein level was measured by flow cytometry and data are expressed as n-fold change (a. u.) to the mFI of not treated cells. One-way ANOVA with Bonferroni post-test were used to assess statistical differences between cell treated with AQ1 and those treated with the vehicle (DMSO).*

An example of scatter plots and histograms obtained with α155 cell line is reported in Figure 18. This would confirm that the occurring morphological changes were not due to a high non selective toxicity of our candidate G4-ligand.

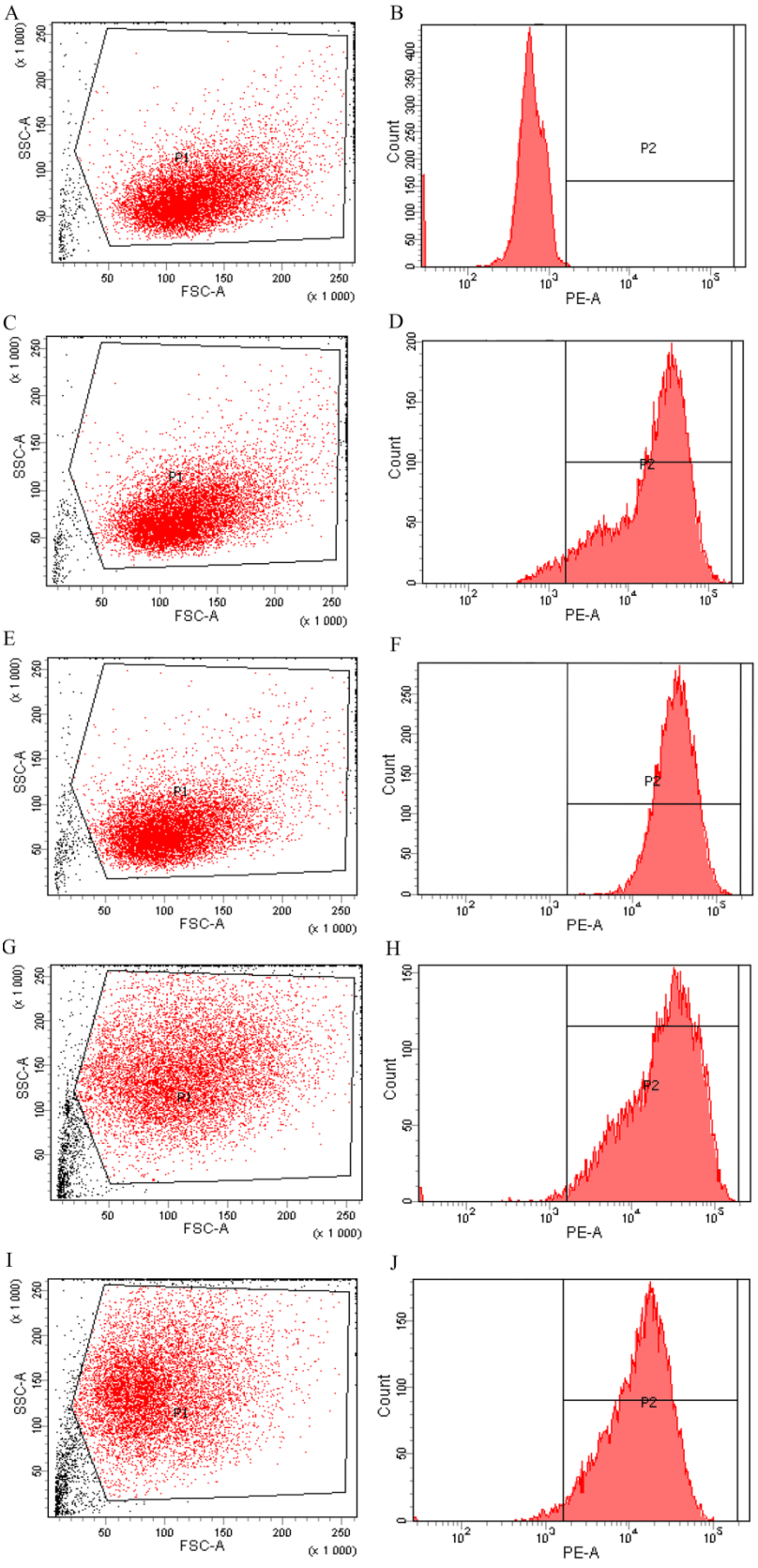

Figure 18: *Flow cytometry analysis of HLA in α155 cell line. Morphological scatter plot with forward scatter (FSC) vs side scatter (SSC) and HLA histogram plot of fluorescence intensity (FI) of different samples: (A) and (B) irrelevant antibody IgG; (C) and (D) control cells; (E) and (F) DMSO treated cells FI; (G) and (H) AQ1 1 µM treated cells; (I) and (J) AQ1 2 µM treated cells.*

3.5 DISCUSSION

The silencing of *c-KIT* is currently a promising therapeutic strategy to treat several types of cancers. Among the different tools, which can be applied to reach this goal, an interesting method is represented by G4-ligands. The advantages rest in the structural knowledge of the target (NMR and X-ray data of the G-rich promoter region of *c-KIT* are currently available) and on the small size of the potential ligands for these targets (thus allowing affordable subsequent optimization steps). To set the basis for a rational design of novel compounds working according to this mechanism, we started with a screening program of a library of compounds to clarify the molecular features required by a G4-ligand in order (a) to bind the selected KIT1 and KIT2 sequences and, (b) to consequently cause the downregulation of *c-KIT* expression in cancer cells.

As regards the target recognition step, the combination of two different binding assays (thermal stabilization of the G4 form of KIT1/KIT2 and the displacement of a G4-bound dye) allowed us to identify three potential candidates out of 39 tested derivatives. They belong to the AQ or AN series thus supporting that the tricyclic aromatic structure can properly recognize the desired targets.

Most of publications focused on *c-KIT* and G4 topic, use MCF7 and HGC27 cell lines as experimental *in vitro* models (Bejugam et al., 2007; Gunaratnam et al., 2009; Waller et al., 2009; McLuckie et al, 2011). Thus, our choice to test candidate G4-ligands on these cells reflects the need to use *in vitro* models suitable for this type of studies. Through the Alamar Blue cytotoxicity test, both AQ1 and AN6 provided lower IC_{50} values in HGC27 cell line than in MCF7 cell line. We could attribute such evidence to the different doubling time of the two cell lines (17 for HCG27 and 38 hours and MCF7). Indeed, the obtained IC_{50} values are usually and comparatively lower in cell lines with a shorter doubling time that, therefore, perform a higher number of cell cycles in an equal period of time (Baguley et al., 2002). The third ligand (AQ7) did not show any relevant antiproliferative effects even at the highest tested concentration (10 μM); moreover, no transcriptional effects were noticed on *c-KIT* expression; consequently, we decided to exclude it for the ensuing experiments. Nevertheless, this result is important because the affinity of AQ1 and AQ7 for the target sequence was comparable.

Overall, the most interesting results have been obtained with AQ1, followed by AN6.

The exposure to AQ1 resulted in a significant inhibition of *c-KIT* mRNA levels in both cell lines. Moreover, this transcriptional effect was confirmed at the protein level by flow cytometry. This inhibitory effect was more pronounced in MCF7 than in HGC27 cells, probably due to the different constitutive expression of the gene in the two cell lines. An analogous behavior has already been observed by Bejugam et al. (2007), in a similar study with a different G4-ligand. Once characterized the inhibitory effect of AQ1 on *c-KIT* expression, a set of confirmatory studies were undertaken by using cellular models commonly recruited to study the effects of TKIs on *c-KIT* expression (Gabillot-Carré et al., 2006; Saleh et al., 2014). Firstly, the experiment with ROSA cells clearly demonstrated that the observed inhibition of proliferation was effectively due to the binding of AQ1 to *c-KIT* promoter. Moreover, the α155 and HMC1.2 cell lines showed a high sensitivity to AQ1, while the prostate cancer cell line PC3 did not. This further result supports that AQ1 binds specifically the oncogene *c-KIT* affecting mostly the proliferation of α155 and HMC1.2 cell lines which growth strictly depends on *c-KIT*. In the PC3 cell line, that do not express the proto-oncogene, the proliferation is less inhibited and this could demonstrate the absence of functional binding with other potential G4 structures in the genome (Simak et al., 2000). Worth mentioning, in the present study we also demonstrated that HMC1.2, a cell line naturally possessing the mutation D816V in the *c-KIT* protein and therefore resistant to imatinib, was highly responsive to AQ1. It is well known that some *c-KIT* mutations could represent a limitation in the use of the TKIs; for example, mutations involving exon 17 such as D816V and occurring in around 80% of adult mastocytosis and some mutations of exon 9 in GIST (Liegl et al., 2008; Ustun et al., 2011). Present results are therefore very encouraging and unveil the potentialities of this compound also against tumor harboring *c-KIT* mutations in the coding region. The decrease of *c-KIT* mRNA and protein amounts, noticed in MCF7 and HGC27, were also confirmed on α155 and HMC1.2 cell lines. To the best of our knowledge this is the first screening of candidate G4-ligands undertaken in a panel of designed target-specific cell lines and ever published so far.

An important aspect that needs to be considered about G4-ligands is their affinity towards several different G4 structures that could be bound by the same molecule along the genome. However, it has been hypothesized that ligands capable

of binding several G4 structures might present an increased inhibitory effect due to interference on multiple cellular pathways (Chen et al., 2012). Boddupally et al., in 2012, when studied the effects of G4-ligands on *MYC'*s G4, demonstrated how two G4-ligands, previously proved to have high affinity toward *MYC'*s G4 in cell-free models, inhibited cell growth by modulating, at the same time, the expression of several genes. For this reason we decided to check for possible ligand interactions with other oncogenes that contain, in the promoter, one or more putative G4 sequences. In particular, we evidenced an inhibition of AQ1 against *BCL2* in both MCF7 and HGC27 (confirmed also in α155 and HMC1.2 cell lines; data not shown). Huang et al. (2004) clarified that the anthraquinones decreased *BCL2* expression and favored apoptosis. Present results confirmed this finding, despite the slighter inhibition noticed at the protein level, which has already been reported in other similar studies with other G4-ligands (Shen et al., 2013). At the same time, it is well documented that SCF, the endogenous *c-KIT* ligand, maintains the survival of human mast cells by repressing apoptosis through the expression of *BCL2* (Mekori et al., 2001); therefore, it is actually impossible to attribute the observed mRNA inhibition to a direct interaction of AQ1 with the G-rich region of *BCL2* or to an indirect repression due to the decrease of *c-KIT* mRNA.

In line with *in solution* data, the experiments in which we tested AN6 in *c-KIT*-dependent cell lines showed that this ligand effectively binds the G4 sequence of *c-KIT*, as demonstrated by the anti-proliferative effect measured in ROSA^{KITD816V} cells, where *c-KIT* expression is regulated by another promoter. At the same time, the proliferation studies conducted in the panel of cell lines showed a common and similar inhibition of cell replication irrespectively of their dependence upon *c-KIT* expression. This result might be justified with (a) a possible non-specific effect of AN6 on different cellular pathways or, (b) a lower affinity of AN6 for the G4 within *c-KIT* promoter, which might allow for a clearer detection of AN6-mediated effects on different cellular pathways. The AN6 exposure in MCF7 and HGC27 cell lines showed minor effect on *c-KIT* mRNA; however, c-kit protein was markedly inhibited. These contradictory results could derive from post-transcriptional modifications and/or the involvement of other pathways in c-kit mechanisms of regulation. To support such a hypothesis, we observed a decrease in *MYC* and *hTERT* and even an increase in *KRAS*, *PDGFA* and *PDGFRβ* gene expression. Noteworthy, the possible up-regulation of some target genes following the exposure to candidate

G4-ligands has already been described previously (Halder et al., 2012); therefore, more detailed studies are required to further decipher the exact mechanism underlying G4-mediated changes in oncogene transcription. Overall, taking into account that *c-KIT* was the gene target of the present study as well as that no differences in proliferation were noticed among the different cell lines, we cannot consider AN6 as a good candidate and worthy of further investigations.

In conclusion, this work exhaustively demonstrated the capability of a putative G4-ligand, that is AQ1, to decrease c-KIT mRNA and protein amounts and, consequently, block proliferation in different but target-designed cellular models. Present results constitute a solid starting point for further studies about this promising molecule(s). Future studies will be addressed to demonstrate the specific binding of AQ1 to *c-KIT* promoter and elucidate the exact molecular mechanism of cell damage induced by the treatment of AQ1 and resulting in the blockage of cell proliferation.

4. Targeting Canine *c-KIT* Promoter by Candidate DNA G-quadruplex Ligands

Adapted from: **Zorzan E., Da Ros S., Zorro Shahidian L., Palumbo M., Giantin M., Sissi C., and Dacasto M., 2015. Targeting Canine *c-KIT* Promoter by Candidate DNA G-quadruplex Ligands. Manuscript in preparation.**

4.1 ABSTRACT

G-quadruplexes (G4) are DNA secondary structures formed by stacked G-tetrads frequently located in telomeres and promoter regions of proto-oncogenes. Recently, two G-rich sequences, canine KIT1 (d_kit1) and KIT2 (d_kit2), folding into G4, have been identified in canine *c-KIT* promoter. In this study, three compounds known to stabilize specifically *KIT1* and *KIT2* G4 structures are tested in a canine cell line, in order to identify a promising G4 ligand able to decrease *c-KIT* expression in dog.

The 50% inhibitory concentration (IC_{50}) of each ligand was determined by using the Alamar Blue cytotoxicity test in the canine mast cell tumor (MCT) cell line C2. The constitutive gene expression of *c-KIT* and other proto-oncogenes (*BCL2, VEGFα, VEGFR2, KRAS, TERT*) mRNA was measured by quantitative RT-PCR (qPCR). Therefore, ligand time- and dose-dependent effects upon *c-KIT* and other target genes were evaluated by using qPCR.

In canine cells, target genes were shown to be constitutively expressed and measurable up to 96 hours of culture. Two compounds named AQ1 and AN6 significantly inhibited *c-KIT* mRNA and protein expression independently from times and ligand concentrations used.

From these preliminary data, both ligands could represent promising candidate for targeting canine *KIT*-dependent tumors such as MCT. However, such an assumption needs to be confirmed with further molecular studies.

4.2 INTRODUCTION

The G4 structure is formed in guanine-rich DNA sequences and consists in a stable, four-stranded structure alternative to the double helix conformation. Four guanine residues connected through Hoogsteen hydrogen bonds constitute a G-quartets and three or more quartets stacked one upon the other formed a G4 (Zhao et al., 2007). Bioinformatics analysis revealed that around 400,000 putative G4 forming sequences are present in the human genome. They are mainly located within the telomeres and in the promoter region of oncogenes, suggesting that these particular conformations may be involved in multiple cellular processes as telomerase maintenance, RNA transcription and translation (Bidzinska et al, 2013). Such hypothesis is supported by promising results, in terms of antiproliferative effects and gene regulation, obtained targeting G4 with small molecules that stabilize these structures. The first evidence of the role of G4 structures in the regulation of gene transcription derived from studies carried out on the v-myc avian myelocytomatosis viral oncogene homolog (MYC, Siddiqui-Jain et al., 2002). Recently, other studies demonstrated that two G4 sequences are located in the proximal promoter of the v-kit Hardy-Zuckerman 4 feline sarcoma viral oncogene homolog (c-*KIT*) proto-oncogene (Rankin et al., 2005; Fernando et al., 2006). It codes for a tyrosine kinase receptor implicated in cell survival, proliferation and differentiation; furthermore, the occurrence of activating mutations and/or overexpression of this gene can result in aberrant functions and oncogenic cellular transformation in mast cells, interstitial cells of Cajal and myeloid cells (Balasubramanian et al., 2011). Recent encouraging results were published about the human *c-KIT* stabilization by different classes of G4 ligands: trisubstituted isoalloxazines, bis-indole carboxamides, benzo[a]phenoxazines, anthraquinone and bisanthrene derivatives (Bejugam et al., 2007; Dash et al., 2008; McLuckie et al., 2011; Zorzan et al., chapter 3 of the present thesis).

In the canine species, the constitutive activation of c-kit and mutations occurring in its DNA sequence are considered relevant pathogenic events in the development of cutaneous mast cell tumor (MCT), the most common skin tumor of dogs (Marconato et al., 2014).

The advent of target therapy, and in particular the use of a new class of drugs called tyrosine kinase inhibitors, brought some benefits in the treatment of canine

MCT; however, potential resistance effects and a different selectivity of the drug depending by the mutational status of the gene sequence could occur (London et al., 2009; Bonkobara, 2015).

The presence of G4 sequence in genomes other than the human one has already been investigated, particularly in prokaryotes (Rawal et al., 2006), chicken (Du et al., 2007) and warm-blooded animals such as rat, mouse, dog and zebrafish (Zhao et al., 2007; Verma et al., 2008). Also in animals, the maximum frequency of G4 DNA motifs occur in the gene transcriptional regulatory region, comprised among the -500 and +499 base pairs, in particular in the 100 bp preceding the transcription starting site.

The recent discovery that canine *c-KIT* promoter presents, alike the human one, two putative G4 sequences surrounding a predicted Sp1 binding site, addressed us to test, in a canine MCT cell line, three candidate human G4 ligands previously investigated in two human established cell lines (Zorzan, chapter 3 of the present thesis). The conclusions published in Da Ros and co-authors in 2014 remarked that *KIT1* G4 was very similar among the two species, human and dog, while KIT2 sequence presented more differences that could vary the molecule binding. The aim of the present work was to establish the possibility to find a promising G4 ligand able to decrease *c-KIT* expression in dog and prevent malignant cell proliferation.

4.3 MATERIALS AND METHODS

4.3.1 Ligands

Information and characteristic of ligands tested in the present study (named AQ1, AQ7 and AN6) are reported in chapter 3 of the present thesis.

4.3.2 Cell cultures

The canine MCT cell line C2, expressing mutated *c-KIT* (48 bp internal tandem duplication in the juxtamembrane domain) was kindly provided by Dr. Patrice Dubreuil (Centre de Recherche en Cancérologie de Marseille, France). Cells were cultured in RPMI 1640 medium supplemented with 10% FBS, 2 mM L-glutamine, 1 mM sodium pyruvate and 1% penicillin/streptomycin (Gibco, Thermo Scientific, Waltham, USA).

Cell number and viability were checked by using Trypan Blue dye exclusion test (Sigma-Aldrich Co., St. Louis, USA). Cell cultures were checked for Mycoplasma contamination through PCR Mycoplasma Test Kit (PromoKine, Heidelberg, Germany). For all the experiments, cells were used from passage 5 to passage 15 maximum.

4.3.3 Characterization of the G4 sequence

The canine c-*KIT* proximal promoter region was amplified through PCR and cloned into TOPO TA vector as previously reported (Da Ros et al., 2014). Around 8 different colonies and plasmids were sequenced for the obtainment of the exact *c-KIT* G4 sequence present in C2 cell line.

4.3.4 G4-ligands cytotoxicity

Cells were seeded in microplates at a concentration of 2 x 10^4 cells per well; then, they were treated with AQ1, AQ7 and AN6 at concentrations ranging from 0.01 µM up to 10 µM. Additional wells exposed to the vehicle (DMSO, 0.1% final concentration) and medium alone were included in each experiment, too. After an exposure of 72 hours, proliferation and cytoxicity were checked by adding 20 µl of CellTiter-Blue® Cell Viability Assay (Alamar Blue, Promega, Madison, USA) to each well and the fluorescence was measured at 560 nm (excitation wavelength) and 590 nm (emission wavelength), by using a VICTOR™X4 Multilabel Plate Reader (Perkin Elmer, Waltham, USA). Three separate experiments were executed and each concentration was tested in sestuplicate.

4.3.5 Time-dependent constitutive expression of target genes

mRNA levels of seven genes known to contain putative G4 structures in their promoter were measured in cultured cells during 96 hours without treatment. Cells were seeded onto 6-well plates at a final concentration of 6 x 10^5 cells/well and collected after 6, 24, 48, 72 and 96 hours. Cell pellets were washed once with PBS 1X 0.02% EDTA and, finally, resuspended in 0.5 ml of TRIzol® reagent. The procedure of total RNA extraction, its quality and quantity evaluation and retrotranscription into cDNA are reported in chapter 3 of the present thesis.

The full list of primers used in the present study for qPCR analysis is reported in Table 1.

Gene	Sequence	Source	UPL probe
c-KIT	F: CCTTGGAAGTAGTAGATAAAGGATTCA R: CAGATCCACATTCTGTCCATCA	designed *ex novo*	#60
BCL2	F: ACAACGGAGGCTGGGAATG R: CCTTCAGAGACAGCCAGGAGAA	designed *ex novo*	#110
MYC	F: GCTGCACGAGGAGACACC R: TCAATTTCTTCTTCGTCCTCTTG	designed *ex novo*	#77
TERT	F: TGACGTGGAAGATGAAGGTG R: CTCTCTCCGACGGTGTTC	designed *ex novo*	#128
KRAS	F: TGTGGTAGTTGGAGCTGGTG R: TCCCTCATTGCACTGTACTCCT	designed *ex novo*	#62
VEGFA	F: CGT GCC CAC TGA GGA GTT R: GCC TTG ATG AGG TTT GAT CC	Giantin et al., 2012	#9
VEGFR2	F: GGAACCCAATCAGAGACCCA R: GTCTTTGCCATCCTGCTGAG	designed *ex novo*	#31
ATP5β	F: TCTGAAGGAGACCATCAAAGG R: AGAAGGCCTGTTCTGGAAGAT	Giantin et al., 2014	#120
GOLGA1	F: GGTGGCTCAGGAAGTTCAGA R: TATACGGCTGCTCTCCTGGT	Aresu et al., 2011	#149
CGI-119	F: TCTACAATCTAAGAGAGATTTCAGCAA R: TTCCTGACAAGCACAAAATCC	Aresu et al., 2011	#15
CCZ1	F: TGAAGCACTGCATTTAATTGTTTAT R: CTTCGGCAAAAATCCAATGT	Giantin, submitted manuscript	#148

Table 1: *Primers and probes used for the qPCR analysis either obtained from previous publications or specifically designed for this study. UPL=Universal Probe Library; VEGFR= vascular endothelial growth factor receptor; ATP5β= ATP synthase, H^+ transporting, mitochondrial F1 complex, beta polypeptide; GOLGA1= the Golgin A1; CGI-119= the transmembrane BAX inhibitor motif containing 4; CCZ1= CCZ1 vacuolar protein trafficking and biogenesis associated homolog.*

Candidate genes included were *c-KIT*, *c-MYC*, *VEGF*, *VEGFR2*, *KRAS*, *BCL2* and Telomerase Reverse Transcriptase (*TERT*). To design genes primers, the Primer3 software (*http://primer3.ut.ee/*) was used. Assay specificity was evaluated either *in*

silico, by using the BLAST tool, than experimentally by Power SYBR Green I (Life Technologies, Carlsbad, CA) amplification and melting curve analysis.

Quantitative real-time RT-PCR (qPCR) reactions (10 µl final volume) were performed as previously reported (Zorzan et al., chapter 3 of the present thesis) with 2.5 µl of 1:150 diluted cDNA. The analysis was performed in a LightCycler 480 Instrument (Roche Applied Science, Indianapolis, IN) using standard PCR conditions (95°C for 10 min; 45 cycles at 95°C for 10 s and at 60°C for 30 s; 40°C for 30 s). Calibration curves, using 3-fold serial dilutions of a cDNA pool, were performed, and corresponding values of slope, efficiency (E) and dynamic range are reported in Table 2. The qPCR assays with E (%) comprised between 90% and 110% were considered as acceptable.

Name	Slope	Efficiency (%)	Dinamic range	Error
c-KIT	-3.32	99.9	17.67-28.85	0.00544
BCL2	-3.42	95.9	26.36-36.46	0.0232
VEGFA	-3.29	101.4	22.04-31.05	0.00528
CGI-119	-3.43	95.7	23.23-31.64	0.00665
GOLGA1	-3.28	101.8	25.60-36.74	0.00866
ATP5*β*	-3.26	102.7	19.17-30.39	0.00585
CTBP1	-3.37	98.2	23.63-34.85	0.0104
CCZ1	-3.34	99.2	25.30-33.35	0.0116
KRAS	-3.33	99.7	20.97-32.11	0.00849
MYC	-3.34	99.4	22.40-33.06	0.0109
TERT	-3.21	105.1	27.12-37.92	0.0162
VEGFR2	-3.33	99.6	24.87-36.25	0.0393

***Table 2**: qPCR assay standard curve values for C2 cell line.*

The obtained qPCR data were analyzed using the LightCycler480 software release 1.5.0 (Roche Applied Science, Indianapolis, USA) and the second derivative

method; the mRNA relative quantification (RQ) was performed by using the ΔΔCt method (Livak et al., 2001). Four internal control genes (ICGs), e.g. ATP synthase, H^+ transporting, mitochondrial F1 complex, beta polypeptide (*ATP5β*), the Golgin A1 (*GOLGA1*), the transmembrane BAX inhibitor motif containing 4 (*CGI-119*) and CCZ1 vacuolar protein trafficking and biogenesis associated homolog (*CCZ1*). These genes were amplified in all samples, but only ICGs genes whose expression was not statistically modulated during experimental conditions were used for the relative quantification. A cDNA pool was used as calibrator.

Experiments were performed in triplicate and, for each experiment, two biological replicates were included.

4.3.6 Transcriptional effects of G4-ligands on target genes

Cells were incubated with vehicle (DMSO, 0.1% final concentration) or two sub-cytotoxic doses of G4-ligands. After 6, 12 and 24 hours of incubation, cell pellets were collected as described above. Methods used for RNA extraction, reverse transcription and qPCR were the same described above. The ICGs expression was checked within every experimental condition and the choice of the most suitable ICGs to be used for normalization was cell line- and ligand-dependent. A cDNA pool was used as calibrator. Experiments were performed in triplicate and, for each experiment, three biological replicates were included.

4.3.7 Confirmatory post-translational effects of G4-ligands

The first day of experiment, 5.4 x 10^6 cells/well were seeded in Petri dishes and treated with AQ1 (final concentration 1.5 µM) or just with the vehicle (DMSO, 0.1% final concentration) for 24 hours. Cell pellets were washed with PBS 1X 0.02% EDTA, resuspended in RIPA buffer (50 mM Tris-HCl pH 7.4, 1% Triton X-100, 0.5% Na-deoxycholate, 0.1% SDS, 150 mM NaCl, 2 mM EDTA, 0.2 mM Sodium Orthovanadate, 1% protein inhibitor cocktail), incubate 30 min on ice and centrifuged for 10 min at high speed. Proteins were separated in 4-12% NuPAGE® Novex® Bis-Tris Gels by using the XCell SureLock™ Mini-Cell electrophoresis system (Thermo Scientific, Waltham, USA), and then transferred onto nitrocellulose filters through the iBlot™ Dry Blotting System (Thermo Scientific, Waltham, USA). On each gel, one prestained molecular marker (Thermo Scientific PageRuler Plus Prestained Protein Ladder, Thermo Scientific, Waltham, USA), one unstained molecular marker

(MagicMark™ XP Western Protein Standard, Thermo Scientific, Waltham, USA), and a *c-KIT* positive control (TF1 cells stable transfected with KITD816V and kindly provided by Drs. Patrice Dubreuil and Paulo De Sepulveda CRCM, Marseille, France) were loaded.

Membranes were incubated with goat anti-human c-KIT (C-14, Santa Cruz Biotechnology, Dallas, Texas, USA), and goat anti-human GAPDH (V-18, Santa Cruz Biotechnology, Dallas, Texas, USA) primary antibodies, both diluted 1:1000. The secondary antibody was a peroxidase conjugated anti-goat IgGs (Merck Spa, Milano, Italy). The peroxide signal was detected with the Super Signal West Pico Chemioluminescent Substrate Kit (Thermo Scientific, Waltham, USA).

Images were captured by Canon MG 5150 and the integrate optimal density of each band was measured with the program ImageJ. Data were normalized with GAPDH values, and the TF1 KITD816V was used as reference.

4.3.8 Statistical analysis

Data statistical analysis was performed by using GraphPad Prism version 5.00 for Windows (GraphPad Software, San Diego, USA). Any details about statistical analysis used in the proliferation experiment and in the qPCR expression analysis are reported in chapter 3 of the present thesis.

Immunoblotting data were expressed as a percentage of control integrated density, where control is represented by normal cells in culture. Variations between DMSO control cells and AQ1-treated cells were statistically evaluated by using the Student t-test.

4.4 RESULTS

4.4.1 Sequencing of the C2 c-KIT proximal promoter

Before testing the effects of the putative G4 ligands on canine cells, we confirmed that C2 cells possessed the exact KIT1 and KIT2 sequences already characterized by Da Ros et al. (2014); in particular, we focused our attention on nucleotide -159, owing to the polymorphism previously detected in dog samples (-159 G>A). The exact sequences of KIT1 and KIT2 are the following: KIT1: AGGGAGGGCGCCGGGAGGAGGG; KIT2: AGGAGGGGCGCGGGGAAGGGG.

4.4.2 Cytotoxicity tests and qPCR results

To identify a potential ligand for canine *KIT1* and *KIT2* G4 structures, three compounds were tested in canine C2 MCT cell line. By using the Alamar Blue cytotoxity test, the dose-response curve of each ligand was determined and the corresponding IC_{50} value identified. The IC_{50} values for AQ1, AN6 and AQ7 were 1,27 µM (R^2: 0.9813), 5,87 µM (R^2: 0.9721) and IC_{50}>10 µM, respectively. In Figure 1, dose-response curves for AQ1 and AN6 are reported.

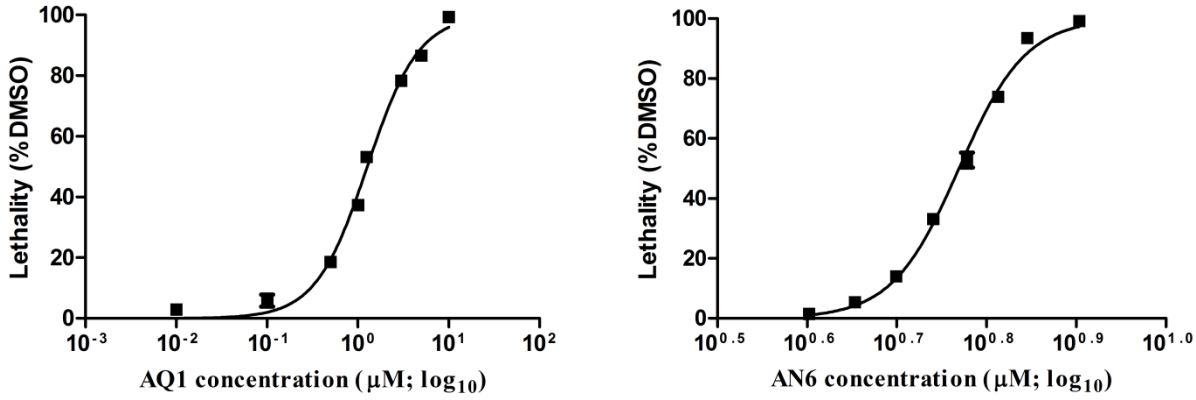

Figure 1*: Dose-response curves of AQ1 and AN6 tested in canine C2 MCT cell line. Data are expressed as mean values ± standard deviation of three independent experiments, each one performed in different passages.*

The constitutive expression analysis was indicative of a variable expression for almost all the genes taken into account in the present study (see Figure 2). The *c-KIT* and *KRAS* expressions were not affected by time of culture, while a significant decrease, after 24 or 48 hours, was noticed for *BCL2*, *MYC* and *hTERT* expressions. The unique gene showing increased (up to 96 hours) mRNA level depending on time was VEGFA.

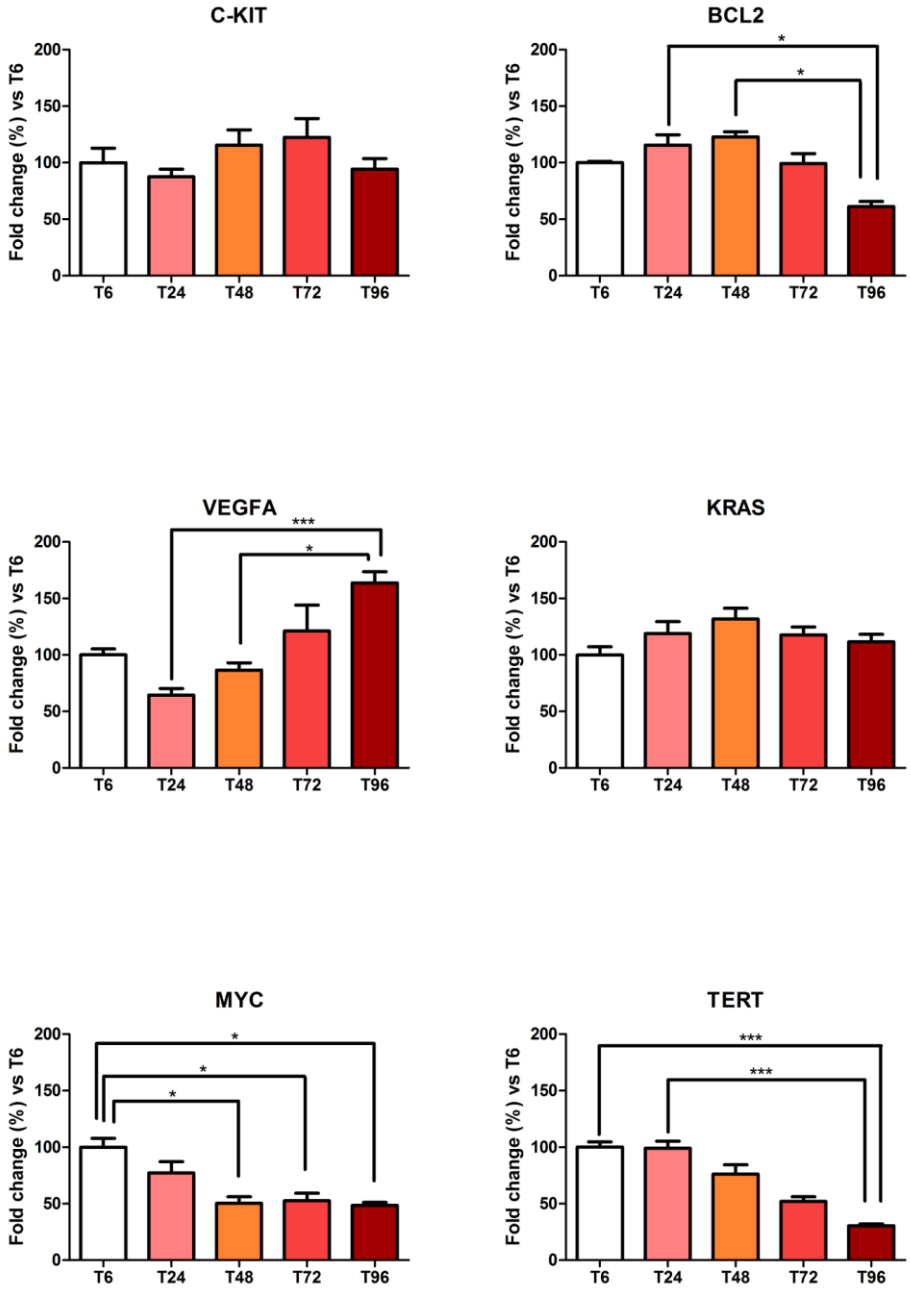

***Figure 2**. Effects of culturing time on gene expression. Total RNA was isolated from C2 cells and c-KIT, BCL2, VEGFA, KRAS, MYC and hTERT mRNA levels were measured by using a qPCR approach. Data (arithmetic means ± S.D.) are expressed as n-fold change (a.u.) normalized to the RQ mean value of cells stopped at T_6, to which an arbitrary value of 100 was assigned. *: P<0.05; ***: P<0.001.*

Taking into consideration these results, we decided to treat cells with the three putative ligands at two sub-cytotoxic doses and three different time points: T_6, T_{12} and T_{24} hours.

With regard to AQ7, as already seen in human cell lines, no significant effects on mRNA levels of target genes were ever detected for the genes included in the study (data not shown).

Concerning AQ1, Figure 3 shows a significant decrease in *c-KIT* mRNA at T_{12} and T_{24} with both concentrations. No differences between the two concentration were noticed. Transcriptional results were confirmed at the protein level, as shown in Figure 3. The densitometric analysis revealed a 2-fold significant inhibition of c-kit protein level following the exposure to 1.5 µM AQ1.

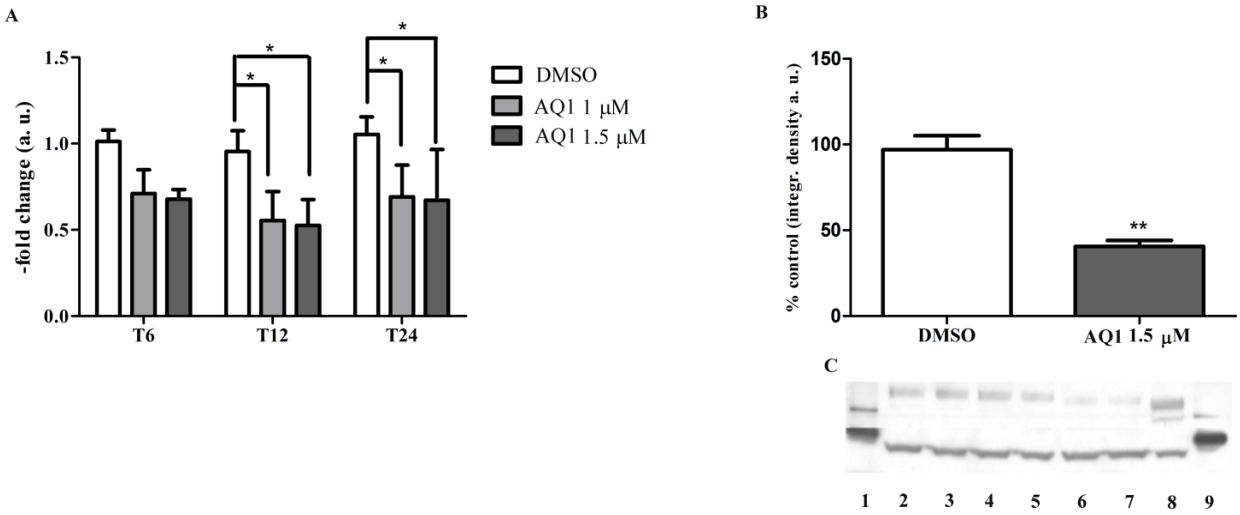

Figure 3: *Effect of AQ1 on c-KIT mRNA and protein amounts. (A) mRNA was measured using qPCR, and data (arithmetic means ± S.D.) are expressed as n-fold change (a.u.) normalized to the RQ of control cells at each time (T_6, T_{12}, T_{24}) to which an arbitrary value of 1 was assigned. Two-way ANOVA and Bonferroni post-test were used to find out statistical differences between doses and time of treatment. The c-KIT protein amount (B and C) was measured by immunoblotting, and data are expressed as n-fold change (a.u.) with respect to the densitometry untreated cells. Student t-test was used to assess statistical differences between cell treated with AQ1 and those treated with the vehicle only (DMSO).* *,***: P<0.05; P<0.01.*

Concerning the other target genes investigated, no significant effects were ever detected except for *BCL2*, for which a moderate inhibition at T_{12} with the highest dose was noticed (see Figure 4).

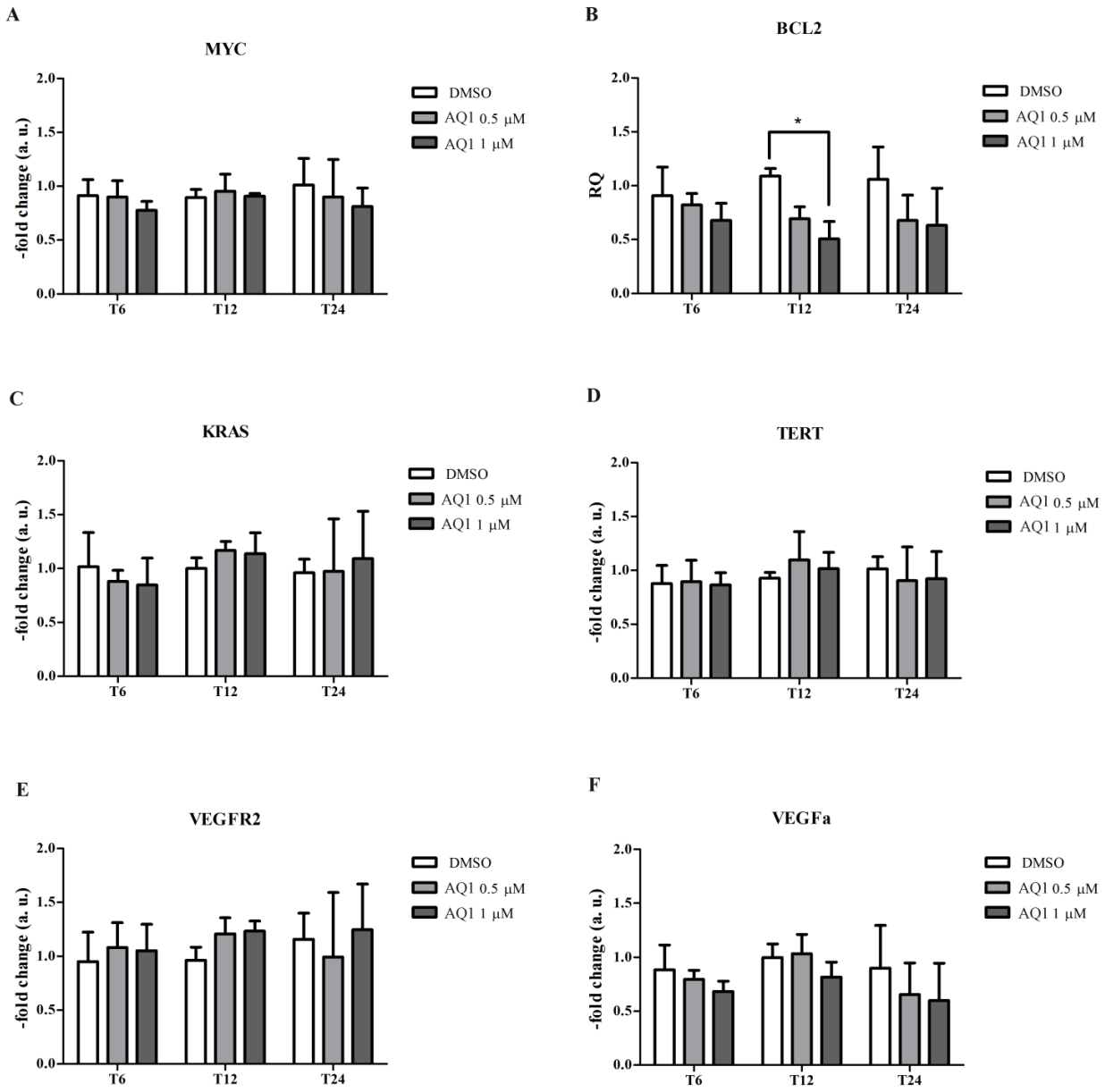

Figure 4: *Effect of AQ1 on MYC* (A), *BCL2* (B), *KRAS* (C), *TERT* (D), *VEGFR2* (E), *VEGFα* (F) *mRNA. mRNA levels were measured using qPCR, and data (arithmetic means ± S.D.) are expressed as n-fold change (a.u.) normalized to the RQ value of corresponding control cells (T_6, T_{12}, T_{24}) to whom an arbitrary value of 1 was assigned. Two-way ANOVA and Bonferroni post-test were used to check for statistical differences between doses and time of treatment.*

About AN6 (Figure 5), the two-way ANOVA showed an overall significant decrease of *c-KIT* mRNA at the highest ligand concentration (4 µM), and a moderate down-regulation at T_{12} with the AN6 lowest dose (2 µM). Confirmatory post-transcriptional investigations (immunoblotting) showed a 2-fold decrease of c-kit protein, after 24 hours of exposure, with 4 µM AN6.

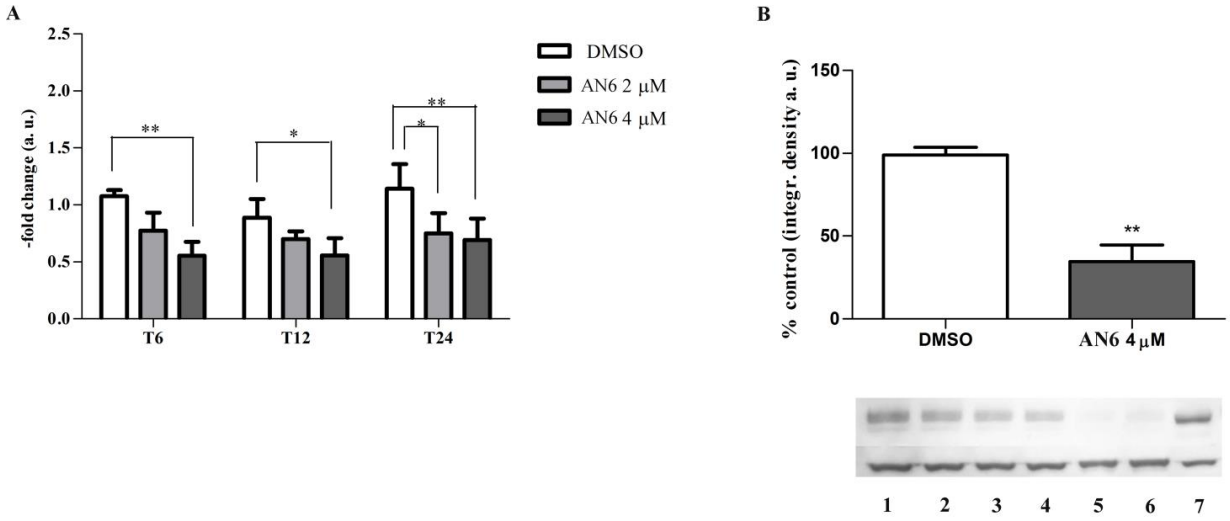

Figure 5: *Effect of AN6 on c-KIT mRNA and protein amounts. (A) mRNA was measured using qPCR, and data (arithmetic means ± S.D.) are expressed as n-fold change (a.u.) normalized to the RQ of control cells at each time (T_6, T_{12}, T_{24}) to which an arbitrary value of 1 was assigned. Two-way ANOVA and Bonferroni post-test were used to find out statistical differences between doses and time of treatment. The c-KIT protein amount (B and C) was measured by immunoblotting, and data are expressed as n-fold change (a. u.) with respect to the densitometry of untreated cells. Student t-test was used to assess statistical differences between cell treated with AN6 and those treated with the vehicle only (DMSO).* *,***: P<0.05; P<0.01.*

Other target gene mRNA levels did not show time- or treatment-dependent significant variations, with the exception of VEGFR2, for which a significant increase after 12 hours (T12) of exposure was noticed at the highest ligand concentration (Figure 6).

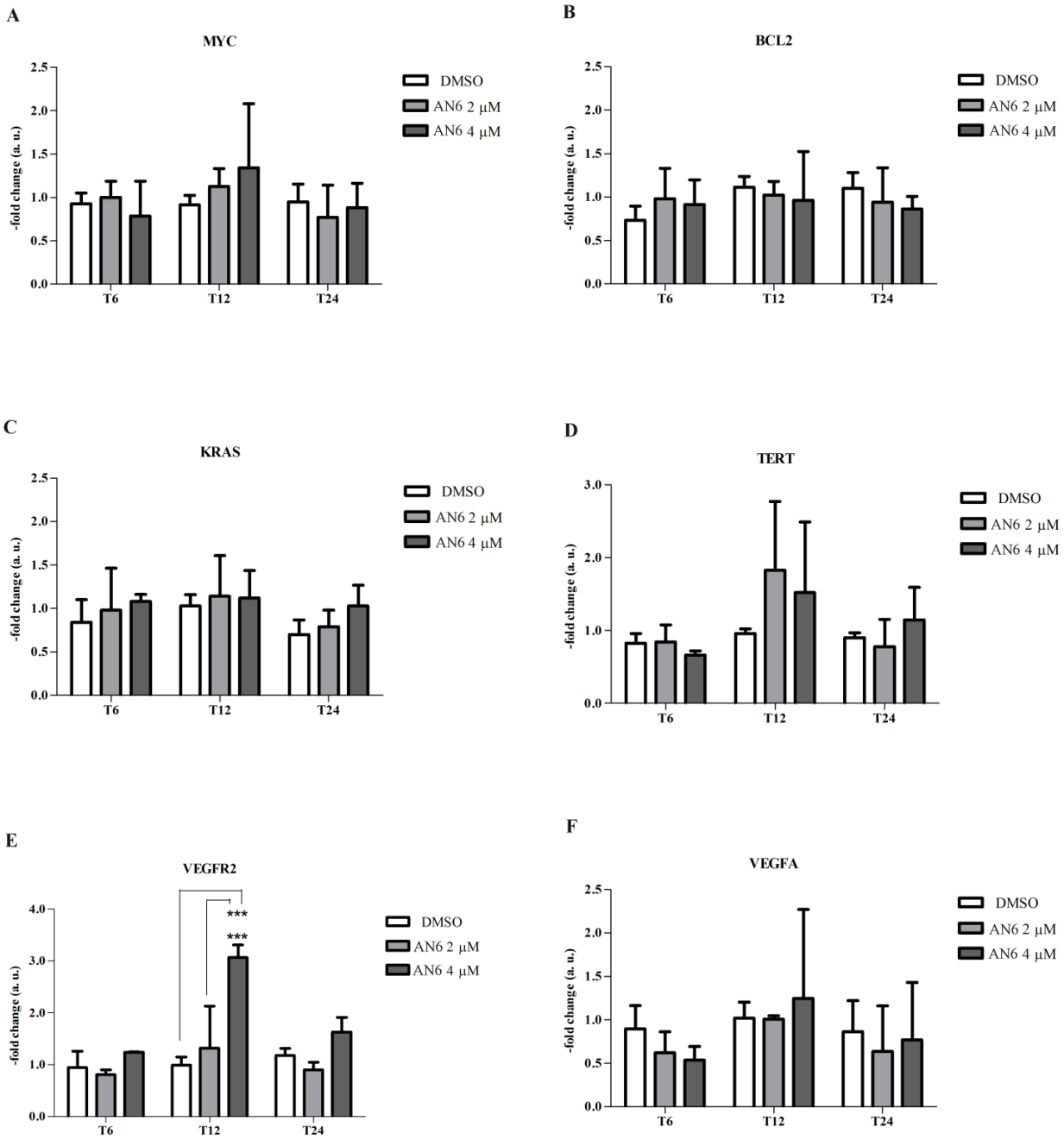

Figure 6: *Effect of AQ1 on MYC* (A), *BCL2* (B), *KRAS* (C), *TERT* (D), *VEGFR2* (E), *VEGFα* (F) *mRNA. mRNA levels were measured using qPCR, and data (arithmetic means ± S.D.) are expressed as n-fold change (a.u.) normalized to the RQ value of corresponding control cells (T_6, T_{12}, T_{24}) to whom an arbitrary value of 1 was assigned. Two-way ANOVA and Bonferroni post-test were used to check for statistical differences between doses and time of treatment.*

4.5 DISCUSSION

The discovery of G4 structures in specific, biologically important regions of the genome known to be essential for cancer cells to proliferate, made them a significant drug target; therefore, several compounds targeting these structures have been discovered and shown a promising anticancer activity. A number of molecules, showing good potentialities in term of G4 stabilization have been proposed as candidate anticancer drugs. However, the compounds discovered so far are either moving very slowly to clinical trials or have not yet fully passed pre-clinical investigations (Shalaby et al., 2013). In this sense, the discovery of two *c-KIT* G4 sequences in dog similar to human ones could be of help either to better understand the G4 biological functions *in vivo*, than to develop new G4-ligand candidates with realistic drug-like structures, higher selectivity and decreased side effects. Worth mentioning, even the domestic dog suffers of *c-KIT*-related tumors and indirectly could benefit from these novel strategies.

In the present study, three candidate G4 ligands, previously evaluated in human *in vitro* models, were tested in the canine C2 MCT cell line, which has been shown to be successfully used in TKIs validation studies (Dubreuil et al., 2009; Halsey et al., 2014). In term of cytotoxicity, AQ1 was proved to be as the most cytotoxic ligand, while AQ7 showed a value of $IC_{50} > 10$ µM, likewise to human cells. Considering the qPCR results, AQ7 did not elicit appreciable effects on *c-KIT* transcription, corroborating human data. Based on these results, it should be hypothesized that AQ7 might be unable to enter within the cell or, rather, it may possess a lower efficacy compared to other ligands.

Independently from the incubation times and concentrations used, AQ1 significantly down-regulated *c-KIT* mRNA. Nevertheless, if compared with human data, such an inhibition is less pronounced (2-fold decrease) than in human mast cell leukemia cells HMC1.2 (5-fold decrease). The inhibitory effect on *c-KIT* expression was confirmed also at the protein level in cells treated with the highest dose (1.5 µM).

Among the other tested oncogenes, only *BCL2* disclosed an inhibitory trend under treatment with AQ1, and such a down-regulation was significant at 12 hours in cells exposed to the highest G4-ligand concentration. This result was not unexpected; as a matter of fact, AQ1 caused a marked inhibition of *BCL2* mRNA also in human cells as reported in chapter 3 of the present thesis. This is partly confirmed by the

evidence, that anthraquinones compounds decrease *BCL2* levels and increase apoptosis (Huang et al., 2006).

By contrast, the bisantrene derivative AN6, let to a significant inhibition of *c-KIT* expression in canine cells while in humans such an effect was never observed. Even in this case, post-translational investigations confirmed the inhibition of gene transcription. Comparing results obtained in human and canine cells treated with this ligand, we should suppose that the different behavior observed between the two species could depend on differences between *KIT1* and *KIT2* G4. Multiple mutagenesis studies in human have already confirmed the direct correspondence between G-rich sequence composition, G4 conformation and ligand interaction; so, any modification in G4 sequences could influence the effectiveness of the ligand bond (Siddiqui-Jain et al., 2002; Patel et al., 2007; Tian et al., 2010).

Besides this, approximately 30–40% of human promoters contain a putative G4 motif, and actually there are no information about canine genome. Since many genes containing potential G4 structures are overexpressed in cancer tissues, striking importance assumes the development of highly selective G4 ligands avoiding an overall gene transcription inhibition, that could potentially result in non-specific toxicity. As regard AQ1, results are encouraging for both species. However, for AN6 some species specific differences seem to be present, and further investigations are needed to clarify in depth the affinity of this candidate compound against *c-KIT*.

To the best of our knowledge this work represent the first attempt to explore the capability of putative G4 ligands to inhibit *c-KIT* transcription in dog cancer, and particularly in a canine tumor cell line derived from MCTs. These preliminary results demonstrate that these ligands may decrease the *c-KIT* expression in cancer cells and seem encouraging particularly for canine *c-KIT*-dependent tumors such as MCTs.

Further studies are needed to demonstrate the specific action of these ligands against *c-KIT* G4. In this sense, chromatin immunoprecipitation and/or gene reporter assays might demonstrate whether AQ1 and AN6 really bind *KIT1* and *KIT2*. Furthermore, other *in vitro* models could be useful for an in depth characterization of molecular phenomena regulating gene inhibition and subsequent effects on kinase cascade and related pathways.

5. Concordance of *c-KIT* Mutational Status in Matched Primary and Metastatic Cutaneous Canine Mast Cell Tumors at Baseline

Adapted with the permission of Wiley from: **Marconato L.,* Zorzan E.,* Giantin M., Di Palma S., Cancedda S., and Dacasto M., 2014. Concordance of c-kit Mutational Status in Matched Primary and Metastatic Cutaneous Canine Mast Cell Tumors at Baseline: Implications for Clinical Practice. Journal of Veterinary Internal Medicine, 28: 547-553.**
* These authors contributed equally to this work.

5.1 ABSTRACT

Background: Mutation analysis of *c-KIT* is advisable before starting treatment with tyrosine kinase inhibitors in dogs with mast cell tumor (MCT), including those with metastatic disease. Testing is usually performed on primary tumors, assuming that *c-KIT* mutation status does not change in metastasis.

Hypothesis/Objectives: To give an insight into the mutational processes and to make a recommendation on the use of *c-KIT* mutational analysis in the clinical setting.

Animals: Twenty-one client-owned dogs with metastatic MCT.

Methods: Dogs undergoing resection or biopsy for both primary and matched metastatic MCT were prospectively enrolled. Total RNA or DNA was extracted from primary MCT and corresponding metastases. Exons 8, 9 and 11 were amplified by PCR and sequenced. Genetic features between primary MCT and metastases were compared. Their correlation with clinicopathological features was investigated.

Results: Concordance (mutated or wild type, WT) of mutational status, evaluable in 21 primary and matched metastatic (20 nodal and 1 splenic) MCTs, was 100%. Three new *c-KIT* mutations were identified. No significant correlation was noticed between *c-KIT* mutation and clinicopathological features.

Conclusions and Clinical Importance: *c-KIT* mutational status is conserved between any primary and its matched secondary tumor, suggesting that both can be used for *c-KIT* mutational testing. Targeted therapies might be also used to treat metastatic disease.

5.2 INTRODUCTION

The proto-oncogene *c-KIT* (*c-KIT*), which encodes for the transmembrane receptor c-kit, is known to play a critical role in mast cell development and tumors (Ma et al., 1999). In dogs, approximately 9 to 30% of mast cell tumors (MCTs) show *c-KIT* mutations, including internal tandem duplications (ITDs) in the juxtamembrane domain, resulting in constitutive activation of KIT in the absence of ligand binding (London et al., 1999; Ma et al., 1999), and activating point mutations in *c-KIT* extracellular domains (e.g., exons 8 and 9; Letard et al., 2008). In general, ITDs are associated with an increased risk of metastasis and local recurrence, higher tumor proliferation index, and aberrant KIT localization (London et al., 1999; Downing et al., 2002; Webster et al., 2006; Webster et al., 2007).

The importance of the mutational status has been elucidated by 2 clinical trials, which showed a lower objective response rate and a shorter survival time when tyrosine kinase inhibitors (TKIs) including toceranib and masitinib, respectively, were administered to dogs with wild-type (WT) tumors (Hahn et al., 2008; London et al., 2009). Although TKI-based therapy is used in dogs with MCT to also treat metastatic disease in the lymph nodes (London et al., 2009), *c-KIT* status is generally evaluated in the primary lesions because metastatic sites are rarely removed or biopsied before treatment. However, it is still unknown whether *c-KIT* status differs in metastases compared with primary tumors. The rationale for using small molecule inhibitors of oncogenic proteins as cancer therapies depends, at least in part, on the assumption that metastatic tumors are primarily clonal with respect to the mutant oncogene. If this is not the case, targeted therapies might only be partially efficacious. Therefore, it is of primary importance to verify the correlation between primaries and related metastases with regard to *c-KIT* status.

In people, controversy exists regarding the stability of mutational status in various tumors throughout the course of the disease, leading to metastases with different mutational status from that of the primary tumor (Ganceberg et al., 2002; Scartozzi et al., 2004; Italiano et al., 2006). In veterinary medicine there are only 2 studies comparing immunohistochemical phenotypes between primary mammary carcinomas and their related lymph node metastasis (Beha et al., 2012; Brunetti et al., 2013). In cats, concordance between primary mammary carcinoma and

matched metastasis was detected in 57.1% of cases (Brunetti et al., 2013), whereas in dogs in 65% of cases (Beha et al., 2012).

To the authors' knowledge, very few studies have been conducted in dogs on the rate of concordance in terms of *c-KIT* mutations. One study showed *c-KIT* ITD heterogeneity in different sites of multiple MCTs in 2 dogs (Amagai et al., 2013); in another study, *c-KIT* ITDs were used to provide evidence of tumor clonality in multiple MCTs developing over 1-2 years in 2 dogs (Zavodovskaja et al., 2004).

In the current study, we prospectively analyzed matched primary and metastatic MCT specimens for *c-KIT* intra- and inter-tumor heterogeneity, (1) to give an insight into the mutational processes, and (2) to make a recommendation on the use of *c-KIT* mutational analysis in the clinical setting. Moreover, the treatment with TKIs is associated with potential toxicity and high costs; additionally, resistance to certain TKIs is often due to secondary mutations of *c-KIT* (London et al., 2009; Gao et al., 2013), therefore it is important to critically review all aspects of the mutational testing to enhance upfront patient selection.

We hypothesized a discordance of *c-KIT* mutational status between matched primary and metastatic MCT, thereby recommending the use of *c-KIT* mutational testing on all involved sites.

5.3 MATERIALS AND METHODS

5.3.1 Case selection - Inclusion Criteria

Dogs with histologically confirmed MCT undergoing complete clinical staging and total or partial surgical excision of the primary tumor and corresponding metastasis were prospectively recruited. Treatment with neoadjuvant medical therapy (including steroids, chemotherapy, targeted therapy) was not permitted.

Background information recorded for each dog included: signalment, body weight, and primary tumor description (location, dimension, presence of ulceration, grade according to Patnaik and Kiupel's systems; Blackwood et al., 2012). Initial staging included history and physical examination, complete blood cell count with differential, serum biochemistry, coagulation profile, cytological

evaluation of the cutaneous nodule and regional lymph node, thoracic radiographs (3 views), abdominal ultrasound, fine-needle aspirates of liver and spleen regardless of their sonographic appearance, and cytologic examination of bone marrow obtained from the iliac crest. Lymph nodes or viscera were considered metastatic, if mast cells appeared in clusters or sheets, in very large numbers or atypical on morphology, as previously documented (Stefanello et al., 2009). Histologically, nodal metastatic spread was supported by the localization of mast cells in the subcapsular sinuses; special histochemical stains (Giemsa) were used to detect poorly granulated mast cells.

Written informed consent was obtained from all owners.

5.3.2 Tumor Specimens

Tumor samples were obtained by partial or total surgical resection from each primary MCT and matched metastasis before starting any medical treatment. To formulate a histologic diagnosis, samples were fixed in 10% buffered formalin, processed, and embedded in paraffin by using a standardized protocol. Slides were reviewed by a single board-certified pathologist (SDP), and histopathological criteria for diagnosis were based on those previously published for canine MCT (Patnaik et al., 1984; Kiupel et al., 2011).

With regards to *c-KIT* sequencing analysis, either one tissue core (2-mm diameter) or fine-needle aspirates (FNA) were obtained from each primary MCT sample and matched metastases. Specimens were submersed in a stabilization and storage solution (RNAlater® Solution, Life Technologies, Foster City, CA) and refrigerated at -20°C until use. Whenever the primary tumor was surgically excised by other veterinarians, 10 µm sections of the corresponding formalin-fixed and paraffin-embedded (FFPE) block were used for nucleic acid extraction.

5.3.3 Nucleic Acid Extraction

Total RNA was extracted from biopsies and FNA (Kobayashi et al., 2012) by using a nucleic acid isolation reagent (TRIzol® Reagent, Applied Biosystems, Foster City, CA) and a commercial kit (High Pure RNA Isolation Kit, Roche Applied Science, Indianapolis, IN), respectively, according to the manufacturer's instructions. Whenever nucleic acids were extracted from FFPE primary tumor sections, another commercial kit (AllPrep DNA/RNA FFPE kit, Qiagen, Milan,

Italy) was used. In this case, the genomic DNA was preferred to RNA because of the poor quality of the extracted RNA.

Nucleic acids yield and purity (260/280 and 260/230 nm absorbance ratios) were measured by using a spectrophotometer Nanodrop ND-1000 Spectrophotometer (Nanodrop Technologies, Wilmington, UK), whilst their quality was checked by 1% agarose gel electrophoresis. Two μg of total RNA were reverse transcribed by using a commercial kit (High Capacity cDNA Reverse Transcription Kit, Life Technologies, Foster City, CA). Both cDNA and DNA were finally stored at -20°C until use.

5.3.4 *c-KIT* Genotyping

Exons 8, 9, and 11 considered the hotspot regions for activating protein mutations were screened by PCR and direct sequencing (Letard et al., 2008; Torres-Cabala et al., 2009). To amplify either *c-KIT* exons 8, 9, and 11 (starting from cDNA) or exon 11 (from DNA), previously published primers pairs and PCR conditions were used (Giantin et al., 2012). Conversely, exons 8 and 9 primers for genomic DNA amplification were designed *ex novo* (Primer3 software, *http://primer3.ut.ee/*) and forward and reverse primers as well as the expected amplicon sizes are reported in Table 1.

exon	primer sequence (5'-3')	expected amplicon size (bp)
8	F: ACTCACTGGTTCCGATGCTC	408
	R: CCCTTAAAAAGCCACATGGA	
9	F: CACCCTTGGTTGAAAAAGGA	458
	R: ATATGGCAGGCAGAGCCTAA	

Table 1. *Primers for genomic DNA amplification and sequencing of c-KIT exons 8 and 9*

Amplifications were carried out in a thermocycler (TPersonal, Biometra GmbH, Goettingen, Germany) by using a commercially available PCR kit (GoTaq® Flexi DNA polymerase, Promega Corp., Madison, WI). Two μL of 5-fold diluted DNA were used as template, while primers (Eurofins MWG Operon,

Ebersberg, Germany) concentrations were 16.5 pmoles each. Amplicons were visualized in 1.5% agarose gel.

Whenever the presence of additional bands of different length (roughly 30 bp) was noticed, these ones were at first individually excised from the agarose gel and, then, purified with a commercial kit (High Pure PCR Cleanup Micro Kit, Roche Applied Science, Indianapolis, IN), according to the manufacturer's instructions. Hence, PCR products were sequenced, by using the same PCR primers, with either a capillary electrophoresis machine (ABI Prism 3100 Genetic Analyzer, Life Technologies, Foster City, CA) or an automatic sequencer (ABI 3730XL DNA Analyzer, Life Technologies, Foster City, CA).

Sequences were analyzed with a commercially available software (FinchTV software, Geospiza Inc., Seattle WA). Alignments with the WT *c-KIT* mRNA sequence NM_001003181.1, to discover potential single nucleotide polymorphisms (SNPs), ITDs or deletions, were performed by using an open source software Multalin (http://multalin.toulouse.inra.fr/multalin/).

5.3.5 Treatment and Response Criteria

The type of treatment was at the investigator's personal discretion, and included surgery, radiation therapy, chemotherapy, TKI or a combination of these. Response was determined by using RECIST criteria (Eisenhauer et al., 2009). Briefly, disappearance of all lesions was defined as complete response (CR); a decrease of at least 30% in the diameter of a lesion was defined as partial response (PR); the appearance of new MCTs or at least a 20% increase of the diameter of a lesion was defined as progressive disease (PD); less than 30% reduction or 20% increase in the diameter of a lesion was defined as stable disease (SD).

5.3.6 Statistical Analysis

To evaluate the relationship between *c-KIT* mutations and clinicopathological factors, data were analyzed by Fisher's exact test and Pearson χ^2 test. To this purpose, the following clinicopathological features were taken into account: gender (male or female), reproductive status (intact or neutered), breed (purebred or crossbred; predisposition to biologically aggressive MCTs [meaning advanced grade or clinical stage], e.g. Shar-pei and Labrador retriever), age ($<$ or $\geq$ 10 years), weight ($<$ or $\geq$ 10 kg), dimension of the primary lesion ($<$ or $\geq$ 3 cm),

clinical stage (II or III or IV), substage (a or b), and histological grading (both Patnaik and Kiupel's systems) (Kiupel et al., 2005; Murphy et al., 2006; White et al., 2011; Blackwood et al., 2012; Dobson, 2013). The anatomic site was categorized as benign or malignant, as some locations have been described as biologically aggressive (e.g. inguinal/perineal, head and neck, digit; Blackwood et al., 2012). Survival time was defined as the time interval between the initiation of treatment and death. Dogs dead from disease or MCT-related causes were classified as events; those dead for unrelated causes or lost to follow up at the time of the study closure were censored.

Statistical calculations were performed using a commercial software package (GraphPad Prism 5, San Diego, California, USA). For all statistical analysis, significance was set at $P < .05$.

5.4 RESULTS

5.4.1 Dogs and MCT Demographics

Between July 2011 and August 2013, 21 dogs met the inclusion criteria and were enrolled. There were 6 Labrador retrievers, 5 crossbred dogs, 3 Boxers, and one each of the following: Breton, Shih-Tzu, Shar-pei, Beagle, American Staffordshire terrier, German hound, and Dogue de Bordeaux. Twelve dogs were spayed females, 3 intact females, 4 intact males, and 2 castrated males. Median age was 8 years (range, 3 to 14 years), and median body weight was 26.7 kg (range, 7.4 to 50.2 kg).

Eighteen (86%) dogs had single lesions, and 3 (14%) had concurrent multiple tumors. In these latter ones, the biggest MCT was sampled for both histopathological and mutational analysis. MCTs were in various locations, including 6 (29%) dogs with tumors on distal limbs; 4 (19%) dogs with their tumors on the head; 3 (14%) dogs with digital MCTs; 2 (10%) dogs with tumors on proximal limbs; 2 (10%) dogs with vulvar tumors; and 1 (5%) dog with a MCT on the abdominal wall. All dogs with multiple tumors had them in the same regional areas (axillary region, head, and abdominal wall).

Histopathology was available for all primary MCTs: 14 (66%) dogs had Patnaik's grade 2 MCTs, 6 (29%) dogs had grade 3 MCTs, and 1 (5%) dog had a grade 1 MCT. Regarding the Kiupel's grading system, 11 (52%) tumors were classified as low grade MCTs, and 10 (48%) as high grade MCTs.

All dogs had metastatic disease: 20 (95%) dogs had regional lymph node involvement and, among these, 2 also had hepatic metastasis, 2 had splenic and hepatic metastasis, 1 had hepatic, splenic and marrow metastasis, 1 had splenic metastasis, and 1 had cutaneous metastasis. One (5%) dog had involvement of liver and spleen without regional lymph node metastasis. Lymph node metastases were confirmed in all 20 dogs by means of histopathology; the remaining dog without lymph node metastasis had only cytologic diagnosis of liver and spleen involvement.

Overall, 11 (52%) dogs had stage II disease, 8 (38%) dogs had stage IV disease, and 2 (10%) dogs had stage III disease. Sixteen (76%) dogs were asymptomatic (substage a), and 5 (24%) dogs had signs of systemic effects of MCT (vomiting, diarrhea, pruritus, and regional edema).

5.4.2 *c-KIT* Mutation Status

All specimens of primary tumors and paired metastases were suitable for *c-KIT* genotyping. Mutations of *c-KIT* sequence were detected in 3 (14%) MCTs: 1 in exon 8 (Figure 1), and 2 in exon 11 (Figure 2). Two of them were noticed in dogs with grade 3 MCTs, and 1 in a dog with a grade 2 MCT.

A new 28 amino acids (AAs) deletion affecting 10 AA codons, namely from Histidine-421 (H421) to Glutamine-430 (Q430), coupled with a contemporary insertion of 10 base pairs (bp) coding for four AAs (Leucine-Threonine-Phenylalanine-Methionine, LTFM), was detected in exon 8 (Figure 1).

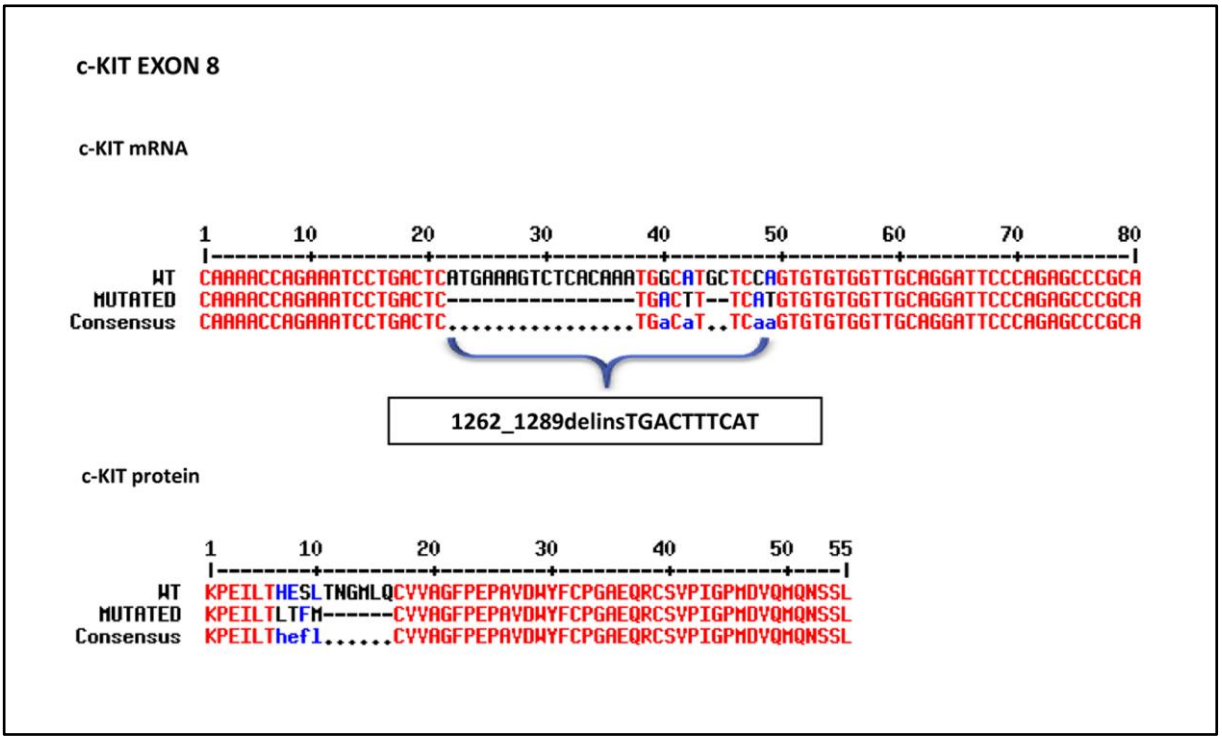

Figure 1. *Direct sequencing of c-KIT exon 8 from canine MCTs. Both wild type (WT) and mutated nucleotide and protein alignments sequences are reported. In cDNA obtained from primary tumor and matched metastasis (the corresponding lymph node), a deletion of 10 AAs (HESLTNGMLQ), associated with an insertion of 4 AAs (LTFM), was detected. This new c-KIT mutation was termed 1262_1289delinsTGACTTTCAT, according to the nomenclature for human sequence variations (Den Dunnen and Antonarakis, 2001).*

This mutation was named 1262_1289delinsTGACTTTCAT, in agreement with the nomenclature for human sequence variations (Den Dunnen and Antonarakis, 2001). Moreover, 2 new ITDs were found in exon 11 (Figure 2): a first one, consisting in the insertion of 12 AAs at the residue 571 ($ITD^{571-582}$), and a second one based on an addition of 14 AAs at the residue 574 ($ITD^{574-587}$).

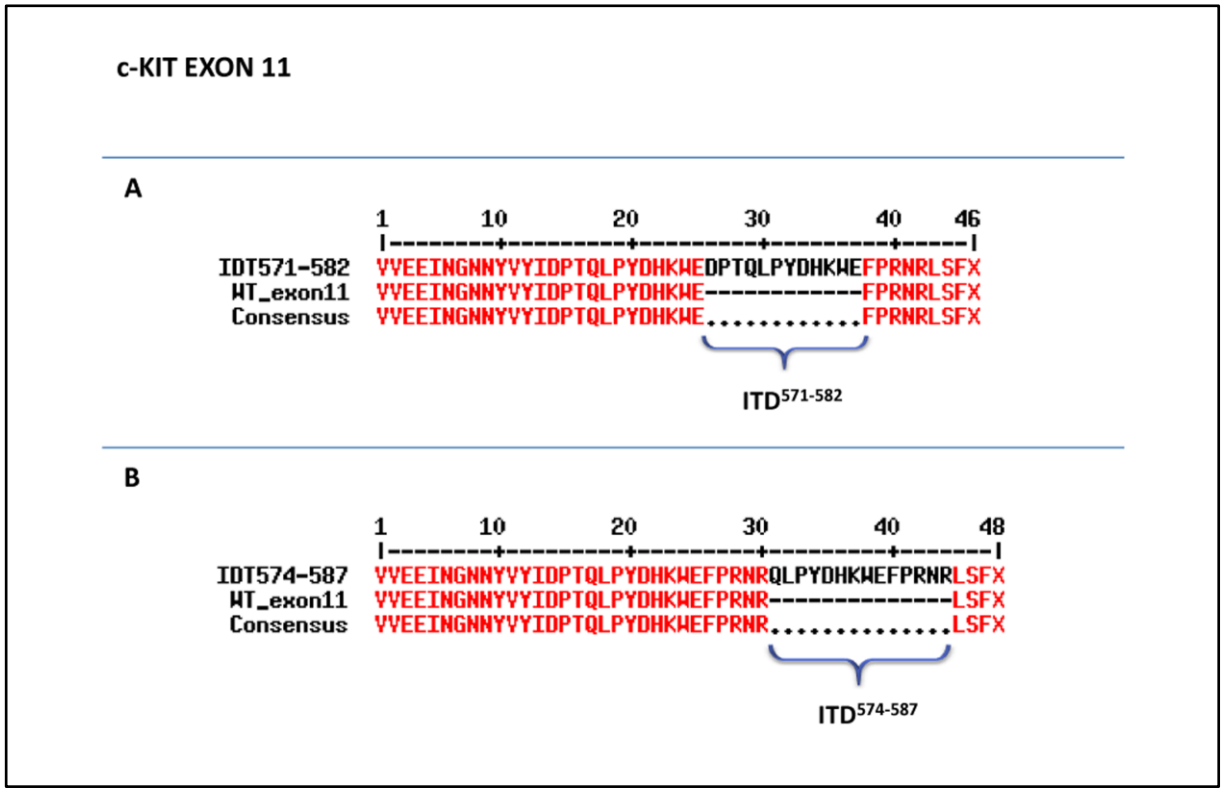

Figure 2. *Direct sequencing of mutant c-KIT exon 11 from canine MCTs. Both wild type (WT) and mutated nucleotide and protein alignments sequences are reported. Two ITDs, namely ITD*$^{571\text{-}582}$ *and ITD*$^{574\text{-}587}$*, were detected in cDNA obtained from primary tumor and matched metastasis (the corresponding lymph node).*

Furthermore, 2 already known silent SNPs were detected in exon 8 (1275G>A),[3] and in exon 11 (1759C>T; Zemke et al., 2002). The relative frequencies were 33% (7/21) and 5% (1/21), respectively.

Noteworthy, the comparison of *c-KIT* mutations and SNPs in primary tumors and corresponding metastases showed a concordance rate of 100%. Likewise, all dogs with a primary WT *c-KIT* genotype showed a WT *c-KIT* in their matched metastases.

5.4.3 Treatment and Clinical Follow-up

Eleven (52%) dogs (including the 3 dogs with *c-KIT* mutation) underwent surgical excision of their MCT. Four of these animals also received systemic chemotherapy (vinblastine and prednisone) as front-line treatment, 3 dogs received vinblastine and TKIs, 1 dog was treated with curative radiation therapy and TKIs, and 1 with curative radiation therapy and vinblastine. Two (10%) dogs received systemic chemotherapy (vinblastine and prednisone) as their only treatment. Six

(28%) dogs were treated with palliative radiation therapy; 4 out of these 6 also received vinblastine and prednisone, and 4 other ones TKI. Finally, 2 (10%) dogs were only treated with TKIs.

Overall, 11 (52%) dogs achieved CR, 7 (33%) dogs PR, 2 (10%) dogs SD, whereas 1 (5%) dog did not respond to the treatment and experienced PD. At the end of the study, 10 (48%) dogs were still alive with a median follow-up of 205 days (range, 41 to 473 days), and 11 (52%) dogs died or were euthanized because of progression of their MCT (n=10) or for tumor-unrelated causes (n=1). The overall median survival was 51 and 149 days for dogs harboring *c-KIT* mutations and with WT *c-KIT* gene, respectively.

5.4.4 Relationship between *c-KIT* Mutational Status and Clinicopathological Features

No significant correlation was found between primary *c-KIT* mutation and the considered clinicopathological characteristics (Table 2).

Variables		*c-KIT* mutation		
		positive	negative	*P* value
age (years)				
	<10	2	9	1.000*
	>10	1	9	
sex				
	male	2	4	0.184*
	female	1	14	
breed				
	pure breed	3	13	0.549*
	crossbred	0	5	
breed predisposition to aggressive MCTs				
	yes	2	5	0.247*
	no	1	13	
weight (kg)				
	<10	1	1	0.271*
	>10	2	17	
primary lesion, anatomic site				
	benign	0	11	0.090*
	malignant	3	7	
primary lesion, dimension (cm)				
	<3	1	9	1.000*
	>3	2	9	
metastatic lymph node				
	yes	3	17	1.000*
	no	0	1	
stage				
	I-II	0	11	0.097**
	III	1	1	
	IV	2	6	
substage				
	a	1	15	0.128*
	b	2	3	
histological grade (Patnaik)				
	I	0	1	0.283**
	II	1	13	
	III	2	4	
histological grade (Kiupel)				
	low	1	10	0.586*
	high	2	8	

Table 2. *Relationship between c-KIT mutational status and clinicopathological features in 21 primary MCTs. *: Fisher exact test; **: Pearson χ^2 test.*

5.5 DISCUSSION

In the current study, we compared *c-KIT* mutational status of exons 8, 9 and 11 between primary MCT and matched metastasis, and found a perfect (100%) concordance.

Metastatic MCT represents a major health problem in the canine population, but the introduction of a novel class of targeted antineoplastic agents directed against KIT, TKI, has significantly changed the therapeutic options available for these dogs (Hahn et al., 2008; London et al., 2009). Indeed, the important role of targeted therapy against molecules contributing to tumor development, progression, and metastasis has attracted considerable attention (London, 2009).

Because the identification of the mutational status of *c-KIT* could help to select dogs that have a high probability of benefiting from TKI (London et al., 2009), it is of primary importance to verify the degree of correlation between primaries and related metastases with regard to *c-KIT* status. Indeed, mutations are mainly evaluated at the primary site and there is little data available regarding the possible concordance in mutational status between the primary tumor and the corresponding metastases (London et al., 2009; Hahn et al., 2008). However, the death of metastatic cells is the main goal of treatment in a metastatic setting. These cells might be biologically different from the primary tumor, which has implications for the clinical management of MCT.

It is well known that the progression of cancer develops from a single mutated cell, followed by malignant clonal expansion secondary to additional genetic and genomic alterations. As a consequence, the ongoing acquisition of these alterations can result in the emergence of neoplastic subclones with varying genotypes and, consequently, phenotypes (Fidler and Kripke, 1977) leading to discordance between the primary tumor and its metastases. In people, several tumors including melanoma (Karatona et al., 2007), gastrointestinal stromal tumor (GIST; Liegl et al., 2008), and lung cancer (Taniguchi et al., 2008), show intra-tumor and inter-tumor heterogeneity, indicating the presence of more than one clone of cancer cells within a given neoplastic mass, and the presence of different genetic alterations in different metastatic sites from a single patient, respectively. Therefore, determining if there is homogeneous mutational status between primary

tumor and its metastatic sites has important clinical implications, over all to select the appropriate treatment.

To our knowledge, the question of mutational status in metastases versus primary MCT has not been addressed so far.

Compared to previously published studies, the mutational status of our case series, including both primary and secondary metastatic tumors, showed a similar proportion of *c-KIT* mutations (Giantin et al., 2012). Two already known SNPs were found in exon 8 and 11 (Zemke et al., 2002; Letard et al., 2008); furthermore, 3 novel mutations (1 in exon 8 and 2 in exon 11), with unknown clinical relevance, were found.

The data presented in this study provide evidence that the WT or mutated *c-KIT* genotype is conserved in primary MCTs and their matched, concurrent metastases. Although a similar behavior has been reported in human melanomas (Torres-Cabala et al., 2009), this result is somewhat surprising, in the light of genomic instability and heterogeneity that characterize most malignant tumors. In fact, it is generally accepted as true that loss of primary mutation and/or gain of secondary mutation might occur in patients regardless of the use chemotherapy or targeted therapy; such a phenomenon can be explained by the fact that cells with different mutations coexist within the primary tumor, and clonal selection for mutations during tumor progression might lead to different *c-KIT* mutations status in metastatic sites from that of the primary tumors (Amagai et al., 2013; Dai et al., 2013).

In the present analysis, discordant cases were not observed, pointing out that in canine MCTs *c-KIT* status is maintained in all cases unchanged during the metastatic process.

Another question, still matter of debate, is whether activating *c-KIT* mutations might be related to a poor prognosis in canine MCTs (Giantin et al., 2012; Takeuchi et al., 2013). Based on our results, dogs with *c-KIT* mutations had a shorter survival time when compared with dogs with WT MCTs. However, due to the different treatments and the limited number of mutated cases, conclusions on the prognostic relevance of *c-KIT* mutations cannot be drawn. Also, a number of variables, including gender, reproductive status, breed, age, weight, dimension of the primary lesion, clinical stage, substage, and histological grading, were evaluated to determine whether they were correlated to *c-KIT* status. None of these

variables were found to be significantly associated with the presence of *c-KIT* mutations, although the small population might have led to an insufficient power to detect differences between subgroups.

Although the current report is limited by the small sample size, our observations indicate that *c-KIT* mutation in the primary tumors might predict *c-KIT* mutated metastases with a reasonably high probability, suggesting that *c-KIT* mutation represents a very early mutational step in MCT pathogenesis and plays a central role in tumor progression. The implication of these results for general oncology practice is that both tissues of primary tumor or metastasis can be used for *c-KIT* mutation testing. However, the low number of mutated cases analyzed at the present time does not allow drawing any definitive conclusions about the *c-KIT* asset in synchronous and metachronous metastases, as well as their association with response to therapy.

Clearly, further molecular studies, carried out on dogs with metastatic MCT and receiving chemotherapy and/or TKI, are needed to clarify whether *c-KIT* genotype might be somewhat affected by anticancer drugs.

Finally, it must be stressed that the results of our study are valid for lymph node metastases and cannot be extrapolated to other metastatic locations, as only one dog with splenic involvement was evaluated here. The lymph node is the predominant site of metastases in the majority of dogs with metastatic MCT; therefore the results of our study of 20 lymph node metastases provide a reference for clinical decision-making as to TKI therapy. Nevertheless, as the molecular patterns might differ between metastatic sites (Stefanello et al., 2009; Amagai et al., 2013), and because *c-KIT* secondary mutations are likely to occur following TKIs administration (Wang et al., 2009; Ando et al., 2011; Gao et al., 2013), more results need to be obtained by testing additional metastatic sites, including spleen and liver, before and after targeted therapies. Also, the identification of new *c-KIT* ITDs underscores the need of further molecular investigations on their prognostic significance.

In conclusion, the mutational status seems to be stable during MCT metastasis, which is encouraging for TKI use in the clinical setting.

6. Mutational Hotpots of TET2, IDH1, IDH2, SRSF2, SF3B1, KRAS, and NRAS from Human Systemic Mastocytosis Are Not Conserved in Canine Mast Cell Tumors

Adapted with the permission of Plos One from: **Zorzan E., Hanssens K., Giantin M., Dacasto M., Dubreuil P., 2015. Mutational hotspot of TET2, IDH1, IDH2, SRSF2, SF3B1, KRAS, and NRAS from human systemic mastocytosis are not conserved in canine mast cell tumors. Plos One 12; 10(11): e0142450.**

6.1 ABSTRACT

Introduction: Both canine cutaneous mast cell tumor (MCT) and human systemic mastocytosis (SM) are characterized by abnormal proliferation and accumulation of mast cells in tissues and, frequently, by the presence of activating mutations in the receptor tyrosine kinase V-Kit Hardy-Zuckerman 4 Feline Sarcoma Viral Oncogene Homolog (*c-KIT*), albeit at different incidence (>80% in SM and 10-30% in MCT). In the last few years, it has been discovered that additional mutations in other genes belonging to the methylation system, the splicing machinery and cell signaling, contribute, with *c-KIT*, to SM pathogenesis and/or phenotype. In the present study, the mutational profile of the Tet methylcytosine dioxygenase 2 (TET2), the isocitrate dehydrogenases 1 and 2 (IDH1 and IDH2), the serine/arginine-rich splicing factor 2 (SRSF2), the splicing factor 3b subunit 1 (SF3B1), the Kirsten rat sarcoma viral oncogene homolog (KRAS) and the neuroblastoma RAS viral oncogene homolog (NRAS), commonly mutated in human myeloid malignancies and mastocytosis, was investigated in canine MCTs.

Methods: Using the Sanger sequencing method, a cohort of 75 DNA samples extracted from MCT biopsies already investigated for *c-KIT* mutations were screened for the "human-like" hot spot mutations of listed genes.

Results: No mutations were ever identified except for TET2 even if with low frequency (2.7%). In contrast to what is observed in human TET2 no frame-shift mutations were found in MCT samples.

Conclusion: Results obtained in this preliminary study are suggestive of a substantial difference between human SM and canine MCT if we consider some target genes known to be involved in the pathogenesis of human SM.

6.2 INTRODUCTION

In dogs, cutaneous mast cell tumor (MCT) is the most common skin tumor, and it accounts for up to 10-30% of all cases. MCTs occur mostly in the dermis and subcutaneous tissue but some visceral forms can also be located in other sites e.g. gastrointestinal tract and spine bone marrow as well as liver, oral cavity, urethra, salivary gland, nasopharynx and spleen (Ohmori et al., 2008; Blackwood et al., 2012; Takeuchi et al., 2010). It is commonly identified as a solitary neoplastic mass in the skin and/or subcutaneous tissue of older dogs, with a mean age of onset of approximately 9 years of age. Some dog breeds, such as Boxers, Labrador Retrievers and Shar Pei, are more prone to develop MCTs (Webster et al., 2007; Warland and Dobson, 2012).

Activating mutations of the tyrosine kinase receptor c-kit, which binds to stem cell factor (SCF), a known hematopoietic cytokine, have been described in canine MCTs. Mutations in *c-KIT* occur in 15-50% of MCTs, and have been associated with a more aggressive tumoral phenotype (Webster et al., 2006), possibly due to an increased proliferation and a resistance to apoptosis (Gleixner et al., 2007; Letard et al., 2008). The most common type of mutations identified in canine MCTs are internal tandem duplications (ITD) involving exon 11 (Zemke et al., 2002; Webster et al., 2006) but also deletions and point mutations in exons 8, 9 and 11 can occur (Ohmori et al., 2008; Takeuchi et al., 2013).

Human mastocytosis is a rare and clonal hematopoietic disease described as the proliferation and the accumulation of abnormal mast cells in the bone marrow and organs (Hanssens et al., 2014). Mastocytosis is schematically divided into cutaneous mastocytosis (CM) and systemic mastocytosis (SM). Localized mast cell tumors as mastocytomas and mast cell sarcoma are very rare. CM is usually diagnosed at birth or in childhood and spontaneously regress over time. However, some types are locally invasive, clinically very severe and, consequently, hard to treat. In most adult patients, the disease is systemic, although also the skin is often affected.

Most cases of SM are associated with the presence of activating mutations in the *c-KIT* proto-oncogene. The most frequent KIT genetic alteration is the substitution of aspartic acid to valine at position 816 (KIT D816V), that leads to the constitutive activation of the kinase domain of the receptor (Arock et al., 2015).

It has been recently discovered as further cooperating events may contribute to the phenotype and/or the pathogenesis of SM (Traina et al., 2012; De Vita et al., 2014) e.g. mutations in tet methylcytosine dioxygenase 2 (TET2) which have been reported in 40% of KIT D816V-positive SM cases (Tefferi et al., 2009). The enzyme TET2 regulates gene methylation and expression, catalyzing the conversion of 5-methylcytosine (5-mC) to 5-hydroxymethylcytosine (5-hmC) (Ito et al., 2011). In SM, it has recently been reported a more aggressive disease and an overall worse prognosis when there is the coexistence of KIT D816V and TET2 mutations (Soucie et al., 2012). Other mutations were identified in isocitrate dehydrogenase 1 and 2 (IDH1 and IDH2, respectively). They affect both histone modifications and DNA methylation, catalyzing the decarboxylation of isocitrate to alpha-ketoglutarate (or 2-oxoglutarate, 2-OG). Hotspot mutation sites are represented by heterozygous substitution clusters in conserved arginines R132 of IDH1 and R140 and R172 of IDH2 (Itzykson et al., 2013). Further additional mutations were found in genes encoding for components of the splicing machinery involved in the intron splicing during pre-mRNA maturation, in particular the serine/arginine-rich splicing factor 2 and the splicing factor 3b, subunit 1 (respectively SRSF2 and SF3B1). Overall, recent data are suggestive of a specific hierarchy, where TET2 gene alterations arise in early progenitor cells, while SRSF2 mutation can occur relatively later during the ontogeny but both prior to KIT mutation during the disease progression (Hanssens et al., 2014). Likewise, neuroblastoma RAS Viral (V-Ras) oncogene homolog (NRAS) mutations have also been reported in SM, having the potential to precede KITD816V in clonal development (Wilson et al., 2011).

Besides SM, loss-of-function mutations in TET2 as well as alterations in other genes mentioned above have been also reported in a variety of hematological malignancies, including acute myeloid leukemias (AMLs), chronic myelomonocytic leukemia (CMML), myeloproliferative neoplasms (MPNs), myelodysplastic syndromes (MDS) and lymphoid malignancies (Delhommeau et al., 2009; Langemeijer et al., 2009; Tefferi et al., 2009; Li et al., 2011; Moran-Crusio et al., 2011). To the best of our knowledge, no data on mutational status of these genes are available for canine MCTs.

In the present study, hypothesizing analogies in molecular mechanisms and gene dysfunctions with human SM and hematopoietic diseases, the mutation profile of genes commonly mutated in myeloid malignancies has been evaluated in a cohort

of 75 MCTs, most of them previously screened for *c-KIT* mutations (Letard et al., 2008).

6.3 MATERIALS AND METHODS

6.3.1 Samples and ethical statement

All tissue biopsies and blood samples were not specifically taken for the purposes of this study; they were part of authors *in-house* collections and were already used in previous studies (Hahn et al., 2008; Letard et al., 2008; Da Ros et al., 2014).

Tissue biopsies were originally collected as part of routine treatment procedures from dogs affected by at least one histologically-confirmed MCT (Patnaik grade II or III) (Patnaik et al., 1984), recurrent after surgery (as standard of care) and/or nonresectable. Female and male dogs, regardless of breed, were previously recruited with owner consent from veterinary clinics in France and in United States.

Blood samples were collected in Italy from 39 healthy random-source adult kennel dogs undergoing routine examination as described in details previously (Da Ros et al., 2014). An Institutional Animal Care and Use Committee approval number was not requested because of an agreement between the Faculty of Veterinary Medicine of University of Padua (Italy) and the kennel for the execution of routinary clinical checkups as described in details previously (Da Ros et al., 2014). Animal care was carried out in accordance with good veterinary practices.

6.3.2 DNA extraction, PCR and sequence analysis

Genomic DNA was extracted from 75 frozen canine MCT tissue samples using QIAamp DNA Mini Kit (Qiagen France, Paris, France), according to manufacturer's protocol. In the 23% of the cohort samples, different *c-KIT* mutations were previously identified in exons 8, 9 and 11 (Letard et al., 2008). Among them, internal tandem duplications of exon 11 represented 36% of total mutations registered.

In the present study, PCR amplifications of all TET2 coding exons and the hot-spot regions of IDH1 (exon 2), IDH2 (exon 1), SF3B1 (exons 13, 14, 15, 16), SRSF2 (exon 1), NRAS (exons 1, 2) and KRAS (exon 1) were executed. Primer oligonucleotide sequences were designed using the AmplifX software

(http://crn2m.univ-mrs.fr/AmplifX) and CanFam3.1 genome sequences available http://www.ncbi.nlm.nih.gov/. Primer sequences, are reported in Table 1. For every exon analyzed, the extreme parts of the flanking introns were also sequenced (around 100 bp upstream the 5´-end and downstream its 3´-end) to check for the presence of alternative splicing sites. All the detected variations were analyzed by using the tool Berkeley Drosophila Genome Project (BDGP, http://www.fruitfly.org) that computed splice sites predictions. Genes were amplified using Taq Phire® Hot Start II DNA Polymerase (Thermo Fisher Scientific, Walthman, MA, USA). The reaction mix contained the following reagents: 1X Phire® Reaction Buffer, 200 µM dNTPs, 0.5 µM of each primer and 0.15 µL of the enzyme (in a final volume of 22 µL). Approximately, 30 ng of genomic DNA were added to each PCR reaction and amplified through the following thermal protocol: an initial denaturation step at 98°C for 30 sec, an amplification step of 35-40 cycles (denaturation at 98°C for 5 sec, annealing at the primer-specific temperature for 5 sec and elongation at 72°C for 5-10 sec depending on the length of the PCR product) and a final elongation step at 72°C for 1 min. PCR products were purified and sequenced in an ABI 3730 sequencer. Sequence PCR reactions were performed with both primer forward (F) and reverse (R) using the Big Dye Terminator V1.1. (Applied Biosystem, Life Technologies, Carlsbad, USA) and the mix included: 3.2 pmol of oligo F or R, 1µL of Big Dye Terminator V1.1, 1X reaction buffer and water (in a final volume of 10 µL). The thermal protocol consisted in: an initial denaturation (1 min at 96°C) followed by 25 cycles of 10 sec at 96°C, 5 sec at 50°C and 2 min at 60°C.

GENE AND PRIMER SEQUENCES (5´-3´)	**EXON**	**TEMP. ANNEALING**	**PRODUCT LENGHT**
KRAS F: CTCATCTGTGGTCAACTGAA R: AGCCAATGGAACCCAAGTA	1	60°C	466 bp
IDH1 F: TGGCACTGTCTTCAGGGAAGCTAT R: TGGGCAACCAAGGACAGGAAAA	2	70°C	163 bp
IDH2 F: CTCCATCTCTGTCCTCGTAGAGT R: TTAGCACCGCTGCCATCCTTT	4	67°C	343 bp
NRAS F: TCTCTAGTTGTGGCTCGCCCATTA R:CAAAAGCCAGAGGTAGGGTCAGT	1	65°C	223 bp

F:GCTAGGAGCTTATCTAACCTTGGC R: TGCGGTATCCTCATTTCCTGTTCC	2	60°C	367 bp
SF3B1 F: ACTGGAGGATCAAGAGCGTCAT R: GCTGTCGTGTTACGGACATACT	13	67°C	1101 bp
F: ATGCTAGAGTGGAAGGTCGAGA R: TGTGTTGGCGGATACCCTT	14	67°C	855 bp
F: GACCATTAGCGCTTTGGCCATT R: GTTCCACAACACTGCTTCACCA	15-16	67°C	529 bp
TET2 F: AGCCTGATGGAACAGGATAGA R: GCCTGACTGTTAATGGCA	3	60°C	782 bp
F:CAAGAAAGTAATCCAGGCAAAGGC R: AATACCGTTCAGAGCTGCCA	3	60°C	718 bp
F: CCTGTCCCTTCCAGAAACCAGAAA R: TGTTGGGTTATGCTTGAGGTGTTC	3	60°C	605 bp
F: CCCCAACCAAAGTAACACAGCTCT R: GCTTTGGATGAAGGGTCTGTCTTG	3	60°C	702 bp
F: GGCATCACTGCGGTCAGTTCTT R: ATTCTGTCCTTGCTCCAATCCCA	3	60°C	715 bp
F: TCCCAAGGCAACAATGATCAGC R: GGGGTGGAATCTCTTGCTTAGTTG	3	60°C	760 bp
F: CTCCCCAGAAGGACATTCAAAAG R: CTCTCTTGCACAGCACAAGCAT	3	60°C	784 bp
F: GGATAAGCTTTGTGGATGTAGCCT R: GCTCGCAGACTATTAGTCCTGT	4	60°C	371 bp
F: TCCAGTTTGCTTGGCTTAGAC R: GAGCAACGTTCATTTCAACTAGC	5	60°C	380 bp
F: AATGCCCTAGTTGTGACCCAG R: AAATGTCGGTTCAACTCCCTTCCC	6	60°C	421 bp
F: CCAGAATCCAAGATTGGTAGCC R: GACTGCTTACTTCATCTGTACTCA	7	60°C	295 bp
F: TCATTTGGATCTAGGCTGTAGGGG R: AACAGAACACTGTGGCTTCACT	8	65°C	336 bp
F: CGAGAGTCTTTCTGACCTGTTC R: AAGGTCACCTTTGCAACAGC	9	60°C	398 bp
F: AGGCATGTCACTAATCTGGTCCAA R:GGGACTTCAGGGAAGATTCTGGTA	10	60°C	638 bp
F: GGGGTTCTCACATACATTTAAGCA R: GAGCTGTTGAACATGCCTGG	11	65°C	920 bp
F: ACTTCATGGGAGCCACCTCTAGAT R: AGACAGGTTGGTTGGTTGGTTGTG	11	60°C	853 bp

Table 1. *Forward (F) and reverse (R) primer sequences of canine genes included in the present study and used for polymerase chain reaction with the corresponding annealing temperature and product length.*

Blood samples of 39 healthy dogs were collected and DNA extraction was performed as previously reported (Da Ros et al., 2014). Around 30 ng of genomic DNA were used in PCR reaction to amplify TET2 exon 11 and the products obtained were subsequently sequenced as described above.

Sequences were analyzed and aligned by using the SeqScape software v3.0 (Life Technologies, Carlsbad, USA) and identity percentage between dog protein sequences and mouse, rat, dog and cat were assessed through BLAST (https://blast.ncbi.nlm.nih.gov/Blast).

6.3.3 Statistical analysis

To evaluate the possible relationship between the presence of glutamine repetitions in canine TET2 exon 11 and *c-KIT* mutations or the tendency to develop MCT, a Pearson χ^2 correlation test was performed by GraphPad Prism version 5.00 for Windows (GraphPad Software, San Diego, USA). A value of $P< 0.05$ was considered significant.

6.4 RESULTS

6.4.1 Gene sequences homology among canine and human species

In myeloproliferative disorders and particularly in SM, the majority of the genes considered in this study possess hot spot sites for mutations; therefore, in the first part of the study, a comparison between human and canine genomic sequences was performed to verify the potential conservation of the same mutations sites in dog and, subsequently, their localization. To give a general overview, the percentages of protein sequence identities in target genes between the canine and the other most commonly studied species (human, cat, mouse and rat) are reported in Table 2. In general, a high degree of conservation was noticed among them and, for our purposes, the CanFam3.1 genome sequence proved to be definitely complete and reliable.

Gene	Human	Cat	Mouse	Rat
TET2	84%	91%	58%	60%
IDH1	97%	99%	95%	96%
IDH2	96%	99%	97%	96%
NRAS	100%	100%	100%	100%
KRAS	99%	97%	96%	96%
SF3B1	100%	100%	100%	100%
SRSF2	100%	NA	100%	100%

Table 2. *List of target genes and percentage of protein sequence identity between dog and other reference species (Homo sapiens, Felis catus, Mus musculus, Rattus norvegicus). NA: sequence not available in the databases.*

The amino acids residues considered hot spot sites for mutations in humans as R132 for IDH1, R140 and R170 for IDH2, G12 and Q61 for NRAS and G12 for KRAS were recognized in dog. Since in humans TET2 mutations occur almost all over the sequence, all the corresponding canine coding exons were amplified; the two sequences shared the 84% of amino acid identity (Table 2). On the other hand, the canine SRSF2 partial sequence obtained in this study differed, either in exons and introns, from NCBI release. Anyway, the analog of human hot spot site (P95) was conserved also in dog. The updated partial sequence was submitted to NCBI with the following accession number: KT072629.

6.4.2 Target gene mutational status in MCTs samples

All genes were successfully amplified in all the 75 samples except for SRSF2, that was amplifiable in only 37 samples cause of its complexity and GC-richness.

In our MCT cohort, surprisingly, no mutations were ever found analyzing sequencing results of IDH1, IDH2, NRAS, KRAS, SF3B1 and SRSF2 genes (data not shown).

Among samples, some intronic variants not related with splicing sites were detected in the target genes. These alterations, with the relative allelic frequencies and population distribution, are collected in Table 3.

Gene	Intron/Exon	Variation	Population Frequency	Allelic frequencies
TET2	exon 3	c.732G>A p. =	3/75 (4%)	G : 0.98, A : 0.02
TET2	exon 3	c. 2315G>A: p.Gly772Asp	4/75 (5.3%)	G : 0.97, A : 0.03
TET2	intron 3	c.3439+75del	6/75 (8%)	T : 0.96, delT : 0.04
TET2	intron 8	c.4075-38del	5/75 (6.67%)	T : 0.97, delT : 0.03
TET2	intron 10	c.4212+63_4212+65insCAG	62/75 (82.7%)	WT : 0.31, insCAG : 0.69
TET2	intron 10	c.4568-65C>T	6/75 (8%)	C : 0.95, T : 0.05
TET2	exon 11	c.4914T>C:p=	58/75 (77.3%)	T : 0.41, C : 0.59
TET2	exon 11	c.5213A>G: p.Asn1728Ser	57/75 (76%)	G : 0.41, A : 0.59
TET2	exon 11	c.5278G>A: p.Ala1760Thr	1/75 (1.33%)	G : 0.01, A : 0.99
IDH1	intron 2	c. 292+37T>C	3/75 (4%)	T : 0.98, C : 0.02
NRAS	intron 2	c. 290+44C>T	18/75 (24%)	C : 0.87, T : 0.13
KRAS	intron 1	c. 93+104A>T	8/75 (10.67%)	A : 0.95, T : 0.05
KRAS	intron 1	c. 93+139T>C	8/75 (10.67%)	T : 0.95, C : 0.05
SRSF2	intron 1	362+59_362+62dup	21/37 (58%)	WT : 0.64, Dup : 0.36

Table 3. *List of genetic variations grouped for gene, relative population frequency and allelic frequencies in the MCT cohort of samples.*

6.4.3 TET2 mutational status in dog MCT

In canine TET2 only two samples evidenced the presence of mutation in their coding sequence: one sample showed a heterozygous non-synonymous substitution (c.491A>G: p. Asp164Gly) in exon 3 while another sample was homozygous for a complete codon deletion (c.2226-2228del: p. His742del) always in exon 3. Both MCTs were histologically classified as Patnaik grade II. As regards to *c-KIT* mutations, the former had a wild-type sequence, while the second one had an internal tandem duplication occurring in exon 11 ($ITD^{572-583}$). Since the frequency of TET2 mutations was low (2.7%), a correlation between TET2 and *c-KIT* mutational status and/or MCT histological grading, was not possible.

Also for TET2 gene, some intronic variants not related with splicing sites, and single nucleotide polymorphisms (SNPs) in the coding sequence were detected in the samples. These alterations, with the relative allelic frequencies and population distribution, are collected in Table 3.

Deepening in sequence analysis, other genetic variations were detected, in two specific regions of the gene. The protein database Uniprot (http://www.uniprot.org/) recognized them as polyglutamine rich-regions because they are rich in glutamine residues: one is located in exon 3 and another one in exon 11. The alignment of canine sequence with the same human, cat, mouse and rat sequence portion showed that poly-glutamines residues were quite conserved among species and dog possessed the highest number of glutamine repetitions (Figure 1).

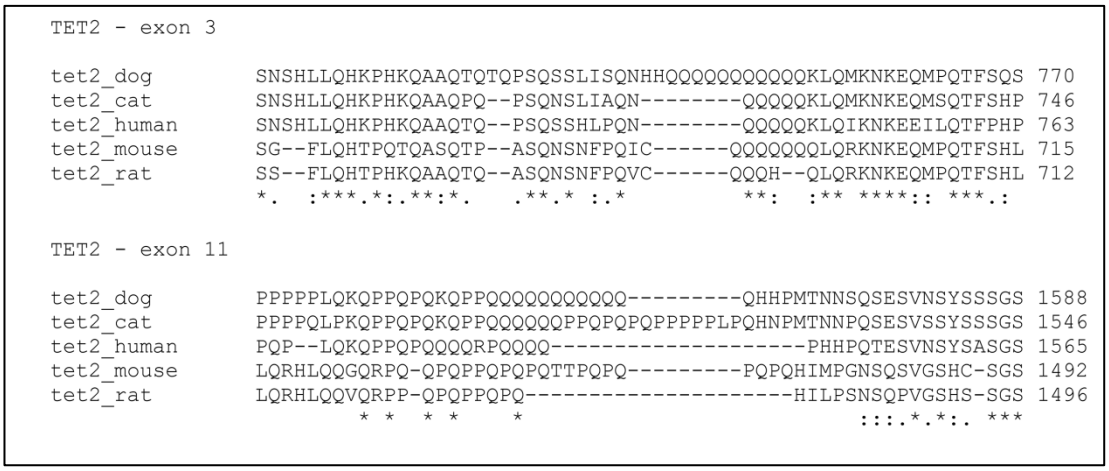

Figure 1. *Sequence alignment between dog, cat, human, mouse and rat specific glutamine-rich regions located in exon 3 and 11 of TET2 gene. The image was obtained using the tool ClustalW2 (http://www.ebi.ac.uk/Tools/msa/clustalw2/).*

In details, in canine exon 3, 65 out of 75 MCTs (86,66%) showed the deletion of glutamine 753 (c. 2250_2252del; p.Gln753del). In exon 11, different rearrangements in the number of glutamine repetitions were detected among samples. All variations observed in our cohort of samples with relative frequencies in the group are listed in Table 4. Performing a Pearson χ^2 analysis between the number of glutamine repetitions in each sample and the presence of *c-KIT* mutations, no statistical correlations were evident (P=0.3427). Furthermore, the number of glutamine repetitions in exon 3 and 11 did not correlate with the histologic grade (Fisher exact test, P= 0.5808 and Pearson χ^2, P= 0.2308, respectively).

Variation	Population Frequency	Glutamine repetitions
Wild-type sequence	59/75	12
c. 4682insGCA; p. 1562insQ	5/75	13
c.4686_4697del; p. 1564_1567del	4/75	8
c.4686_4694del; p. 1564_1566del	3/75	9
c.4698_4700del; p.1568del	4/75	11

***Table 4**. List of genetic variations detected in the glutamine rich region of TET2 exon 11 with relative population frequency and total glutamine residues number in the 75 MCT samples.*

Afterwards, to better understand if these sequence rearrangements might have a correlation with the onset of the disease, we screened the DNA from 39 healthy dogs for the same polyglutamine region in TET2 exon 11. Subsequently, considering as the wild-type phenotype the 12 glutamine repetitions presented in the reference NCBI sequence (XM_535678-4) we categorized all samples (healthy and pathologic) in three groups: samples that evidenced less than 12 glutamines (Q<12), wild-type dogs and samples with more than 12 glutamines (Q>12). From the contingency table and the Pearson χ^2 test, no significant correlation emerged between the number of glutamine repetitions and the risk to develop mast cell tumor (Figure 2).

***Figure 2.** Association between the number of glutamine (Gln) repetitions and healthy/pathologic state in 114 canine blood and MCT samples. Pearson χ^2 test ($p = 0.3454$; not significant).*

6.5 DISCUSSION

Mast cells (MCs) neoplastic disorders occur in both canine and human species sharing many but not all biological and clinical features. Spontaneous MCT has been proposed as a model to study biological and therapeutic approach for human neoplastic MCs diseases, i. e. mastocytosis (Ranieri et al., 2015). At the same time, due to the implications of *c-KIT* aberrations in the development of MCs tumors, canine MCT could represent a useful model to study human *c-KIT* driven malignancies and TKIs, targeting c-kit. Therefore, comparative studies of MCs disorders may represent an opportunity to improve our knowledge on both mastocytosis and *c-KIT* driven tumors for diagnosis in case of *c-KIT* wild type state and/or with the aim to develop novel treatment options that can be translated in human patients.

In this respect, starting from a list of genes that showed recurrent somatic mutations in human myeloproliferative diseases and mastocytosis, we screened a cohort of 75 canine MCTs for hot-spot mutations sites.

No mutations were identified in IDH1 and IDH2 genes in our cohort of MCTs while, in SM, IDH2 mutations occurred for 6.9% of cases (Hanssens et al., 2014). To the best of our knowledge, only one study has been published in dog (Reitman et al., 2010) where no mutations in both these genes were found in canine gliomas. Considering the high percentage of mutations in the human analog tumor (~80% in grades II-III) these results were surprising and might suggest a minor role of these genes in the pathogenesis of canine gliomas and MCT.

In SM, two genes involved in spliceosome machinery, SRSF2 and SF3B1, showed a mutation occurrence of 24% and 5.6% respectively (Hanssens et al., 2014). However, no mutations were detected in canine MCT. No data about the relevance of these genes and their mutational status in canine oncology are actually available; therefore, present results, are the first data ever published so far.

On the other hand, more information are available about NRAS and KRAS, in dog cancer. Present results showing the absence of mutations obtained in our MCTs samples are consistent with a number of previously published studies in which RAS mutations have been shown to be extremely rare in the most common types of canine tumor such as mammary tumors, soft-tissue tumors (included MCTs), melanomas and lymphoproliferative disorders (Watzinger et al., 2001; Terragni et al., 2014). In

contrast, higher mutational frequencies of RAS genes have been obtained in human lung, pancreatic, gastrointestinal, brain and liver tumor, in acute myelogenous leukemia, in follicular and undifferentiated papillary thyroid tumors (Richter et al., 2005). Therefore and likewise to IDH1/2 we might hypothesized that RAS mutations do not play a major role in the pathogenesis of canine MCT and this supposition is in line with previously published data (Watzinger et al., 2001).

About TET2, the high percentage of mutations found in aggressive form of human mastocytosis (20.8%) was not confirmed in canine MCT (2.7%). Moreover, the typical frame-shift mutations observed in humans and coding for a truncated protein with consequently loss of function, was never observed. These results surprised the authors and, until this moment, represented the first attempt, in veterinary medicine, to investigate the role of TET2 mutations in a canine tumor since no information are available in previous published studies.

Noteworthy, a frequent rearrangement was observed in a glutamine-rich region of TET2 exon 11, resulting in variations of the number of glutamine repetitions (from 8 to 13) among cases. Very little information are actually published in human oncology about a possible relationship between length of polyglutamine regions in some genes and the risk to develop cancer. The number of CAG repetitions in androgen receptor seems to be correlated with the risk of occurrence of prostate cancer; furthermore polymorphisms in glutamine regions of nuclear receptor coactivator 3 (NCOA3 also known as AIB1) seems to play a role in the susceptibility of some type of breast cancer (Ingles et al., 1997; Kadouri et al., 2004; Yoo et al., 2014). The sequencing analysis conducted in a little group of healthy dogs and matched statistically with results of MCT samples did not reveal any significant relationship between number of glutamine repetitions and the risk of MCT development.

In conclusion, this preliminary study aimed to investigate, in canine MCT, the mutational status of genes known to be involved in human myeloproliferative disorders. The study was undertaken in a relatively small cohort of canine samples, and only human analogue hot-spot sites for mutation were took into consideration. Further investigations are needed to better characterize the pathogenic pathways involved in both diseases. Among these ones, to sequence the entire IDH1, IDH2, NRAS, KRAS, SRSF2 and SF3B1 genes and, subsequently, to analyze interesting genes that were excluded from this preliminary study (i. e. Additional Sex Combs

Like 1 alias ASXL1, Janus Kinase 2 alias JAK2). Clearly, the advent of deep sequencing methods might be more useful in this sense, giving a more wide observation on genome modifications and allowing the identification of new hot-spot mutation sites in canine genes. This approach will permit to clarify the possible value of canine MCT as a comparative animal model for human SM.

7. CONCLUSIONS AND FUTURE PERSPECTIVES

The *c-KIT* gain of function mutations and overexpression are driven events in several highly malignant human (GIST, AML, melanoma) and canine tumors (MCT, melanoma). Tyrosine kinase inhibitors are a class of anti-cancer drugs inhibiting the phospho-activation of c-kit protein, but despite their use is directly linked to tumor regression, the onset of resistance is likely to occur, sometimes after several years of therapy, in most patients. The heterogeneity of patterns of mutations in the protein and in the resistance mechanisms suggests that the clinical challenges of resistance still remain to be overcome (Gunaratnam et al., 2009).

The first part of this thesis described an alternative approach to inhibit human *c-KIT* by using an anthraquinone derivative (AQ1). The compound was previously selected among a library of putative G4 ligands by the Department of Pharmaceutical Sciences. In this work, AQ1 blocked the proliferation of multiple cancer *in vitro* models. It also decreased *c-KIT* expression in human cancer cells with an inhibition rate that is, to the best of our knowledge, one of the highest ever noticed. Contextualizing this study in the G4 research field, one of its merits stands in the use of multiple cancer cell lines to test AQ1 in different cancer types. Also the two-variants statistical approach represented an innovation aspect in these types of complex studies that could provide more robust results. Moreover the use, for the first time, of *in vitro* model engineered for expressing a promoter free from G4 could be an helpful tool to check deeper the specificity of ligands. Actually, a major impediment to the validation of G4 DNA as a new anti-cancer drug target is the lack of small molecules that bind to G4 DNA with high affinity (Kd<1 nM) and high specificity (Luedtke et al., 2009). However, the potentialities of G4 compounds as alternative to the current TKIs therapies (imatinib) were evidenced in the treatment of *c-KIT* mutated cells comparing to the wild type.

In the past decades, the domestic dog has gained increasing interest as one of the most suitable animal model for comparative oncologic studies on tumor molecular mechanisms as well as for the identification and validation of new therapeutic targets. The lack of information about G4 presence in dogs, prompt us to investigate canine *c-KIT* promoter. Two putative G4 sequences were identified; these ones comprise a putative Sp1 transcriptional binding site and mimic the situation

present in the human DNA (Da Ros et al., 2014). The treatment of a canine MCT cell line with the same ligands used for human cells evidenced two putative efficient *c-KIT* inhibitors, suggesting that differences in the G-strands base composition can affect affinity and, consequently, the ligand binding.

Besides this encouraging results in both species, further experiments are needed to confirm the validity of these ligands as possible therapeutic tools. For example, gene reporter assays should be performed to verify whether ligands inhibit gene transcription through a specific binding to G4 conformations in both human and canine cells. Particularly in dogs, transcription regulatory elements found in *c-KIT* promoter are still undefined; moreover, the Sp1 domain, comprised between the two G4 regions, has not yet been characterized. Further studies, aiming to investigate the *c-KIT* downstream activation pathways, should also be undertaken to clarify which type of cellular damage occur following the exposure to AQ1 and AN6.

Results exposed in chapter 5 represented the first investigation in veterinary medicine about the *c-KIT* mutational status in mast cell tumor and relative metastases. In our study, the perfect concordance between primary lesion and relative metastases was detected, and it has important clinical implications; both matrices can be sampled by veterinarians for the mutational screening analysis and, the eventual *c-KIT* targeted therapeutic approach should be successful also against metastases. The small cohort of samples could represent a limit of this study and also the heterogeneity in the treatment protocols used. In this respect, future perspectives might be the analysis of an increased number of MCTs that underwent the same treatment. Furthermore, distal metastases should be inserted in the investigation as well as the multicentric MCTs to ascertain whether multiple masses are likely to present the same *c-KIT* mutational profile.

In general, further efforts should be spent to better understand MCT molecular biology; in this respect, the last study here presented offered an insight about the possible involvement of common genes in the pathogenesis of human systemic mastocytosis and canine MCT. The absence of mutations in genes considered as hotspots for SM suggest that the two diseases might differ in terms of gene-related pathogenetic pathways. From a comparative point of view, data obtained suggest researchers to be cautious in assuming canine MCT as a model for SM. A limit of the present work consist in the screening of only a restricted number of genes; as a matter of fact, the use of high-throughput methodologies, such as next generation

sequencing techniques, might give a wider view of cell pathways involved in tumor progression. Worth mentioning, a full, in-depth characterization of canine MCT transcriptome has only recently been considered (Giantin et al., 2014; Giantin et al., submitted); nevertheless, most of molecular mechanisms involved in tumoral onset and progression are still unknown and need more efforts to be spent for their characterization.

In conclusions, the research activities conducted in the three-years of Ph.D. program allowed to clarify some scientific gaps about *c-KIT*, and other related genes, in specific tumors, and identify new targets and strategies for canine and human anticancer chemotherapy. This work could lay the foundations of deeper investigations about the therapeutic usefulness of the *c-KIT* G4 ligands AQ1 and AN6, as well as the reliability of canine MCT as a model for other human *c-KIT* dependent tumors.

8. BIBLIOGRAPHY

Abou-Jawde R, Choueiri T, Alemany C, Mekhail T (2003). An overview of targeted treatments in cancer. Clinical Therapeutics, 25: 2121-2137.

Adams GP, Weiner LM (2005). Monoclonal antibody therapy of cancer. Nature biotechnology, 23: 1147-1157.

Amagai Y, Tanaka A, Matsuda A, Jung K, Oida K, Nishikawa S, Jang H, Matsuda H (2013). Heterogeneity of internal tandem duplications in the c-kit of dogs with multiple mast cell tumours. The Journal of Small Animal Practice, 54: 377-380.

An X, Tiwari AK, Sun Y, Ding P, Ashby Jr. CR, Chen Z (2010). BCR-ABL tyrosine kinase inhibitors in the treatment of Philadelphia chromosome positive chronic myeloid leukemia: A review. Leukemia Research, 34: 1255-1268.

Ando K, Oki E, Sugiyama M, Zhao Y, Kojima A, Yamamoto H, Yamashita Y, Saeki H, Taketomi A, Morita M, Kakeji Y, Tsujitani S, Maehara Y (2011). Secondary resistance of extra-gastrointestinal stromal tumors to imatinib mesylate: report of a case. Surgery Today, 41: 1290-1293.

Antonescu C (2011). What lessons can be learned from the GIST paradigm that can be applied to other kinase-driven cancers. The journal of Pathology, 223: 251-261.

Arock M, Akin C, Hermine O, Valent P (2015). Current treatment options in patients with mastocytosis: status in 2015 and future perspectives. European Journal of Hematology, 94: 474-490.

Arock M, Sotlar K, Akin C, Broesby-Olsen S, Hoermann G, Escribano L, Kristensen TK, Kluin-Nelemans HC, Hermine O, Dubreuil P, Sperr WR, Hartmann K, Gotlib J, Cross NCP, Haferlach T, Garcia-Montero A, Orfao A, Schwaab J, Triggiani M, Horny H-P, Metcalfe DD, Reiter A, Valent P (2015). KIT mutation analysis in mast cell neoplasms: recommendations of the European Competence Network on Mastocytosis. Leukemia, 29: 1223-1232.

Arora A, Scholar EM (2005). Role of tyrosine kinase inhibitors in cancer therapy. The journal of pharmacology and experimental therapeutics, 315: 971-979.

Ashman LK, Griffith R (2013). Therapeutic targeting of c-KIT in cancer. Expert Opinion on Investigational Drugs, 22: 103-115.

Baguley BC, Hicks KO, Wilson WR (2002). Tumor cell cultures in drug development. In Anticancer Drug Development (Baguley BC and Kerr DJ eds), pp 269-284, Academic Press, San Diego.

Balasubramanian S, Hurley LH, Neidle S (2011). Targeting G-quadruplexes in gene promoters: a novel anticancer strategy? Nature reviews - Drug discovery, 10: 261-675.

Beha G, Brunetti B, Asproni P, Muscatello LV, Millanta F, Poli A, Sarli G, Benazzi C (2012). Molecular portrait-based correlation between primary canine mammary tumor and its lymph node metastasis: possible prognostic-predictive models and/or stronghold for specific treatments? BMC Veterinary Research, 8: 219-227.

Bejugam M, Sewitz S, Shirude PS, Rodriguez R, Shahid R, Balasubramanian S (2007). Trisubstituted Isoalloxazines as a New Class of G-Quadruplex Binding Ligands: Small Molecule Regulation of c-kit Oncogene Expression. Journal of the American Chemical Society**,** 129: 12926-12927.

Bejugam M, Gunaratnam M, Muller S, Sanders DA, Sewitz S, Fletcher JA, Neidle S, Balasubramanian S (2010). Targerting the c-Kit promoter G-quadruplexes with 6-substituted idenoisoquinolines. ACS Medicinal Chemostry Letters, 1: 306-310.

Besmer P, Murphy JE, George PC, Qiu FH, Bergold PJ, Lederman L, Snyder HW Jr, Brodeur D, Zuckerman EE, Hardy WD (1986). A new acute transforming feline retrovirus and relationship of its oncogene v-kit with the protein kinase gene family. Nature, 320: 415-421.

Bianco S, Musetti C, Krapcho AP, Palumbo M, Sissi C (2013). Ni2+ and Cu2+ complexes of a phenanthroline-based ligand bind to G-quadruplexes at non-overlapping sites. Chemical Communications, 49: 8057-8059.

Bianco S, Musetti C, Waldeck A, Sparapani S, Seitz JD, Krapcho AP, Palumbo M, Sissi C (2010). Bis-phenanthroline derivatives as suitable scaffolds for effective G-quadruplex recognition. Dalton Transactions, 39: 5833-5841.

Bidzinska J, Cimino-Reale G, Zaffaroni N, Folini M (2013). G-quadruplex structures in the human genome as novel therapeutic targets. Molecules, 18: 12368-12395.

Blackwood L, Murphy S, Buracco P, De Vos JP, De Fornel-Thibaud P, Hirschberger J, Kessler M, Pastor J, Ponce F, Savary-Bataille K, Argyle DJ (2012). European consensus document on mast cell tumours in dogs and cats. Veterinary and Comparative Oncology, 10: 1-29.

Bochman ML, Paeschke K, Zakian VA (2012). DNA secondary structures: stability and function of G-quadruplex structures. Nature Reviews Genetic, 13: 770-780.

Boddupally PVL, Hahn S, Beman C, De B, Brooks TA, Gokhale V, Hurley LH (2012). The anticancer activity and cellular repression of c-MYC by the G-quadruplex-stabilizing 11-piperazinyl quindoline is not dependent on direct targeting of the G-quadruplex in the c-MYC promoter. Journal of Medicinal Chemistry, 55: 6076-6086.

Bonkobara M (2015). Dysregulation of tyrosine kinases and use of imatinib in small animal practice. The Veterinary Journal, 205: 180-188.

Brassesco, MS, Cortez MA, Valera ET, Engel EE, Nogueira-Barbosa MH, Becker AP, Scrideli CA, Tone LG (2010). Cryptic SYT/SXX1 fusion gene in high-grade

biphasic synovial sarcoma with unique complex rearrangement and extensive BCL2 overexpression. Cancer Genetics and Cytogenetics, 196: 189-193.

Brunetti B, Asproni P, Beha G, Muscatello LV, Millanta F, Poli A, Benazzi C, Sarli G (2013). Molecular phenotype in mammary tumours of queens: correlation between primary tumour and lymph node metastasis. Journal of Comparative Pathology, 148: 206-213.

Bryan TM, Baumann P (2011). G-quadruplexes: From guanine gels to chemotherapeutics. Molecular Biotechnology, 49: 198-208.

Chanakira A, Dutta R, Charboneau R, Barke R, Santilli SM, Roy S (2012). Hypoxia differential regulates arterial and venous smooth muscle cell proliferation via PDGFR-β and VEGFR-2 expression. American journal of physiology. Heart and circulatory physiology, 302: 1173-1184.

Chen Y, Fu L (2011). Mechanisms of acquired resistance to tyrosine kinase inhibitors. Acta Pharmaceutica Sinica B, 1: 197-207.

Chen Y, Yang D (2012). Sequence, stability, and structure of G-Quadruplexes and their interactions with drugs. Current Protocols in Nucleic Acid Chemistry, 50: 1-17.

Corless CL, Barnett, Heinrich MC (2011). Gastrointestinal stromal tumours: origin and molecular oncology. Nature Reviews Cancer, 11: 865-878.

Costa Casagrande TA, de Oliveira-Barros LM, Fukumasu H, Cogliati B, Chaible LM, Dagli MLZ, Matera JM (2015). The value of molecular expression of KIT and KIT ligand analysed using real-time polymerase chain reaction and immunohistochemistry as a prognostic indicator for canine cutaneous mast cell tumours. Veterinary and Comparative Oncology, 13: 1-10.

Cruse G, Metcalfe DD, Olivera A (2014). Functional deregulation of Kit: link to mast cell proliferative diseases and other neoplasms. Immunology and Allergy Clinics of North America, 34: 219-237.

Da Ros S, Zorzan E, Giantin M, Shahidian LZ, Palumbo M, Dacasto M, Sissi C (2014). Sequencing and G-quadruplex folding of the canine proto-oncogene KIT promoter region: might dog be used as a model for human disease? Plos One, 9: e103876.

Dai B, Cai X, Kong Y-Y, Yang F, Shen XX, Wang LW, Kong JC (2013). Analysis of KIT expression and gene mutation in human acral melanoma: with a comparison between primary tumors and corresponding metastases/recurrences. Human Pathology, 44: 1472-1478.

Dash J, Shirude PS, Hsu SD, Balasubramanian S (2008). Diarylethynyl Amides That Recognize the Parallel Conformation of Genomic Promoter DNA G-Quadruplexes. Journal of American Chemical Society, 130: 15950-15956.

De Vita S, Schneider RK, Garcia M, Wood J, Gavillet M, Ebert BL, Gerbaulet A, Roers A, Levine RL, Mullally A, Williams DA (2014). Loss of Function of TET2

Cooperates with Constitutively Active KIT in Murine and Human Models of Mastocytosis. Plos One, 9: 1-13.

Deininger MWN, Druker BJ (2003). Specific targeted therapy of chronic myelogenous leukemia with imatinib. Pharmacological Reviews, 55: 401-423.

Delhommeau F, Dupont S, Della Valle V, James C, Trannoy S, Massé A, Kosmider O, Le Couedic JP, Robert F, Alberdi A, Lécluse Y, Plo I, Dreyfus FJ, Marzac C, Casadevall N, Lacombe C, Romana SP, Dessen P, Soulier J, Viguié F, Fontenay M, Vainchenker W, Bernard OA, (2009). Mutation in TET2 in myeloid cancers. The New England Journal of Medicine, 360: 2289-2301.

den Dunnen JT, Antonarakis SE (2001). Nomenclature for the description of human sequence variations. Human Genetics, 109: 121-124.

Dobson JM (2013). Breed-predispositions to cancer in pedigree dogs. ISRN Veterinary Science, 941275.

Downing S, Chien MB, Kass PH, Moore PE, London CA (2002). Prevalence and importance of internal tandem duplications in exons 11 and 12 of c-kit in mast cell tumors of dogs. American Journal of Veterinary Research, 63: 1718-1723.

Du Z, Kong P, Gao Y, Li N (2007). Enrichment of G4 DNA motif in transcriptional regulatory region of chicken genome. Biochemical Biophysical Research Communications, 354: 1067-1070.

Dubreuil P, Letard S, Ciufolini M, Gros L, Humbert M, Castéran N, Borge L, Hajem B, Lermet A, Sippl W, Voisset E, Arock M, Auclair C, Leventhal PS, Mansfield CD, Moussy A, Hermine O (2009). Masitinib (AB1010), a potent and selective tyrosine kinase inhibitor targeting KIT. Plos One, 4: e7258.

Eisenhauer EA, Therasse P, Bogaerts J, Schwartz LH, Sargent D, Ford R, Dancey J, Arbuck S, Gwyther S, Mooney M, Rubinstein L, Shankar L, Dodd L, Kaplan R, Lacombe D, Verweij J (2009). New response evaluation criteria in solid tumours: revised RECIST guideline (version 1.1). European journal of Cancer, 45: 228-247.

Fernando H, Reszka AP, Huppert J, Ladame S, Rankin S, Venkitaraman AR, Neidle S, Balasubramanian S (2006). A conserved quadruplex motif located in a transcription activation site of the human c-kit oncogene. Biochemistry, 45: 7854-7860.

Ferrara N, Hillan KJ, Novotny W (2005). Bevacizumab (Avastin), a humanized anti-VEGF monoclonal antibody for cancer therapy. Biochemical and Biophysical Research Communications, 333: 328-335.

Fidler IJ, Kripke ML (1977). Metastasis results from preexisting variant cells within a malignant tumor. Science, 197: 893-895.

Folini M, Pivetta C, Zagotto G, De Marco C, Palumbo M, Zaffaroni N, Sissi C (2010). Remarkable interference with telomeric function by a G-quadruplex selective bisantrene regioisomer. Biochemical Pharmacology, 70: 1781-1790.

Fonseca-Alves CE, Bento DD, Torres-Neto R, Werner J, Kitchell B and Laufer-Amorim R (2015). Ki67/KIT double immunohistochemical staining in cutaneous mast cell tumors from Boxer dogs. Research in Veterinary Science, 102: 122-126.

Frost D, Lasota J, Miettinen M (2003). Gastrointestinal stromal tumors and leiomyomas in the dog: a histopathologic, immunohistochemical, and molecular genetic study of 50 cases. Veterinary Pathology, 40: 42-54.

Fulda S (2015). Targeting apoptosis for anticancer therapy. Seminars in Cancer Biology, 31: 84-88.

Gabillot-Carré M, Lepelletier Y, Humbert M, De Sepuvelda P, Hamouda NB, Zappulla JP, Liblau R, Ribadeau-Dumas A, Machavoine F, Letard S, Baude C, Hermant A, Yang Y, Vargaftig J, Bodemer C, Morelon E, Lortholary O, Recher C, Laurent G, Dy M, Arock M, Dubreuil P, Hermine O (2006). Rapamycin inhibits growth and survival of D816V-mutated c-kit mast cells. Blood, 108: 1065-1072.

Gancberg D, Di Leo A, Cardoso F, Rouas G, Pedrocchi M, Paesmans M, Verhest A, Bernard-Marty C, Piccart MJ, Larsimont D (2002). Comparison of *HER-2* status between primary breast cancer and corresponding distant metastatic sites. Annals of Oncology, 13: 1036-1043.

Gao J, Tian Y, Li J, Sun N, Yuan J, Shen L (2013). Secondary mutations of c-KIT contribute to acquired resistance to imatinib and decrease efficacy of sunitinib in Chinese patients with gastrointestinal stromal tumors. Medical Oncology, 30: 522.

Gerber DE (2008), Targeted Therapies: A New Generation of Cancer Treatments. American Family Physician, 77: 311-319.

Giantin M, Granato A, Baratto C, Marconato L, Vascellari M, Morello EM, Vercelli A, Mutinelli F, Dacasto M (2014). Global gene expression analysis of canine cutaneous mast cell tumor: could molecular profiling be useful for subtype classification and prognostication? Plos One, e95481.

Giantin M, Vascellari M, Morello EM, Capello K, Vercelli A, Granato A, Lopparelli RM, Nassuato C, Carminato A, Martano M, Mutinelli F, Dacasto M (2012). c-KIT messenger RNA and protein expression and mutations in canine cutaneous mast cell tumors: correlations with post-surgical prognosis. Journal of Veterinary Diagnostic Investigation, 24: 116-126.

Gil da Costa RM (2015). C-kit as a prognostic and therapeutic marker in canine cutaneous mast cell tumours: from laboratory to clinic. The Veterinary Journal, 205: 5-10.

Gleixner K, Rebuzzi L, Mayerhofer M, Gruze A, Hadzijusufovic E, Sonneck K, Vales A, Kneidinger M, Samorapoompichit P, Thaiwong T, Pickl WF, Yuzbasiyan-

Gurkan V, Sillaber C, Willmann M, Valent P (2007). Synergistic antiproliferative effects of KIT tyrosine kinase inhibitors on neoplastic canine mast cells. Experimental Hematology, 35: 1510-1521.

Gomez D, Wenner T, Brassart B, Douarre C, O'Donohue MF, El Khoury V, Shin-Ya K, Morjani H, Trentesaux C, Riou JF (2006). Telomestatin-induced telomere uncapping is modulated by POT1 through G-overhang extension in HT1080 human tumor cells. Journal of Biological Chemistry, 281: 38721-38729.

Gregory-Bryson E, Bartlett E, Kiupel M, Hayes S, Yuzbasiyan-Gurkan V (2010). Canine and human gastrointestinal stromal tumors display similar mutations in c-KIT exon 11. BMC Cancer, 10: 1-9.

Gunaratnam M, Swank S, Haider SM, Galeasa K, Reszka AP, Beltran M, Cuenca F, Fletcher JA, Neidle S (2009). Targeting human gastrointestinal stromal tumor cells with a quadruplex-binding small molecule. Journal of Medicinal Chemistry, 52: 3774-3783.

Hahn KA, Ogilvie G, Rusk T, Devauchelle P, Leblanc A, Legendre A, Powers B, Leventhal PS, Kinet JP, Palmerini F, Dubreuil P, Moussy A, Hermine O (2008). Masitinib is safe and effective for the treatment of canine mast cell tumors. Journal of Veterinary Internal Medicine, 22: 1301-1309.

Halder R, Riou J, Teulade-Fichou M, Frickey T, Hartig JS (2012). Bisquinolinium compounds induce quadruplex-specific transcriptome changes in HeLa S3 cell lines. BMC Research Notes, 5: 138-149.

Halsey CHC, Gustafson DL, Rose BJ, Wolf-Ringwall A, Burnett RC, Duval DL, Avery AC, Thamm DH (2014). Development of an *in vitro* model of acquired resistance to toceranib phosphate (Palladia®) in canine mast cell tumor. BMC Veterinary Research, 10: 105-117.

Hanahan D, Weinberg R (2000). The hallmarks of cancer. Cell Press, 100: 57-70.

Hanssens K, Brenet F, Agopian J, Georgin-Lavialle S, Damaj G, Cabaret L, Chandesris MO, de Sepulveda P, Hermine O, Dubreuil P, Soucie E (2014). SRSF2-p95 hotspot mutation is highly associated with advanced forms of mastocytosis and mutations in epigenetic regulator genes. Haematologica, 99: 830-835.

Huang M, Shen A, Ding J, Geng M (2014). Molecularly targeted cancer therapy: some lessons from the past decade. Trends in Pharmacological Sciences, 35: 41-50.

Huang Q, Lu G, Shen H, Chung MCM, Ong CN (2007). Anti-Cancer Properties of Anthraquinones from Rhubarb. Medicinal Research Reviews, 27: 609-630.

Huang S, Jean D, Luca M, Tainsky MA, Bar-Eli M (1998). Loss of AP-2 results in downregulation of c-KIT and enhancement of melanoma tumorigenicity and metastasis. EMBO Journal, 17: 4358-4369.

Ingles SA, Ross RK, Yu MC, Irvine RA, La Pera G, Haile RW, Coetzee GA (1997). Association of prostate cancer risk with genetic polymorphisms in vitamin D receptor and androgen receptor. Journal of the National Cancer Institute, 89: 166-170.

Iqbal S, Zhang S, Driss A, Liu Z, Kim H, Wang Y, Ritenour C, Zhau HE, Kucuk O, Chung LWK, Wu D (2012). PDGF Upregulates Mcl-1 through activation of β-catenin and HIF-1α-dependent signaling in human prostate cancer cells. Plos One, 7: 7-12.

Italiano A, Vandenbos FB, Otto J, Mouroux J, Fontaine D, Marcy PY, Cardot N, Thyss A, Pedeutour F. (2006). Comparison of the epidermal growth factor receptor gene and protein in primary non-small-cell-lung cancer and metastatic sites: implications for treatment with EGFR-inhibitors. Annals of Oncology, 17: 981-985.

Ito S, Shen L, Dai Q, Wu SC, Collins LB, Swenberg A, He C, Zhang Y (2011). Tet proteins can convert 5-methylcytosine to 5-formylcytosine and 5-carboxylcytosine. Science, 333: 1300-1303.

Itzykson R, Kosmider O, Fenaux P (2013). Somatic mutations and epigenetic abnormalities in myelodysplastic syndromes. Best Practice and Research Clinical Hematology, 26: 355-364.

Kadouri L, Kote-Jarai Z, Easton DF, Hubert A, Hamoudi R, Glaser B, Abeliovich D, Peretz T, Eeles RA (2004). Polyglutamine repeat length in the AIB1 gene modifies breast cancer susceptibility in BRCA1 carriers. International Journal of Cancer, 108: 399-403.

Kang MH, Reynolds CP (2009). Bcl-2 inhibitors: targeting mitochondrial apoptotic pathways in cancer therapy. Clinical Cancer Research, 15: 1126-1132.

Katona TM, Jones TD, Wang M, Eble JN, Billings SD, Cheng L (2007). Genetically heterogeneous and clonally unrelated metastases may arise in patients with cutaneous melanoma. The American Journal of Surgical Pathology, 31: 1029-1037.

Kiupel M, Webster JD, Bailey KL, Best S, DeLay J, Detrisac CJ, Fitzgerald SD, Gamble D, Ginn PE, Goldschmidt MH, Hendrick MJ, Howerth EW, Janovitz EB, Langohr I, Lenz SD, Lipscomb TP, Miller MA, Misdorp W, Moroff S, Mullaney TP, Neyens I, O'Toole D, Ramos-Vara J, Scase TJ, Schulman FY, Sledge D, Smedley RC, Smith K, W Snyder P, Southorn E, Stedman NL, Steficek BA, Stromberg PC, Valli VE, Weisbrode SE, Yager J, Heller J, Miller R (2011). Proposal of a 2-tier histologic grading system for canine cutaneous mast cell tumors to more accurately predict biological behavior. Veterinary Pathology, 48: 147-155.

Kiupel M, Webster JD, Miller RA, Kaneene JB (2005). Impact of tumour depth, tumour location and multiple synchronous masses on the prognosis of canine cutaneous mast cell tumours. Journal of Veterinary Medicine A, 52: 280-286.

Klein CA (2009). Parallel progression of primary tumours and metastases. Nature Reviews Cancer, 9: 302-312.

Kobayashi M, Sugisaki O, Ishii N, Yamada O, Ito K, Kuroki S, Sasaki Y, Ono K, Washizu T, Bonkobara M (2012). Canine intestinal mast cell tumor with c-kit exon 8 mutation responsive to imatinib therapy. The Veterinary Journal, 193: 264-267.

Krause DS, Van Etten RA (2005). Tyrosine kinases as targets for cancer therapy. The new England Journal of Medicine, 353: 172-187.

Langemeijer SMC, Kuiper RP, Berends M, Knops R, Aslanyan MG, Massop M, Stevens-Linders E, van Hoogen P, van Kessel AG, Raymakers RA, Kamping EJ, Verhoef GE, Verburgh E, Hagemeijer A, Vandenberghe P, de Witte T, van der Reijden BA, Jansen JH (2009). Acquired mutations in TET2 are common in myelodysplastic syndromes. Nature Genetics, 41: 838-842.

Largy E, Hamon F, Teulade-Fichou MP (2011). Development of a high-throughput G4-FID assay for screening and evaluation of small molecules binding quadruplex nucleic acid structures. Analytical and Bioanalytical Chemistry, 400: 3419-3427.

Lemmon MA, Schlessinger J (2010). Cell signaling by receptor tyrosine kinases. Cell, 141: 1117-1134.

Lennartsson J, Rönnstrand L (2012). Stem cell factor receptor/c-kit: from basic science to clinical implications. Physiological Reviews, 92: 1619-1649.

Letard S, Yang Y, Hanssens K, Palmerini F, Leventhal PS, Guéry S, Moussy A, Kinet JP, Hermine O, Dubreuil P (2008). Gain-of- function mutations in the extracellular domain of KIT are common in canine mast cell tumors. Molecular Cancer Research, 6: 1137-1145.

Li Z, Cai X, Cai CL, Wang J, Zhang W, Petersen BE, Yang FC, Xu M (2011). Deletion of Tet2 in mice leads to dysregulated hematopoietic stem cells and subsequent development of myeloid malignancies. Blood, 118: 4509-4518.

Liang J, Wu YL, Chen BJ, Zhang W, Tanaka Y, Sugiyama H (2013). The c-Kit receptor-mediated signal transduction and tumor-related diseases. International Journal of Biological Sciences**,** 9: 435-443.

Liegl B, Kepten I, Le C, Zhu M, Demetri GD, Heinrich MC, Fletcher CD, Corless CL, Fletcher JA (2008). Heterogeneity of kinase inhibitor resistance mechanisms in GIST. The Journal of Pathology, 216: 64-74.

Livak KJ, Schmittgen TD (2001). Analysis of relative gene expression data using real time quantitative PCR and the 2(-Delta Delta C(T)) Method. Methods, 25: 402-408.

London CA (2009). Tyrosine kinase inhibitors in veterinary medicine. Topics in Companion Animal Medicine, 24: 106-112.

London CA, Galli SJ, Yuuki T, Hu ZQ, Helfand SC, Geissler EN (1999). Spontaneous canine mast cell tumors express tandem duplications in the proto-oncogene c-kit. Experimental Hematology, 27: 689-697.

London CA, Malpas PB, Wood-Follis SL, Boucher JF, Rusk AW, Rosenberg MP, Henry CJ, Mitchener KL, Klein MK, Hintermeister JG, Bergman PJ, Couto GC, Mauldin GN, Michels GM (2009). Multi-center, placebo-controlled, double-blind, randomized study of oral toceranib phosphate (SU11654), a receptor tyrosine kinase inhibitor, for the treatment of dogs with recurrent (either local or distant) mast cell tumor following surgical excision. Clinical Cancer Research, 15: 3856-3865.

London CA, Seguin B (2003). Mast cell tumors in the dog. Veterinary Clinics of North America: Small Animal Practice, 33: 473-489.

Luedtke NW (2009) Targeting G-Quadruplex DNA with small molecules. Chimia, 63: 134-139.

Ma Y, Longley BJ, Wang X, Blount JL, Langley K, Caughey GH (1999). Clustering of activating mutations in c-kit's juxtamembrane coding region in canine mast cell neoplasms. The Journal of Investigating Dermatology, 112: 165-170.

Maeda K, Nishiyama C, Ogawa H, Okomura K (2010). GATA2 and Sp1 Positively Regulate the c-kit Promoter in Mast Cells. The journal of immunology, 185: 4252-4260.

Malaise M, Steinbach D, Corbacioglu S (2011). Clinical implications of c-Kit mutations in acute myelogenous leukemia. Current Hematologic Malignancy Reports, 4: 77-82.

Marconato L, Zorzan E, Giantin M, Di Palma S, Cancedda S, Dacasto M (2014). Concordance of c-kit Mutational Status in Matched Primary and Metastatic Cutaneous Canine Mast Cell Tumors at Baseline: Implications for Clinical Practice. Journal of Veterinary Internal Medicine, 28: 547-553.

Marostica G (2015). Effetti di un ligando G-quadruplex sui profili di espressione di c-KIT e BCL2 in una linea cellulare di mastocitoma canino. Tesi di laurea triennale in Biotecnologie. Padova: Università degli Studi di Padova.

McLuckie KI, Waller ZA, Sanders DA, Alves D, Rodriguez R, Dash J, McKenzie GJ, Venkitaraman AR, and Balasubramanian S (2011). G-quadruplex-binding benzo[a]phenoxazines down-regulate c-KIT expression in human gastric carcinoma cells. Journal of the American Chemical Society 133: 2658-2663.

Mekori YA, Gilfillan AM, Akin C, Hartmann K, Metcalfe DD (2001). Human mast cell apoptosis is regulated through Bcl-2 and Bcl-X_L. Journal of Clinical Immunology, 21: 171-174.

Metcalfe DD (2008). Mast cells and mastocytosis. Blood, 112: 946-956.

Michelon V (2015). Messa a punto di un protocollo di immunoelettroforesi per la valutazione degli effetti post-trascrizionali di ligandi G-quadruplex in una linea cellulare di mastocitoma canino. Tesi di laurea triennale in Biotecnologie. Padova: Università degli Studi di Padova.

Milelli A, Tumiatti V, Micco M, Rosini M, Zuccari G, Raffaghello L, Bianchi G, Pistoia V, Díaz JF, Pera B, Trigili C, Barasoain I, Musetti C, Toniolo M, Sissi C, Alcaro S, Moraca F, Zini M, Stefanelli C, Minarini A (2012). Structure-activity relationships of novel substituted naphthalene diimides as anticancer agents. European Journal of Medicinal Chemistry, 57: 417-428.

Miller MJ, Foy KC, Kaumaya PT (2013). Cancer immunotherapy: present status, future perspective, and a new paradigm of peptide immunotherapeutics. Discovery Medicine, 215: 166-176.

Moran-Crusio K, Reavie L, Shih A, Abdel-Wahab O, Ndiaye-Lobry D, Lobry C, Figueroa ME, Vasanthakumar A, Patel J, Zhao X, Perna F, Pandey S, Madzo J, Song C, Dai Q, He C, Ibrahim S, Beran M, Zavadil J, Nimer SD, Melnick A, Godley LA, Aifantis I, Levine RL (2011). Tet2 loss leads to increased hematopoietic stem cell self-renewal and myeloid transformation. Cancer Cell, 20: 11-24.

Moye AL, Porter KC, Cohen SB, Phan T, Zyner KG, Sasaki N, Lovrecz GO, Beck JL, Bryan TM (2015). Telomeric G-quadruplexes are a substrate and site of localization for human telomerase. Nature communications, 6: 1-12.

Murphy S, Sparkes AH, Blunden AS, Brearley MJ, Smith KC (2006). Effects of stage and number of tumours on prognosis of dogs with cutaneous mast cell tumours. The Veterinary Record, 158: 287-291.

Musetti C, Lucatello L, Bianco S, Krapcho AP, Cadamuro SA, Palumbo M, Sissi C (2009). Metal ion-mediated assembly of effective phenanthroline-based G-quadruplex ligands. Dalton Transaction, 21: 3657-3660.

Nahta R, Yu D, Hung M, Hortobagyi GN, Esteva FJ (2006). Mechanisms of Disease: understanding resistance to HER2-targeted therapy in human breast cancer. Nature Clinical Practice Oncology, 3: 269-280.

Nanjunda R, Musetti C, Kumar A, Ismail MA, Farahat AA, Wang S, Sissi C, Palumbo M, Boykin DW, Wilson WD (2012). Heterocyclic dications as a new class of telomeric G-quadruplex targeting agents. Current Pharmaceutical Design, 18: 1934-1947.

Ohmori K, Kawarai S, Yasuda N, Tanaka A, Matsuda H, Nishimura R, Tanaka A, Matsuda H, Nishimura R, Sasaki N, Tsujimoto H, Masuda K (2008). Identification of c-kit mutations-independent neoplastic cell proliferation of canine mast cells. Veterinary immunology and immunopathology, 126: 43-53.

Onel B, Lin C, Yang D (2014). DNA G-quadruplex and its potential as anticancer drug target. Science China Chemistry, 57: 1605-1614.

Ozvegy-Laczka C, Cserepes J, Elkind NB, Sarkadi B (2005). Tyrosine kinase inhibitor resistance in cancer: role of ABC multidrug transporters. Drug Resistance Updates, 8: 15-26.

Pardanani A (2015). Systemic mastocytosis in adults: 2015 update on diagnosis, risk stratification, and management. Annual journal of Hematology, 90: 251-262.

Park GH, Plummer HK 3rd, Krystal GW (1998). Selective SpI binding is critical for maximal activity of the human *c-kit* promoter. Blood, 92: 4138-4149.

Patel DJ, Phan AT, Kuryavyi V (2007). Human telomere,oncogenic promoter and 5'-UTR G-quadruplexes: diverse higher order DNA and RNA targets for cancer therapeutics. Nucleic Acids Research, 35: 7429-7455.

Patnaik AK, Ehler WJ, MacEwen EG (1984). Canine cutaneous mast cell tumor: morphologic grading and survival time in 83 dogs. Veterinary Pathology, 21: 469-474.

Patruno, R, Marech I, Zizzo N, Ammendola M, Nardulli P, Gadaleta C, Introna M, Capriuolo G, Rubini RA, Ribatti D, Gadaleta CD, Ranieri G (2014). C-kit expression, angiogenesis, and grading in canine mast cell tumour: a unique model to study c-kit driven human malignancies. BioMed Research International, 2014: 1-8.

Pittoni P, Piconese S, Tripodo C, Colombo MP (2011). Tumor-intrinsic and -extrinsic roles of c-Kit: mast cells as the primary off-target of tyrosine kinase inhibitors. Oncogene**,** 30: 757-769.

Rankin S, Reszka AP, Huppert J, Zloh M, Parkinson GN, Todd AK, Ladame S, Balasubramanina S, Neidle S (2005). Putative DNA quadruplex formation within the human c-kit oncogene. Journal of the American Chemical Society, 127: 10584-10589.

Ranieri G, Marech I, Pantaleo M, Piccinno M, Roncetti M, Mutinati M, Rizzo A, Gadaleta CD, Introna M, Patruno R, Sciorsci RL (2015). In *vivo* model for mastocytosis: A comparative review. Critical Reviews in Oncology/Hematology, 93: 159-169.

Rasteiro AMF (2015). *In vitro* comparative studies on new targets for cancer therapy, and characterization of their biomolecular effects. Dissertação de Mestrado Integrado em Medicina Veterinária. Lisboa: Faculdade de Medicina Veterinária - Universidade de Lisboa.

Rawal P, Kummarasetti VBR, Ravindran J, Kumar N, Halder K, Sharma R, Mukerji M, Das SK, Chowdhury S (2006). Genome-wide prediction of G4 DNA as regulatory motifs: role of *Escherichia coli* global regulation. Genome Research,16: 644-655.

Reimann-Berg N, Murua Escobar H, Nolte I (2012). Relevance of chromosome 13 aberrations in canine tumours. Tierärztliche Praxis Ausgabe K: Kleintiere - Heimtiere, 40: 267-270.

Reitman ZJ, Olby NJ, Mariani CL, Thomas R, Breen M, Bigner DD, McLendon RE, Yan H (2010). IDH1 and IDH2 hotspot mutations are not found in canine glioma. International Journal of Cancer, 127: 245-246.

Richter A, Murua Escobar H, Gunther K, Soller JT, Winkler S, Nolte I, Bullerdiek J (2005). RAS gene hot-spot mutations in canine neoplasias. The Journal of Heredity, 96: 764-765.

Rosenzweig SA (2012). Acquired resistance to drugs targeting receptor tyrosine kinases. Biochemical Pharmacology, 82: 1041-1048.

Sabattini S, Scarpa F, Berlato D, Bettini G (2015). Histologic grading of canine mast cell tumor: is 2 better than 3? Veterinary Pathology, 52: 70-73.

Sailasuta A, Ketpun D, Piyaviriyakul, P, Theerawatanasirikul S, Theewasutrakul P, Rungsipipat A (2014). The relevance of CD117-immunocytochemistry staining patterns to mutational exon-11 in c-kit detected by PCR from fine-needle aspirated canine mast cell tumor cells. Veterinary Medicine International, 787498: 1-8.

Saleh R, Wedeh G, Herrmann H, Bibi S, Cerny-Reiterer S, Sadovnik I, Blatt K, Hadzijusufovic E, Jeanningros S, Blanc C, Legarff-Tavernier M, Chapiro E, Nguyen-Khac F, Subra F, Bonnemye P, Dubreuil P, Desplat V, Merle-Béral H, Willmann M, Rülicke T, Valent P, Arock M (2014). A new human mast cell line expressing a functional IgE receptor converts to tumorigenic growth by KIT D816V transfection. Blood, 124: 111-120.

Scartozzi M, Bearzi I, Berardi R, Mandolesi A, Fabris G, Cascinu S (2004). Epidermal growth factor receptor (EGFR) status in primary colorectal tumors does not correlate with EGFR expression in related metastatic sites: implications for treatment with EGFR-targeted monoclonal antibodies. Journal of Clinical Oncology, 22: 4772-4778.

Schrama D, Reisfeld RA, Becker JC (2006). Antibody targeted drugs as cancer therapeutics. Nature Reviews, 5: 147-159.

Shahidian LZ (2013). Characterization of *in vitro* models for the study of candidate G-quadruplex ligands targeting the human c-kit proto-oncogene promoter. Dissertação de Mestrado Integrado em Medicina Veterinária. Lisboa: Faculdade de Medicina Veterinária - Universidade de Lisboa.

Shalaby T, Fiaschetti G, Nagasawa K, Shin-ya K, Baumgartner M, Grotzer M (2013). G-Quadruplexes as potential therapeutic targets for embryonal tumors. Molecules, 18: 12500-12537.

Shen F, Jin J, Li J, Wang Y, Zhu S, Lu Y, Ou T, Huang Z, Huang M, Huang Z (2013). The G-quadruplex ligand, SYUIQ-FM05, targets proto-oncogene *c-kit* transcription and induces apoptosis in K562 cells. Pharmaceutical Biology, 51: 447-454.

Siddiqui-Jain A, Grand CL, Bearss DJ, Hurley LH (2002). Direct evidence for a G-quadruplex in a promoter region and its targeting with a small molecule to repress c-MYC transcription. In: Proceedings of the National Academy of Sciences of the United States of America, 99: 11593-11598.

Simak R, Capodieci P, Cohen DW, Fair WR, Scher H, Melamed J, Drobnjak M, Heston WD, Stix U, Steiner G, Cordon-Cardo C (2000). Expression of c-kit and kit-ligand in benign and malignant prostatic tissues. Histology Histopathology, 15: 365-374.

Soucie E, Hanssens K, Mercher T, Georgin-Lavialle S, Damaj G, Livideanu C, Chandesris MO, Acin Y, Létard S, de Sepulveda P, Hermine O, Bernard OA, Dubreuil P (2012). In aggressive forms of mastocytosis, TET2 loss cooperates with c-KITD816V to transform mast cells. Blood, 120: 4846-4849.

Stefanello D, Valenti P, Faverzani S, Bronzo V, Fiorbianco V, Pinto da Cunha N, Romussi S, Cantatore M, Caniatti M (2009). Ultrasound-guided cytology of spleen and liver: a prognostic tool in canine cutaneous mast cell tumor. Journal of Veterinary Internal Medicine, 23: 1051-1057.

Stern M, Herrmann R (2005). Overview of monoclonal antibodies in cancer therapy: present and promise. Critical Reviews in Oncology/Hematology, 54: 11-29.

Stewart EL, Zhixing Tan S, Liu G, Tsao M (2015). Known and putative mechanisms of resistance to EGFR targeted therapies in NSCLC patients with EGFR mutations—a review. Translational lung cancer research, 4: 67-81.

Sun C, Bernards R (2014). Feedback and redundancy in receptor tyrosine kinase signaling: relevance to cancer therapies. Trends in Biochemical Sciences, 39: 465-474.

Syed YY, McKeage K (2015). Aflibercept: a review in metastatic colorectal cancer. Drugs, 75: 1435-1445.

Takeuchi Y, Fujino Y, Watanabe M, Nakagawa T, Ohno K, Sasaki N, Nakagawa T, Ohno K, Sasaki N, Sugano S, Tsujimoto H (2010). Aberrant autophosphorylation of c-Kit receptor in canine mast cell tumor cell lines. Veterinary immunology and immunopathology, 137: 208-216.

Takeuchi Y, Fujino Y, Watanabe M, Takahashi M, Nakagawa T, Takeuchi A, Bonkobara M, Kobayashi T, Ohno K, Uchida K, Asano K, Nishimura R, Nakayama H, Sugano S, Ohashi Y, Tsujimoto H (2013). Validation of the prognostic value of histopathological grading or c-kit mutation in canine cutaneous mast cell tumours: a retrospective cohort study. The Veterinary Journal, 196: 492-498.

Taniguchi K, Okami J, Kodama K, Higashiyama M, Kato K (2008). Intratumor heterogeneity of epidermal growth factor receptor mutations in lung cancer and its correlation to the response to gefitinib. Cancer Science, 99: 929-935.

Tefferi A, Levine RL, Lim KH, Abdel-Wahab O, Lasho TL, Patel J, Finke CM, Mullally A, Li CY, Pardanani A, Gilliland DG (2009). Frequent TET2 mutations in systemic mastocytosis: clinical, KITD816V and FIP1L1-PDGFRA correlates. Leukemia, 23: 900-904.

Tefferi A, Pardanani A, Lim KH, Abdel-Wahab O, Lasho TL, Patel J, Gangat N, Finke CM, Schwager S, Mullally A, Li CY, Hanson CA, Mesa R, Bernard O, Delhommeau F, Vainchenker W, Gilliland DG, Levine RL (2009). TET2 mutations and their clinical correlates in polycythemia vera, essential thrombocythemia and myelofibrosis. Leukemia, 23: 905-911.

Terragni R, Casadei Gardini A, Sabattini S, Bettini G, Amadori D, Talamont C (2014). EGFR, HER-2 and KRAS in canine gastric epithelial tumors: a potential human model? Plos One, 9: doi:10.1371/journal.pone.0085388.

Tobin NP, Foukakis T, De Petris L, Bergh J (2015). The importance of molecular markers for diagnosis and selection of targeted treatments in patients with cancer. Journal of Internal Medicine, 278: 545-570.

Torres-Cabala CA, Wang W-L, Trent J, Yang D, Chen S, Galbincea J, Kim KB, Woodman S, Davies M, Plaza JA, Nash JW, Prieto VG, Lazar AJ, Ivan D (2009). Correlation between KIT expression and KIT mutation in melanoma: a study of 173 cases with emphasis on the acral-lentiginous/mucosal type. Modern Pathology, 22: 1446-1456.

Traina F, Visconte V, Jankowska AM, Makishima H, O'Keefe CL, Elson P, Han Y, Hsieh FH, Sekeres MA, Mali RS, Kalaycio M, Lichtin AE, Advani AS, Duong HK, Copelan E, Kapur R, Olalla Saad ST, Maciejewski JP, Tiu RV (2012). Single nucleotide polymorphism array lesions, TET2, DNMT3A, ASXL1 and CBL mutations are present in systemic mastocytosis. Plos One, 7: e43090.

Urruticoechea A, Alemany R, Balart J, Villanueva A, Viñals F, Capellá G (2010). Recent advances in cancer therapy: an overview. Current Pharmaceutical Design, 16: 3-10.

Usher SG, Radford AD, Villiers EJ, Blackwood L (2009). RAS, FLT3, and C-KIT mutations in immunophenotyped canine leukemias. Experimental Hematology, 37: 65-77.

Ustun C, DeRemer DL, Akin C (2011). Tyrosine kinase inhibitors in the treatment of systemic mastocytosis. Leukemia Research, 35: 1143-1152.

Valent P, Sperr WR, Akin C (2010). How I treat patients with advanced systemic mastocytosis? Blood, 116: 5812-5817.

Verma A, Halder K, Halder R, Yadav VK, Rawal P, Thakur RK, Mohd F, Sharma A, Chowdhury S (2008). Genome-wide computational and expression analyses reveal G-quadruplex DNA motifs as conserved *cis*-regulatory elements in human and related species. Journal of Medicinal Chemistry, 51: 5641-5649.

Waller ZAE, Sewitz SA, Hsu STD, Balasubramanian S (2009). A Small Molecule That Disrupts G-Quadruplex DNA Structure and Enhances Gene Expression. Journal of American Chemical Society, 131: 12628-12633.

Wang W-L, Hornick JL, Mallipeddi R, Zelger BG, Rother JD, Yang D, Lev DC, Trent JC, Prieto VG, Brenn T, Robson A, Calonje E, Lazar AJ (2009). Cutaneous and subcutaneous metastases of gastrointestinal stromal tumors: a series of 5 cases with molecular analysis. The American Journal of Dermatopatholy, 31: 297-300.

Warland J, Dobson J (2013). Breed predispositions in canine mast cell tumour: A single centre experience in the United Kingdom. The Veterinary Journal, 197: 496-498.

Watzinger F, Mayr B, Gamerith R, Vetter C, Lion T (2001). Comparative analysis of ras proto-oncogene mutations in selected mammalian tumors. Molecular Carcinogenesis, 30: 190-198.

Webster JD, Yuzbasiyan-Gurkan V, Miller RA, Kaneene JB, Kiupel M (2007). Cellular proliferation in canine cutaneous mast cell tumors: associations with c-KIT and its role in prognostication. Veterinary Pathology, 44: 298-308.

Webster JD, Yuzbasiyan-Gurkan V, Kaneene JB, Miller R, Resau JH, Kiupel M (2006). The role of c-KIT in tumorigenesis: evaluation in canine cutaneous mast cell tumors. Neoplasia, 8: 104-111.

Wei D, Husby J, Neidle S (2014). Flexibility and structural conservation in a c-KIT G-quadruplex. Nucleic Acids Research, 43: 629-644.

Weidle UH, Schneider B, Georges G, Brinkmann U (2012).Genetically engineered fusion proteins for treatment of cancer. Cancer Genomics and Proteomics, 9: 357-372.

Welle MM, Bley CR, Howard J, Rüfenacht S. (2008). Canine mast cell tumours: a review of the pathogenesis, clinical features, pathology and treatment. Veterinary Dermatology, 19: 321-339.

Weisberg E, Manley PW, Cowan-Jacob SW, Hochhaus A, Griffin JD (2007). Second generation inhibitors of BCRABL for the treatment of imatinib resistant chronic myeloid leukaemia. Nature reviews, 7: 345- 356.

White CR, Hohenhaus AE, Kelsey J, Procter-Gray E (2011). Cutaneous MCTs: associations with spay/neuter status, breed, body size, and phylogenetic cluster. Journal of the American Animal Hospital Association, 47: 210-216.

Wilson TM, Maric I, Simakova O, Bai Y, Chan EC, Olivares N, Carter M, Maric D, Robyn J, Metcalfe DD (2011). Clonal analysis of NRAS activating mutations in KIT-D816V systemic mastocytosis. Haematologica, 96: 459-463.

Yamamoto K, Tojo A, Aoki N, Shibuya M (1993). Characterization of the promoter region of the human c-kit proto-oncogene. Japanese journal of cancer research, 84: 1136-1144.

Yang D, Okamoto K (2010). Structural insights into G-quadruplexes: towards new anticancer drugs. Future Medicinal Chemistry, 2: 619-646.

Yarden Y, Kuang WJ, Yang-Feng T, Coussens L, Munemitsu S, Dull TJ, Chen E, Schlessinger J, Francke U, Ullrich A (1987). Human proto-oncogene *c-kit*: a new cell surface receptor tyrosine kinase for an unidentified ligand. EMBO journal, 6: 3341-3351.

Yoo S, Pettersson A, Jordahl KM, Lis RT, Lindstrom S, Meisner A, Nuttall EJ, Stack EC, Stampfer MJ, Kraft P, Brown M, Loda M, Giovannucci EL, Kantoff PW, Mucci LA (2014). Androgen Receptor CAG repeat polymorphism and risk of TMPRSS2:ERG positive prostate cancer. Cancer Epidemiology, Biomarkers and Prevention, 23: 2027-2031.

Zagotto G, Ricci A, Vasquez E, Sandoli A, Benedetti S, Palumbo M, Sissi C (2011). Tuning G-quadruplex vs double-stranded DNA recognition in regioisomeric lysyl-peptidyl-anthraquinone conjugates. Bioconjugate Chemistry, 22: 2126-2135.

Zavodovskaja R, Chien MB, London CA (2004). Use of kit internal tandem duplications to establish mast cell tumor clonality in 2 dogs. Journal of Veterinary Internal Medicine, 18: 915-917.

Zemke D, Yamini B, Yuzbasiyan-Gurkan V (2002). Mutations in the juxtamembrane domain of c-KIT are associated with higher grade mast cell tumors in dogs. Veterinay Pathology, 39: 529-535.

Zhao Y, Du Z, Li N (2007). Extensive selection for the enrichment of G4 DNA motifs in transcriptional regulatory regions of warm blooded animals. FEBS letters, 581: 1951-1956.

Zorzan E, Hanssens K, Giantin M, Dacasto M, Dubreuil P (2015). Mutational hotspot of TET2, IDH1, IDH2, SRSF2, SF3B1, KRAS, and NRAS from human systemic mastocytosis are not conserved in canine mast cell tumors. Plos One 12; 10(11): e0142450.

8.1 WEB REFERENCES

http://kohnpharmaceuticals.weebly.com/biochemical-pathways.html

http://primer3.ut.ee/

http://crn2m.univ-mrs.fr/AmplifX

http://www.ncbi.nlm.nih.gov/

http://www.fruitfly.org

https://blast.ncbi.nlm.nih.gov/Blast

http://www.uniprot.org/

http://www.ebi.ac.uk/Tools/msa/clustalw2/

http://cancer.sanger.ac.uk/cosmic

https://qpcr.probefinder.com/organism.jsp

http://multalin.toulouse.inra.fr/multalin/